

**AEROSOL FORMATION FROM
OXIDATION OF
CYCLIC VOLATILE METHYL SILOXANE**

by

Yue Wu

A dissertation submitted to the Faculty of the University of Delaware in partial fulfillment of the requirements for the degree of Doctor of Philosophy in Chemistry and Biochemistry

Fall 2017

© 2017 Yue Wu
All Rights Reserved

**AEROSOL FROMATION FROM
OXIDATION OF
CYCLIC VOLATILE METHYL SILOXANE**

by

Yue Wu

Approved: _____
Brian J. Bahnson, Ph.D.
Chair of the Department of Chemistry and Biochemistry

Approved: _____
George H. Watson, Ph.D.
Dean of the College of Arts and Sciences

Approved: _____
Ann L. Ardis, Ph.D.
Senior Vice Provost for Graduate and Professional Education

I certify that I have read this dissertation and that in my opinion it meets the academic and professional standard required by the University as a dissertation for the degree of Doctor of Philosophy.

Signed:

Murray V. Johnston, Ph.D.
Professor in charge of dissertation

I certify that I have read this dissertation and that in my opinion it meets the academic and professional standard required by the University as a dissertation for the degree of Doctor of Philosophy.

Signed:

Andrew V. Teplyakov, Ph.D.
Member of dissertation committee

I certify that I have read this dissertation and that in my opinion it meets the academic and professional standard required by the University as a dissertation for the degree of Doctor of Philosophy.

Signed:

Sharon L. Neal, Ph.D.
Member of dissertation committee

I certify that I have read this dissertation and that in my opinion it meets the academic and professional standard required by the University as a dissertation for the degree of Doctor of Philosophy.

Signed:

Chin-Pao (C.P.) Huang, Ph.D.
Member of dissertation committee

ACKNOWLEDGMENTS

First, I would like to express my deepest gratitude to my advisor, Dr. Murray Johnston, for his guidance, support and patience throughout my whole five years of graduate research. I feel very honored to have him as my Ph.D. advisor. He has encouraged me to do the best I can as well as to explore my interests in a wide range of research topics. It is lucky to learn from him and work with him during the past five years.

I would also like to thank my committee members: Dr. Andrew Teplyakov, Dr. Sharon Neal, and Dr. Chin-Pao Huang. During the committee meetings, their questions and comments helped me understand more about this research and also opened many new scopes to explore for different projects.

Additionally, I would thank my fellow members from Johnston's group. Particularly I want to thank Dr. Joe DePalma and Dr. Andrew Horan for assistance during the early stage of my lab work. Also it is my great honor to work with the whole Johnston group: Dr. Bryan Bzdek, Justin Krasnomowitz, Christopher Stangl and Michael Apsokardu.

I acknowledge the specialists from the Departmental Mass Spectrometry Facility for helping running a bunch of samples. Specifically, I thank Dr. Steven Chan, Dr. Andrew Horan, and Benjamin Rupert for their kind assistance and suggestions.

I, of course, acknowledge the NSF for providing funding which made this work possible.

Finally, I thank my parents for their support and encouragement during every step in my life. Without parents like them, I would absolutely not be where I am today. I would also like to thank all my friends, especially those who are not in the United States for bearing the time difference to listen to my worries and encourage me.

TABLE OF CONTENTS

LIST OF TABLES	ix
LIST OF FIGURES	xii
ABSTRACT	xvii

Chapter

1 INTRODUCTION	1
1.1 The Importance of Ambient Organic Aerosols	1
1.2 Silicon has been Observed in Ambient Nanoparticles	5
1.3 Cyclic Volatile Methyl Siloxane (cVMS)	6
1.3.1 Occurrence and Fate of cVMS in the Air	7
1.3.2 Analysis of cVMS	9
1.4 Scope of This Dissertation	10
REFERENCES	12
2 MOLECULAR CHARACTERIZATION OF SECONDARY AEROSOL FROM OXIDATION OF CYCLIC METHYLSILOXANES	16
2.1 Silicon Observed in Ambient Nanoparticles	16
2.2 Method Configuration	17
2.2.1 Aerosol Formation and Particle Collection	17
2.2.2 Mass Spectrometer	20
2.3 Molecular Characterization of D ₅ -oxidized Products	21
2.3.1 High Resolution Mass Spectra Interpretation	21
2.3.1.1 Fragmented Oxidation Products of D ₅	25
2.3.1.2 Saturated Oxidation Products of D ₅	26
2.3.2 High Resolution MS/MS Interpretation	28

2.3.2.1	OH Substitution of a CH ₃ Group	28
2.3.2.2	CH ₂ OH Substitution of a CH ₃ Group.....	30
2.3.2.3	Dimers Linkages by O and CH ₂	30
2.3.2.4	Dimers Linkage by CH ₂ CH ₂	34
2.4	Comparison to Previous Work	34
2.5	D ₄ -derived Secondary Aerosol.....	38
2.6	Conclusions.....	41
REFERENCES		43
3	AEROSOL FORMATION FROM OXIDATION OF VOLATILE CYCLIC METHYL SILOXANE DECAMETHYLPENTASILOXANE	45
3.1	Experimental Section	45
3.2	Aerosol Formation in Unseeded Experiments	49
3.3	Aerosol Formation in Seeded Experiments	58
3.4	Product Volatility Estimation	60
3.5	Aerosol Yield and Atmospheric Implication	67
3.6	Morphology of D ₅ -derived Aerosol	72
3.7	Conclusions.....	73
REFERENCES		74
4	SECONDARY AEROSOL FORMATION FROM OXIDATION OF DECAMETHYLOENTASILOXANE MIXED WITH β-PINENE	77
4.1	SOA from Biogenic and Anthropogenic Sources	77
4.2	Aerosol Generation from Photo-oxidation of D ₅ and β-pinene	79
4.3	Chemical Composition of Aerosol Formed in Mixed System.....	80
4.3.1	Molecular Characterization of Mixed Aerosol	80
4.3.2	Chemical Composition of Mixed Aerosol	84
4.4	Aerosol Formation from Mixed Conditions	85
4.4.1	Aerosol Yield Expression	85
4.4.2	Product Volatility Estimation	89
4.4.3	Chemical Resolved Partitioning.....	91
4.5	MS/MS Analysis for Structure Identification of ‘Mixed Products’.....	92
4.6	Conclusions.....	95
REFERENCES		97

5	CONCLUSIONS AND FUTURE DIRECTIONS.....	100
---	--	-----

Appendix

A	SUPPLEMENTAL MOLECULAR FORMULAS FOR IONS DETECTED IN D ₅ -DERIVED AEROSOL.....	102
B	SUPPLEMENTAL MOLECULAR FORMULAS AND VOLATILITIES (LOG C*) OF THE CORRESPONDING CANDIDATE STRUCTURES AT 299.15K FOR PRODUCTS DETECTED IN D ₅ -DERIVED SECONDARY AEROSOL	107

LIST OF TABLES

Table 1-1: Occurrence of cyclic siloxanes in the air published in the past a few years.	7
Table 2-1: Number and Mass-Intensity Weighted Fraction, MIF (%), of fragmented, saturated and unsaturated products of D ₅ oxidation in the positive and negative ion modes, respectively.....	25
Table 2-2: Several fragmented products in D ₅ -derived secondary aerosol. Molecular formulas are written based on likely structures (linear, cyclic) and functional groups....	25
Table 3-1: Experimental conditions for secondary aerosol formation from OH oxidation of D ₅ with/without seed particles. ΔD ₅ is the estimated reacted concentration of gas phase D ₅ , ΔM is the aerosol mass concentration....	47
Table 3-2: Estimation of boiling point and volatility at 299.15K of one OH substituted D ₅ (C ₉ H ₂₈ O ₆ Si ₅)..	62
Table 3-3: Estimation of boiling point and volatility at 299.15K of various siloxanes.	63
Table 3-4: Estimation of volatility at 299.15K for candidate isomers of the ring opened product (C ₁₁ H ₃₆ O ₁₂ Si ₈).....	64
Table 3-5: Empirical parameters for three products model describing the particle mass yield of aerosol produced from unseeded experiments.....	71
Table 4-1: Experimental conditions for secondary aerosol formation from OH oxidation of D ₅ and β-pinene. ΔM is the aerosol mass concentration.	80
Table 4-2: Three model products i describing the partitioning of D ₅ -derived aerosol molecules between the gas and particle phases. Shown are the mass yield α _i , the decadal volatility C* _i (μg/m ³), the atomic ratios (O/Si) _i and (C/Si) _i , and the corresponding empirical formulas on a one-silicon basis....	92
Table A-1: Assigned ring-opened formulas for ions detected in D ₅ -derived aerosol..	102
Table A-2: Assigned saturated formulas for ions detected in D ₅ -derived aerosol.....	104

Table A-3: Assigned unsaturated formulas for ions detected in D₅-derived aerosol..106

Table B-1: Molecular formulas and volatilities (logC*) of the corresponding candidate structures at 299.15K for products detected in D₅-derived secondary aerosol. The products listed were positively detected in all four samples of at least one secondary aerosol studied...107

LIST OF FIGURES

Figure 1-1: Formation of primary and secondary aerosol in the atmosphere.	3
Figure 1-2: Octamethylcyclotetrasiloxane, (D ₄) and Decamethylcyclopentasiloxane (D ₅).....	6
Figure 1-3: Proposed oxidation reaction mechanism of Si-CH ₃ groups.....	9
Figure 2-1: Experimental Setup.....	17
Figure 2-2: Photo-Oxidation Reaction Chamber.	18
Figure 2-3: Representative ESI mass spectra of secondary aerosol from D ₅ oxidation.....	22
Figure 2-4: Representative ESI mass spectra in the positive ion mode of D ₅ -derived aerosol generated under conditions giving high (60 µg/m ³) vs. low (~6 µg/m ³) mass loading..	23
Figure 2-5: Positive ESI mass spectrum of pure D ₅ in ACN with a concentration of 100 µg/ml.....	26
Figure 2-6: Plots of C/Si versus O/Si for saturated products of D ₅ oxidation in the monomer (a) and dimer (b) regions. Each dot represents an assigned molecular formula of a saturated oxidation product. The arrows in the monomer plot extend from unoxidized D ₅ and represent the two types of substitution that can occur. The arrows in the dimer plot take into account difference possible linkages between monomers.	28
Figure 2-7: Product ion spectra for isolation of a) 373 m/z(+), b) 371 m/z(-) and c) 387 m/z(+). These precursors correspond to the oxidation product of D ₅ having one OH substitution for a CH ₃ group and D ₅ having one CH ₂ OH substitution for a CH ₃ group	30

Figure 2-8: Product ion spectrum of 727 m/z(+). a) Complete product ion spectrum. b) An expansion of 350 to 380 m/z(+). Peaks corresponding to an O linkage are marked with red. Peaks corresponding with a CH ₂ linkage are marked with blue. Peaks consistent with both are marked in black. c) Expansion of the product ion spectrum of 795 m/z(+) between 380 and 470 m/z(+). Peaks corresponding with a CH ₂ CH ₂ linkage are marked with blue.	32
Figure 2-9: Dimer structures with a) -O-, b) -CH ₂ -, and c) -CH ₂ CH ₂ - linkages. The OH group in b) could be located anywhere around the siloxane ring. The locations of the two CH ₂ OH groups in c) can be anywhere on the left hand ring, while the location of the OH group can be anywhere on the right hand ring. The C ₁₁ product confirms the existence of a CH ₂ CH ₂ - linkage. Other labeled ions are consistent with, but not unique to, this linkage.	33
Figure 2-10: a) GC-MS total ion chromatogram of D ₅ -derived aerosol. b) EI mass spectra of three peaks in the chromatogram corresponding to D ₅ , OH substituted D ₅ and CH ₂ OH substituted D ₅ . The EI mass spectra match library spectra for these compounds. c) EI mass spectra of what appear to be peaks corresponding to O and CH ₂ linked dimers.	35
Figure 2-11: A Possible pathways for product formation from OH oxidation of D ₅	38
Figure 2-12: Representative ESI mass spectra of secondary aerosol from D ₄ oxidation.	40
Figure 2-13: Plots of C/Si versus O/Si for saturated products of D ₄ oxidation in the a) monomer and b) dimer regions. Each dot represents an assigned molecular formula of a saturated oxidation product. The arrows in the monomer plot extend from unoxidized D ₄ and represent the two main types of substitution that occur. The arrows in the dimer plot take into account different possible linkages between monomers. Circles represent monomer products where all eight CH ₃ groups have been substituted. Formulas to the right of the circles (same C/Si but higher O/Si) must contain peroxy groups..	41
Figure 3-1: a) Number based size distributions from unseeded experiments with secondary mass loadings of 1.2, 5.6 and 12 μg/m ³ , respectively. b) Number based size distributions from a seeded experiment before and after secondary aerosol formation.....	48

Figure 3-2: ESI mass spectra in positive ion mode of secondary aerosol from D ₅ oxidation under various aerosol mass loadings. Ion signal intensities are averaged over four separate measurements from four different samples. Peaks considered as ring opened products are coded blue, dimers are coded black, and monomers are coded red... ..	51
Figure 3-3: Candidate structures for the three types of reaction products found in siloxane secondary aerosol.	52
Figure 3-4: Product MS/MS ion spectra for isolation of (a) 607 m/z(+), (b) 729 m/z(+), and (c) 373 m/z(+).	53
Figure 3-5: Positive ESI mass spectrum of pure D ₅ in ACN/H ₂ O 50/50 by volume with a concentration of 100 µg/ml sonicating for 3 hours.....	54
Figure 3-6: Volume-to-surface area ratio vs. mass loading for the unseeded aerosols studied in this work. Error bars represent one standard deviation. Error bars smaller than the symbol are not shown.....	55
Figure 3-7: Signal intensity ratio of a) dimers to ring-opened products and b) monomers to dimers vs. volume/surface area ratio of the secondary aerosol. Error bars represent one standard deviation. Error bars smaller than the symbols are not shown.....	56
Figure 3-8: ESI mass spectra in positive ion mode for a) unseeded and b) seeded aerosol produced by OH oxidation of D ₅ under conditions that give similar mass loadings (after subtraction of seed aerosol) of ~3 µg/m ³ . Ion signal intensities are averaged over four separate measurements from four different samples. Peaks considered as ring opened products are coded blue, dimers are coded black, and monomers are coded red.	60
Figure 3-9: O/Si ratio and estimated C* values for molecular formulas assigned from siloxane secondary aerosol. This figure summarizes the data in Appendix B. Ring opened products are coded blue; dimers are coded black; monomers are coded red.	65
Figure 3-10: Mass-weighted signal intensities summed over the three types of ions in a) unseeded and b) seeded aerosols vs. log C* for candidate structures that correspond to individual ions. These plots are for assigned ions in the mass spectra of Figures 3-6a and 3-6b, respectively. Ring-opened products are coded blue, dimers are coded black, and monomers are coded red.....	67

Figure 3-11: Plot of number and mass concentration as a function of time after reaction was initiated...	69
Figure 3-12: Plot of aerosol yield and aerosol mass concentration versus reacted mass concentration respectively..	70
Figure 3-13: Plot of aerosol yield versus aerosol mass concentration. These data are for unseeded experiments. The dashed line represents the volatility basis set model fit	71
Figure 4-1: ESI mass spectra in positive ion mode of secondary aerosol from mixed D ₅ and β-pinene oxidation under various aerosol mass loadings. Ion signal intensities are averaged over four separate measurements from four different samples. Peaks considered D ₅ -derived aerosol are coded blue, β-pinene SOA are coded red, and mixed products are coded black. Note that the color coding in this figure is different from that in Chapter 3 and for most Figures that follow in Chapter 4...	82
Figure 4-2: a) ESI mass spectra in positive ion mode of oxidation products of D ₅ observed in secondary aerosol from the mixed precursor experiments. Ion signal intensities are averaged over four separate measurements from four different samples. Peaks considered as ring opened products are coded blue, dimers are coded black, and monomers are coded red. The relative abundance is ranged from 0 to 15%; b) Plot of average O/Si as a function of aerosol mass loadings.	83
Figure 4-3: Plot of C/Si versus O/Si showing chemical composition of unseeded (black), seeded (red) and mixed (blue) experiments. The black dashed line represents OH substitutions on siloxane (OH→CH ₃); the red dashed line represents CH ₂ OH substitutions on siloxane (CH ₂ OH→CH ₃).	85
Figure 4-4: Plot of aerosol yield versus aerosol mass concentration of single siloxane experiment (red) and mixed experiment (blue) respectively..	87
Figure 4-5: Volume-to-surface area ratio vs. mass loading for the single siloxane experiments (red) and mixed experiments (blue) studied in this work. Error bars represent one standard deviation. Error bars smaller than the symbol are not shown	87
Figure 4-6: Signal intensity ratio of a) dimers to ring-opened products and b) monomers to dimers vs. volume/surface area ratio of the secondary aerosol. Unseeded aerosol coded black and mixed aerosol coded red. Error bars represent one standard deviation. Error bars smaller than the symbols are not shown.....	88

Figure 4-7: Mass-weighted signal intensities summed over the three types of ions in a) unseeded, b) seeded and c) mixed aerosols vs. $\log C^*$ for candidate structures that correspond to individual ions. These plots are for assigned ions in the mass spectra of Figure 3-7a, b and Figure 4-2c, respectively. Ring-opened products are coded blue, dimers are coded black, and monomers are coded red.....	90
Figure 4-8: ESI mass spectra in positive ion mode of mixed products. Ion signal intensities are averaged over four separate measurements from four different samples. The relative abundance is ranged from 0 to 30%.....	93
Figure 4-9: Product ion spectrum of 299 $m/z(+)$. a) Complete product ion spectrum. b) Representative chemical structure.	94

ABSTRACT

Ambient nanoparticles (defined as smaller than 100 nm in diameter) can disproportionately affect climate and human health relative to their mass loading in the atmosphere. To better understand these effects, knowledge of chemical composition is needed. Organic aerosol constitutes a large portion of this matter and most of this contribution is secondary, meaning that it is formed through reaction of gas phase volatile organic compounds (VOC) with oxidants (OH, O₃, NO₃) to give semi- or non-volatile products. Recently, silicon was reported as a frequent component of ambient nanoparticles. Measurements with Nano Aerosol Mass Spectrometer (NAMS), which provides quantitative elemental composition of particles in the 10-30 nm diameter range, showed that Si was often observed in urban and suburban environments but rarely detected in a remote environment. The location dependence suggests that Si in these particles is associated with human activity. One possible source is atmospheric oxidation of cyclic volatile methylsiloxanes (cVMS), which are commonly used in personal care products. Owing to high vapor pressure, they are easily released into atmosphere where they may react with OH to form semi- or non-volatile products. In this dissertation, the chemical composition and formation mechanisms of secondary aerosol produced from the OH-initiated oxidation of decamethylcyclopentasiloxane is studied by high performance mass spectrometry.

Firstly, high resolution ESI-MS reveals a large number of monomeric ($300 < m/z < 470$) and dimeric ($700 < m/z < 870$) oxidation products. With the aid of high resolution and MS/MS, it is shown that oxidation leads mainly to the substitution of a

CH₃ group by OH or CH₂OH, and that a single molecule can undergo many CH₃ group substitutions. Dimers also exhibit OH and CH₂OH substitutions and can be linked by O, CH₂ and CH₂CH₂ groups.

Secondly, aerosol formation mechanisms were studied with and without the presence of ammonium sulfate seed aerosol. For the unseeded experiments, chemical characterization with high performance mass spectrometry showed that the molecular composition changed substantially with aerosol mass loading in the 1-12 μg/m³ range. Monomers (5 Si atoms/molecule) and dimers (10 Si atoms/molecule) dominated the mass spectra of aerosols at higher mass loadings while ring opened species (neither 5 nor 10 Si atoms/molecule) dominated the mass spectra of aerosols at lower mass loadings. Molecular signal intensity dependencies on the aerosol volume-to-surface area ratio suggest that nonvolatile ring opened species are formed in the gas phase and assist particle formation through condensation, while dimers are formed by accretion reactions within the particle phase as the particles grow. These conclusions are supported by experiments in the presence of seed aerosol with similar siloxane aerosol mass loading but higher volume to surface area ratio, where ring-opened species are much less prevalent than monomers or dimers and the aerosol yield is higher.

The influence of biogenic secondary organic aerosol on D₅ derived aerosol was studied by mixing β-pinene into reactor. The results showed that aerosol chemical composition containing both β-pinene and siloxane components is dominated by β-pinene SOA with slowly increasing siloxane contribution in this mixed system with increasing aerosol mass loading. Additionally, β-pinene SOA was found to serve in a similar manner to ammonium sulfate as a seed aerosol where ring-opened siloxane products are much less prevalent than siloxane monomers or dimers.

Chapter 1

INTRODUCTION

1.1 The Importance of Ambient Organic Aerosol

Ambient aerosol has been defined as a solid particles or liquid droplets suspended in the air. Aerosol particles affect the radiative budget of the Earth's atmosphere¹ through scattering and absorption of light² (i.e., direct climate forcing effect) and by modulating the formation and properties of clouds (i.e., indirect climate forcing effect)³. In addition, aerosols have serious adverse effects on air quality⁴, human health⁵, and ecosystems⁶. To better understand these effects, atmospheric particles can be categorized by the size and chemical composition⁷. Specifically, the size of ambient particles can vary from several nanometers up to 10 μ m, where those from 2.5 to 10 μ m are called coarse particles and those less than 2.5 μ m are called fine particles⁷. Fine particles have a more severe influence on human health than coarse particles because they can penetrate into deeper regions of the human respiratory tract during nose breathing⁸. As a result, atmospheric fine particles are strongly linked with adverse health effects. Fine particulate matter (PM) makes up a large fraction of the total particulate mass in the atmosphere, typically 20-60% in the continental mid-latitudes⁹, and up to 90% in tropical forested areas¹⁰. Despite the abundance of atmospheric PM, the ambient composition is still poorly understood due to large measurement uncertainties and chemical complexity.

According to the different sources, PM could be classified into primary and secondary. The processes of the formation of primary and secondary aerosol are shown in Figure 1-1 respectively. Primary particles are directly emitted into the atmosphere from many sources such as motor vehicle emissions (anthropogenic) or volcanic eruptions (natural). Secondary particles, on the other hand, are formed by

gas-particle conversion process such as nucleation, condensation and multiple chemical reactions¹¹. While the composition across all environments/sizes is not completely known, components formed from the oxidation of gas phase organic molecules (Secondary Organic Aerosol, SOA) have been shown to be a large contributor to overall aerosol mass¹². It has been shown that about 80% of SOA in mass is from biogenic sources¹³. Biogenic SOA is formed from the reaction of biogenic volatile organic compound (VOC) with atmospheric oxidants such as O₃, OH and NO₃ resulting in semi- or non-volatile compounds that migrate to the particle phase through gas-particle transfer⁹⁻¹³. The SOA formation mechanisms are complex and even though we nowadays have a detailed chemical knowledge on the degradation of most VOC, a large part of the SOA formation and ageing is still unclear as well as understanding how different VOC precursors interact with each other during aerosol formation. In addition to biogenic sources (of which monoterpenes are most important), SOA could also be generated from other anthropogenic sources, and of the anthropogenic VOCs, chamber experiments indicate that aromatic compounds from vehicle emissions produce the majority of anthropogenic SOA¹⁴. However, a number of recent studies clearly show that anthropogenic VOCs lead to much more SOA than expected¹⁵⁻¹⁶ suggesting other unknown production pathways.

Recently, there are several field observations where SOA has been attributed to originate from both biogenic and anthropogenic sources and it seems that anthropogenic activities enhance biogenic SOA abundance¹⁷⁻¹⁹. Efforts have been made to quantify the aerosol formation potential (aerosol yield) of both monoterpenes and aromatic compounds. Odum et al. (1997) showed that the aerosol yield of whole gasoline vapor can be explained by the sum of the single SOA yields of its aromatic constituents¹⁴. Most models describing SOA formation assume a thermodynamic equilibrium of organic compounds between the gas and the aerosol phase. However, these models underestimate the organic partitioning into the aerosol phase of many compounds²⁰. As a result, in the

equilibrium gas/particle partitioning framework, an increase in aerosol leads to a shift in partitioning from the gas to the condensed phase, therefore increased anthropogenic emissions of organic particulate matter or semi-volatile OC may lead to a shift of biogenic carbon from the gas to the condensed phase¹⁷. However, the influence of biogenic SOA on anthropogenic SOA is not well understood yet.

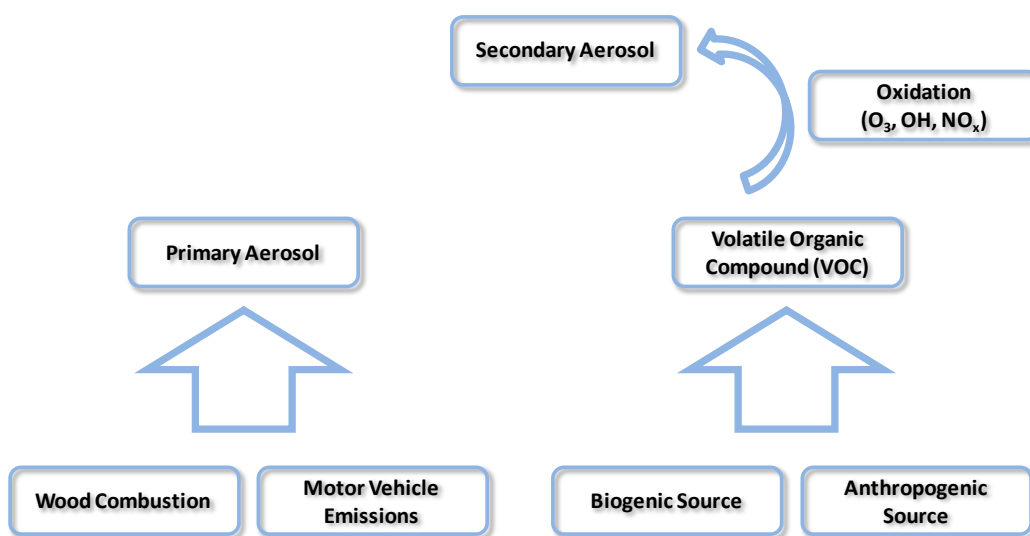


Figure 1-1: Formation of primary and secondary aerosol in the atmosphere.

The composition of SOA on the molecular level is difficult to analyze, and it has been shown that studies conducted so far were only able to resolve a small fraction of the entire organic particle mass²¹. More accurate studies are needed to solve the chemical composition SOA and its time dependence. In recent years, online aerosol mass spectrometers have enabled chemical analyses of aerosols in real time with high time resolution (seconds to minutes)²². A range of mass spectrometers using various particle vaporization and ionization techniques have been developed to solve the complex chemical composition of aerosol. Most of the currently available aerosol mass spectrometers rely on ‘hard’ ionization methods, and therefore observe many ionic fragments²³. A ‘soft’ ionization method that converts the precursor molecules into positive or negative

ions without fragmentation is a key prerequisite for the molecular assignment of organic compounds, which fragment rather extensively under the traditional electron impact ionization conditions²². A number of soft ionization methods have been developed in recent years, and successfully coupled with high resolution mass spectrometers (HR-MS). For example, Bruggemann et al. (2015) presented the development and characterization of a new soft ionization technique that allows mass spectrometric real-time detection of organic compounds in aerosols. Ionization of the analytes occurs in the afterglow region after thermal desorption and produces mainly intact quasimolecular ions, facilitating the interpretation of the acquired mass spectra; Horan et al. (2017) recently introduced a new ionization method, droplet assisted inlet ionization (DAII), where aqueous droplets are produced from airborne nanoparticles allowing for the characterization of airborne nanoparticles with sufficient sensitivity and application to ambient aerosol as well as laboratory experiments²⁴.

The application of HR-MS combined with tandem mass spectrometry (MSⁿ) for structural characterization of SOA constituents, pioneered by the Johnston research group in 2004²⁵⁻²⁸, is currently a rapidly growing area of research in aerosol chemistry. In particular, the chemical composition of secondary organic aerosol formed from the ozone-initiated oxidation of limonene was characterized by high-resolution electrospray ionization mass spectrometry in both positive and negative ion modes²⁸; additionally, Hall et al. (2012) successfully studied the formation mechanisms of oligomers produced in the laboratory by ozonolysis of α -pinene and characterized monomer building blocks within the reactions that couple them together by utilizing the MS and MS/MS measurements with high accuracy and resolving power²⁶. As a result, high-resolution mass spectrometry becomes a more and more powerful tool for detailed characterization of such complex SOA samples.

1.2 Si has been Observed in Ambient Nanoparticles

Silicon (Si) has been reported sporadically in ambient nanoparticles in the past²⁹⁻³¹, but its quantitative contribution to nanoparticle mass has not been assessed. Bzdek et al. (2014) combined nanoparticle elemental composition measurements over several field campaigns to show that Si is a frequent component of atmospheric nanoparticles³². In particular, nanoparticle chemical composition measurements were performed with the Nano Aerosol Mass Spectrometer (NAMS), which provides quantitative elemental composition of nanoparticles in the 10–30 nm diameter size range³³⁻³⁵. Specifically, they analyzed data obtained with the instrument between 2006 and 2012 at urban, suburban, and rural sites around the U.S. and at a pristine forest site in Finland, in measurement campaigns lasting several weeks. A surprising observation during many of these campaigns is that Si was found in a large fraction of ambient nanoparticles. For example, in Pasadena (CA), which is part of the Los Angeles metropolitan area, 40% of the measured nanoparticles contained silicon; in Wilmington (DE), a smaller city in the Philadelphia metropolitan area, the proportion ranged from 5 to 13%³². In these populated areas, the proportion of silicon-containing nanoparticles did not vary greatly with wind direction, suggesting a diffuse source³². At the pristine site in Finland, only about 2% of nanoparticles contained silicon³². Given the greater proportion of silicon-containing nanoparticles in populated areas, the researchers suspected the particles had a human-made source³². Because the method of nanoparticle analysis provides only elemental composition, it is not possible to determine the molecular forms of Si in the nanoparticles³². However, several studies have addressed the atmospheric concentrations and lifetimes of organosilicon compounds such as cyclic siloxanes, which are widely used in personal care products and industrial applications and which have the potential for long-range transport and bioaccumulation³². These sources are related to human activity and could be manifested on both local and regional scales. To test this hypothesis, a

Johnston group collaborator, Professor Charles Stanier at the University of Iowa, made an atmospheric transport model for three of the most common cyclic siloxanes found in personal care products—octamethylcyclotetrasiloxane (D_4), decamethylcyclopentasiloxane (D_5), and dodecamethylcyclohexasiloxane (D_6). The team estimated emission rates for the compounds based on U.S. population data, as well as information based on antiperspirant sales and usage³². They then applied known rates for the reaction of siloxanes with hydroxyl radicals in the atmosphere, to predict the concentration of oxidized cyclic siloxanes across the U.S. These concentrations peaked in populated areas such as Los Angeles and the East Coast, consistent with the team’s field data³².

1.3 Cyclic Volatile Methyl Siloxane

One possible source of silicon in ambient nanoparticles is the atmospheric oxidation of cyclic volatile methylsiloxanes (cVMS). cVMS compounds predominantly made of $-\text{Si}(\text{CH}_3)_2-\text{O}-$ units and the Si-O atoms are singly bonded forming a ring. Octamethylcyclotetrasiloxane, (D_4) and decamethylcyclopentasiloxane (D_5) are shown as examples in Figure 1-2.

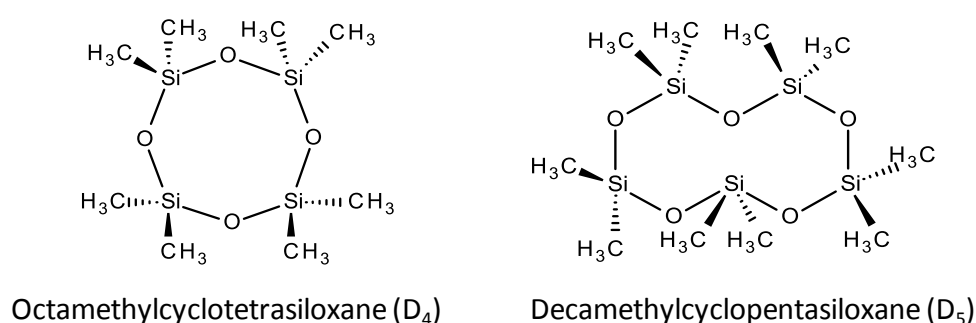


Figure 1-2: cVMS molecules D_4 and D_5 .

Numerical values of several important physicochemical properties of cVMS molecules from D_3 to D_6 were compiled and discussed in previous publications³⁶. Especially some thermochemical properties of D_3 , D_4 , and D_5 (vapor pressure,

liquid density, viscosity, heat capacity, surface tension, thermal conductivity) were measured³⁷. Generally, cVMS are low viscosity silicone fluids with low water solubility and relatively high vapor pressure representing potential for long range transport and bioaccumulation in the environment³⁸.

1.3.1 Occurrence of cVMS in the air

Owing to high vapor pressure, more than 90% of cVMS are released into atmosphere as gases where they may react with OH³⁹ to form semi- or non-volatile products. Table 1-1 then summarizes the results of siloxane concentration measurements published in the past few years in both of indoor and outdoor environments, with a much higher concentration in indoor environments³⁶. Basically, D₃–D₆ were measured indoor and outdoor air at 20 sites worldwide in 2009, mostly in North America and Europe, including five sites in the Arctic region⁴⁰. High levels of D₅ together with some D₆ were found in urban areas, whereas D₃ and D₄ occurred mostly in northwestern America⁴⁰. It seems that D₅ and D₆ occurrence was explained by the use of personal care products while D₃ and D₄ were industrial emissions. For example, Buser et al. reported D₅ and D₆ at levels up to 650 and 79 ng/m³ respectively in ambient air in Zurich, Switzerland⁴¹. Tang et al. examined the sources of VOCs in a university classroom and reported a D₅ concentration of 60±32µg/m³, which represented >90% of all VOCs detected⁴². For D₅ concentrations, rather good accord with predictions from two global contaminant models was found, which led to the conclusion that sources, transport paths, and sinks of D₅ are fairly well-understood³⁶.

matrix	siloxane	location	Concentration	ref.
Indoor and outdoor air	D ₅	Office building in San Francisco Bay area	Indoor 1.1-7.4 ppb, outdoor 0.03-0.08 ppb.	43
Indoor air	D ₅	Commercial building in California	1.3-120 µg/m ³	44
Indoor air	D ₃ -D ₅	Class room in Northrhine-westphalia,	D ₃ : 48 µg/m ³ , D ₄ : 32 µg/m ³ , D ₅ : 23 µg/m ³	45

		Germany		
Outdoor air	D ₅	Rural site of Stockholm, Sweden	0.7-8 ng/m ³ for 4 month	46
Outdoor air	D ₅	Ambient air of Zurich, Switzerland.	650 ng/m ³	41
Outdoor air	D ₃ -D ₅	20 sites in North America and Europe	D ₃ : 117 ng/m ³ , D ₄ : 50 ng/m ³ , D ₅ : 280 ng/m ³	40

Table 1-1: Occurrence of cyclic siloxanes in the air published in the past a few years.

As discussed earlier, the major degradation pathway of cVMS in the atmosphere is oxidation by hydroxyl radical (OH)³⁹, where generation of semivolatile and nonvolatile products can lead to aerosol formation⁴⁷. An atmospheric transport model with built-in OH and D₅ chemistry was used to predict D₅ concentrations in air at a rural site in Sweden, with good agreement between measured and predicted concentrations⁴⁶. Janecek et al. modified the Community Multiscale Air Quality (CMAQ) model by incorporating cVMS and their gas phase oxidation products, and found that oxidized D₅ concentrations could be up to 9 ng/m³ downwind of major urban areas⁴⁸. It has been reported that the atmospheric half-lives of cVMS have been estimated to range from days to weeks (e.g., 30 days for D₃, 15 days for D₄, and 10 days for D₅) indicating the long range transportation in the air⁴⁹. In 1991, Atkinson³⁹ determined the first-order rate constants (k) for gas-phase reactions of D₃, D₄, and D₅ with OH radical at 298 K to be $(0.52 \pm 0.17) \times 10^{-12}$, $(1.01 \pm 0.32) \times 10^{-12}$, and $(1.55 \pm 0.17) \times 10^{-12}$ cm³ molecule⁻¹ s⁻¹, respectively; Sommerlade et al.⁴⁹ measured the rate constant for reaction of D₄ with OH radical to be $(1.26 \pm 0.40) \times 10^{-12}$ cm³ molecule⁻¹ s⁻¹ at 297K and confirmed several identified products by using GC/MS. In a recent study, Safron et al.⁵⁰ measured reaction rates of D₄, D₅, and D₆ with OH between 313 and 353 K in a small scale reaction chamber, using the method of relative rates with cyclohexane as a reference substance. The reported k values of D₄, D₅, and D₆ calculated at 298 K from the resulting Arrhenius

equations are $(1.9 \pm 0.3) \times 10^{-12}$, $(2.6 \pm 0.3) \times 10^{-12}$, and $(2.8 \pm 0.3) \times 10^{-12}$ $\text{cm}^3 \text{ molecule}^{-1} \text{ s}^{-1}$, respectively⁵⁰.

The reaction mechanism between cyclic siloxane and OH radical is complicated. Generally, the first step of the reaction of cVMS and OH is considered to be H-atom abstraction from the methyl group, producing a siloxane methyl radical and water³⁸. Subsequent reactions of the siloxane methyl radical, involving consecutive initiation, self-reaction, chain propagation, and isomerization steps, are still not well understood. Reaction scheme could only be proposed and based on known atmospheric chemistry of similar compounds as shown in Figure 1-3⁵¹.

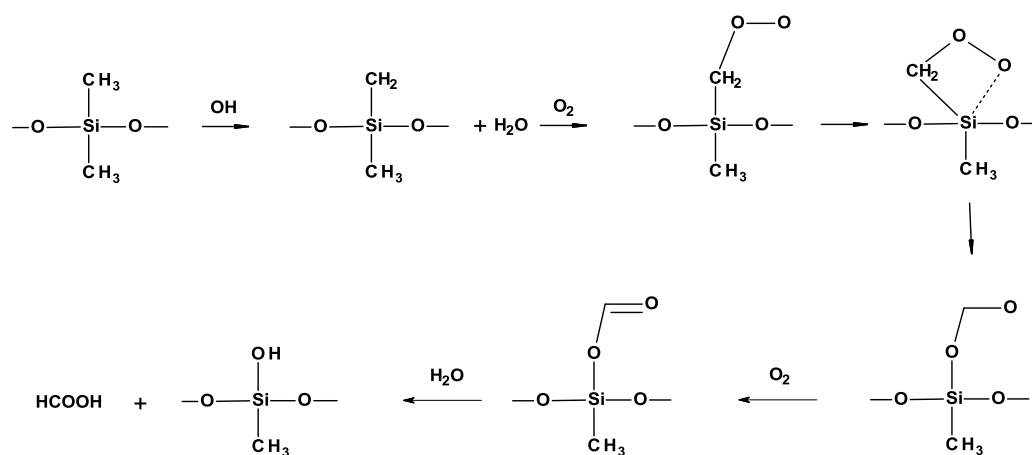


Figure 1-3: Proposed oxidation reaction mechanism of Si-CH₃ groups

1.3.2 Analysis of cVMS

Quantitative analysis of cVMS at trace levels is a demanding task. Methods, intricacies, and potential fallacies of cVMS analysis were well described in reviews^{36,52}. Difficulty of analysis, and thus lack of analytical methods for routine use, is probably one reason why siloxanes were not included in environmental monitoring programs³⁶. It is only recently that analytical methods for determination of individual cVMS in environmental samples have been developed. Quite logically, for volatile analytes such as D₄ and D₅, GC is the method of choice, preferably in combination with MS detection^{47,49,53}. As

discussed above, although degradation by OH radical is the main oxidation pathway of cVMS in the atmosphere, the products and mechanisms are not well understood. In other words, explicit molecular identification of products was not included. This is justified given the lack of knowledge about the distribution of products under atmospherically relevant oxidation conditions. Specific products have been identified in chamber studies using GC/MS analysis of filters, denuders, and extracts from reaction vessels⁴⁹. Studies also propose multistep mechanisms leading to a first generation of stable oxidation products. Sommerlade et al. (1993) detected D₃TOH (one OH substituted D₄) as a major product species from reaction of D₄ using GC/MS⁴⁹. However, D₃TOH only accounted for 46% of the mass of products resolved by GC/MS. Several other products were resolved, and still other products could not be resolved. Fragmentation in the GC/MS may occur as well. Whelan et al. (2004) modeled multigenerational oxidation leading to progressive substitution of methyl groups by alcohol groups, but experimental observations of atmospheric products to support their model are not available³⁸. This dissertation includes the first report of using high resolution mass spectrometry(HR-MS) to characterize the chemical composition in the aerosol phase, which will be discussed late in Chapter 2^{47,53}.

1.4 Scope of this dissertation

As discussed in previous sections, there exists a need for the research of aerosol produced from cVMS-OH oxidation, especially the products on molecular levels and chemical evolution under the atmospheric relevant conditions. Focusing on siloxane-derived aerosol by using multiple mass spectrometry techniques, this dissertation seeks to help bridge those gaps by characterizing the aerosol molecular composition and aerosol formation mechanisms.

Specifically, Chapter 2 describes the chemical composition of secondary aerosol produced from the OH-initiated oxidation of decamethylcyclopentasiloxane (D₅, C₁₀H₃₀O₅Si₅) by high performance mass

spectrometry. Experiments are detailed which give insight into the molecular characterization of oxidized D₅ products by utilizing high resolution MS and MS/MS.

Chapter 3 then describes the molecular composition of secondary aerosol obtained from D₅ oxidation generated both in the presence and absence of ammonium sulfate seed aerosol. Systematic changes in the molecular composition with aerosol mass loading are observed and interpreted on the basis of estimated volatilities of the individual molecular products, which give fundamental insight into the pathways involved in secondary aerosol formation.

Chapter 4 expands the single siloxane precursor to a mixed VOC precursor condition. Aerosol generated from a mixture of D₅ and β-pinene was used to study the influence of biogenic and anthropogenic precursors on each other. High resolution MS/MS is performed to elucidate the chemical structure of the products generated from the mixed oxidation system.

Chapter 5 concludes with an overview of the aerosol generated from OH oxidation of D₅. Remaining questions are needed to study this chemistry under a wider range of experimental conditions and particle phase morphologies that might be encountered in ambient aerosol.

REFERENCES

- (1) Papadimas, C. D.; Hatzianastassiou, N.; Matsoukas, C.; Kanakidou, M.; Mihalopoulos, N.; Vardavas, I. *Atmospheric Chemistry and Physics* **2012**, *12*, 7165-7185.
- (2) Lyamani, H.; Olmo, F.; Aladosarboledas, L. *Atmospheric Environment* **2008**, *42*, 2630-2642.
- (3) Spracklen, D. V.; Carslaw, K. S.; Kulmala, M.; Kerminen, V.-M.; Sihto, S.-L.; Riipinen, I.; Merikanto, J.; Mann, G. W.; Chipperfield, M. P.; Wiedensohler, A.; Birmili, W.; Lihavainen, H. *Geophysical Research Letters* **2008**, *35*.
- (4) Schell, B.; Ackermann, I. J.; Hass, H.; Binkowski, F. S.; Ebel, A. *Journal of Geophysical Research: Atmospheres* **2001**, *106*, 28275-28293.
- (5) Seaton, A.; Macnee, W.; Donaldson, K.; Godden, D. *Lancet* **1995**, *345*, 176-178.
- (6) Tobo, Y.; Prenni, A. J.; DeMott, P. J.; Huffman, J. A.; McCluskey, C. S.; Tian, G.; Pöhlker, C.; Pöschl, U.; Kreidenweis, S. M. *Journal of Geophysical Research: Atmospheres* **2013**, *118*, 10,100-110.
- (7) Tolocka, M. P.; Jang, M.; Ginter, J. M.; Cox, F. J.; Kamens, R. M.; Johnston, M. V. *Environmental Science & Technology* **2004**, *38*, 1428-1434.
- (8) Oberdörster, G.; Oberdörster, E.; Oberdörster, J. *Environmental Health Perspectives* **2005**, *113*, 823-839.
- (9) Carlton, A. G.; Wiedinmyer, C.; Kroll, J. H. *Atmospheric Chemistry and Physics* **2009**, *9*, 4987-5005.
- (10) Griffin, R. J.; Cocker, D. R.; Flagan, R. C.; Seinfeld, J. H. *Journal of Geophysical Research-Atmospheres* **1999**, *104*, 3555-3567.
- (11) Pöschl, U. *Angew Chem Int Ed Engl* **2005**, *44*, 7520-7540.
- (12) Hallquist, M.; Wenger, J. C.; Baltensperger, U.; Rudich, Y.; Simpson, D.; Claeys, M.; Dommen, J.; Donahue, N. M.; George, C.; Goldstein, A. H.; Hamilton, J. F.; Herrmann, H.; Hoffmann, T.; Iinuma, Y.; Jang, M.; Jenkin, M. E.; Jimenez, J. L.; Kiendler-Scharr, A.; Maenhaut, W.; McFiggans, G.; Mentel, T. F.; Monod, A.; Prevot, A. S. H.; Seinfeld, J. H.; Surratt, J. D.; Szmigielski, R.; Wildt, J. *Atmospheric Chemistry and Physics* **2009**, *9*, 5155-5236.

- (13) Griffin, R. J.; Cocker, D. R.; Flagan, R. C.; Seinfeld, J. H. *Journal of Geophysical Research-Atmospheres* **1999**, *104*, 3555-3567.
- (14) Odum, J. R.; Jungkamp, T. P. W.; Griffin, R. J.; Flagan, R. C.; Seinfeld, J. H. *Science* **1997**, *276*, 96-99.
- (15) de Gouw, J. A. *Journal of Geophysical Research* **2005**, *110*.
- (16) Volkamer, R.; Jimenez, J. L.; San Martini, F.; Dzepina, K.; Zhang, Q.; Salcedo, D.; Molina, L. T.; Worsnop, D. R.; Molina, M. J. *Geophysical Research Letters* **2006**, *33*.
- (17) Hoyle, C. R.; Boy, M.; Donahue, N. M.; Fry, J. L.; Glasius, M.; Guenther, A.; Hallar, A. G.; Huff Hartz, K.; Petters, M. D.; Petters, T.; Rosenoern, T.; Sullivan, A. P. *Atmospheric Chemistry and Physics* **2011**, *11*, 321-343.
- (18) Emanuelsson, E. U.; Hallquist, M.; Kristensen, K.; Glasius, M.; Bohn, B.; Fuchs, H.; Kammer, B.; Kiendler-Scharr, A.; Nehr, S.; Rubach, F.; Tillmann, R.; Wahner, A.; Wu, H. C.; Mentel, T. F. *Atmospheric Chemistry and Physics* **2013**, *13*, 2837-2855.
- (19) Baltensperger, U.; Kalberer, M.; Dommen, J.; Paulsen, D.; Alfarra, M. R.; Coe, H.; Fisseha, R.; Gascho, A.; Gysel, M.; Nyeki, S.; Sax, M.; Steinbacher, M.; Prevot, A. S. H.; Sjögren, S.; Weingartner, E.; Zenobi, R. *Faraday Discussions* **2005**, *130*, 265.
- (20) Jang, M. S.; Czoschke, N. M.; Lee, S.; Kamens, R. M. *Science* **2002**, *298*, 814-817.
- (21) Kleindienst, T. E.; Conner, T. S.; McIver, C. D.; Edney, E. O. *Journal of Atmospheric Chemistry* **2004**, *47*, 79-100.
- (22) Brüggemann, M.; Karu, E.; Stelzer, T.; Hoffmann, T. *Environmental Science & Technology* **2015**, *49*, 5571-5578.
- (23) Hearn, J. D.; Smith, G. D. *Analytical Chemistry* **2004**, *76*, 2820-2826.
- (24) Horan, A. J.; Apsokardu, M. J.; Johnston, M. V. *Analytical Chemistry* **2017**, *89*, 1059-1062.
- (25) Tolocka, M. P.; Jang, M.; Ginter, J. M.; Cox, F. J.; Kamens, R. M.; Johnston, M. V. *Environmental Science & Technology* **2004**, *38*, 1428-1434.
- (26) Hall, W. A. t.; Johnston, M. V. *Journal of the American Society for Mass Spectrometry* **2012**, *23*, 1097-1108.
- (27) Chhabra, P. S.; Flagan, R. C.; Seinfeld, J. H. *Atmospheric Chemistry and Physics* **2010**, *10*, 4111-4131.
- (28) Walser, M. L.; Desyaterik, Y.; Laskin, J.; Laskin, A.; Nizkorodov, S. A. *Physical Chemistry Chemical Physics : PCCP* **2008**, *10*, 1009-1022.

- (29) Bein, K. J. *Journal of Geophysical Research* **2005**, *110*.
- (30) Phares, D. J. *Journal of Geophysical Research* **2003**, *108*.
- (31) Rhoads, K. P. *Journal of Geophysical Research* **2003**, *108*.
- (32) Bzdek, B. R.; Horan, A. J.; Pennington, M. R.; Janecek, N. J.; Baek, J.; Stanier, C. O.; Johnston, M. V. *Environmental Science & Technology* **2014**, *48*, 11137-11145.
- (33) Ross Pennington, M.; Johnston, M. V. *International Journal of Mass Spectrometry* **2012**, *311*, 64-71.
- (34) Wang, S.; Johnston, M. V. *International Journal of Mass Spectrometry* **2006**, *258*, 50-57.
- (35) Wang, S. Y.; Zordan, C. A.; Johnston, M. V. *Analytical Chemistry* **2006**, *78*, 1750-1754.
- (36) Rucker, C.; Kummerer, K. *Chemical Reviews* **2015**, *115*, 466-524.
- (37) Palczewska-Tulinska, M.; Oracz, P. *Journal of Chemical and Engineering Data* **2005**, *50*, 1711-1719.
- (38) Whelan, M. J.; Estrada, E.; van Egmond, R. *Chemosphere* **2004**, *57*, 1427-1437.
- (39) Atkinson, R. *Environmental Science & Technology* **1991**, *25*, 863-866.
- (40) Genualdi, S.; Harner, T.; Cheng, Y.; Macleod, M.; Hansen, K. M.; van Egmond, R.; Shoeib, M.; Lee, S. C. *Environmental Science & Technology* **2011**, *45*, 3349-3354.
- (41) Buser, A. M.; Kierkegaard, A.; Bogdal, C.; MacLeod, M.; Scheringer, M.; Hungerbühler, K. *Environmental Science & Technology* **2013**, *47*, 7045-7051.
- (42) Tang, X.; Misztal, P. K.; Nazaroff, W. W.; Goldstein, A. H. *Environmental Science & Technology Letters* **2015**, *2*, 303-307.
- (43) Hodgson, A. T.; Faulkner, D.; Sullivan, D. P.; DiBartolomeo, D. L.; Russell, M. L.; Fisk, W. J. *Atmospheric Environment* **2003**, *37*, 5517-5527.
- (44) Wu, X. M.; Apte, M. G.; Maddalena, R.; Bennett, D. H. *Environmental Science & Technology* **2011**, *45*, 9075-9083.
- (45) Neumann, H.-D.; Buxtrup, M.; Weber, M.; von Hahn, N.; Koppisch, D.; Breuer, D.; Hahn, J.-U. *Gefahrstoffe - Reinhalt. Luft* **2012**, *72*, 291 (in German).

- (46) McLachlan, M. S.; Kierkegaard, A.; Hansen, K. M.; van Egmond, R.; Christensen, J. H.; Skjoth, C. A. *Environmental Science & Technology* **2010**, *44*, 5365-5370.
- (47) Wu, Y.; Johnston, M. V. *Journal of the American Society for Mass Spectrometry* **2016**, *27*, 402-409.
- (48) Janecek, N. J.; Hansen, K. M.; Stanier, C. O. *Atmospheric Chemistry and Physics Discussions* **2017**, 1-27.
- (49) Sommerlade, R.; Parlar, H.; Wrobel, D.; Kochs, P. *Environmental Science & Technology* **1993**, *27*, 2435-2440.
- (50) Xiao, R.; Zammit, I.; Wei, Z.; Hu, W. P.; MacLeod, M.; Spinney, R. *Environmental Science & Technology* **2015**, *49*, 13322-13330.
- (51) Graiver, D.; Farminer, K. W.; Narayan, R. *Journal of Polymers and the Environment* **2003**, *11*, 129-136.
- (52) Wang, D. G.; Norwood, W.; Alae, M.; Byer, J. D.; Brimble, S. *Chemosphere* **2013**, *93*, 711-725.
- (53) Wu, Y.; Johnston, M. V. *Environmental Science & Technology* **2017**, *51*, 4445-4451.
- .
- .

Chapter 2

MOLECULAR CHARACTERIZATION OF SECONDARY AEROSOL FROM OXIDATION OF CYCLIC METHYLSILOXANES

2.1 Silicon observed in ambient nanoparticles.

As described in Chapter 1, ambient nanoparticles (smaller than 100 nm in diameter) can disproportionately affect climate and human health relative to their mass loading in the atmosphere. These particles influence climate by scattering the incoming solar radiation¹⁻³ and/or serving as cloud condensation nuclei (CCN)⁴. They influence human health by penetrating deep into the respiratory system⁵⁻⁷. To better understand these effects, knowledge of the chemical composition is needed⁸. Organic aerosol constitutes a large portion of this matter and most of this contribution is secondary, meaning that it is formed through reaction of gas phase volatile organic compounds (VOC) with oxidants (OH, O₃, NO₃) to give semi- or non-volatile products⁸⁻⁹.

Recently, silicon was reported as a frequent component of ambient nanoparticles^{10,11}. Measurements with Nano Aerosol Mass Spectrometer (NAMS), which provides quantitative elemental composition of particles in the 10-30 nm diameter range^{12,13}, showed that Si was often observed in urban and suburban environments but rarely detected in a remote environment¹⁴. The location dependence suggests that Si in these particles is associated with human activity. One possible source is atmospheric oxidation of cyclic volatile methylsiloxanes (cVMS), which are commonly used in personal care products^{15,16}. cVMS are considered to be environmentally acceptable cleaning agents¹⁷ due to their inertness to ozone¹⁸. Owing to high vapor pressure, they are easily released into atmosphere where they may react with OH¹⁹ to form semi- or non-volatile products. An atmospheric transport model for three most common cVMS in

personal care products: (octamethylcyclotetrasiloxane, D₄; decamethylcyclopentasiloxane D₅; and dodecamethylcyclohexasiloxane, D₆) is consistent with cVMS as a possible source of nanoparticulate Si¹⁴.

In this chapter, the molecular composition of secondary aerosol obtained from cVMS oxidation is studied in detail. D₅ was chosen as the precursor and D₅-derived secondary aerosol was produced in a Photo-oxidation Chamber (PC) to simulate photo-oxidation in the atmosphere by reaction with hydroxyl radical. Several measurements were performed including high-resolution ESI-MS, ESI-MSMS and EI-MS. Previous work used only low-resolution GC-MS analysis, which could only provide partial characterization of the oxidation products¹⁹.

2.2 Method Configuration

2.2.1 Aerosol Formation and Particle Collection

The experimental setup is shown in Figure 2-1.

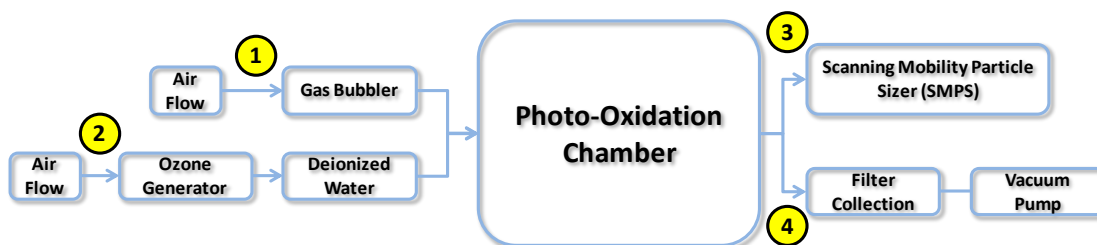


Figure 2-1: Experimental Setup.

Aerosol was generated in a Photo-oxidation chamber (PC) (Figure 2-2) consisting of a 50L box shaped chamber made of a perfluoroalkoxy copolymer²⁰. Before each experiment, the chamber was flushed continuously with clean, dry, air for 2-3 days. After flushing, background particle concentrations in the PC were below 100/cm³ and 0.5 µg/m³. The air was cleaned by passing compressed

air through charcoal and high efficiency particulate matter air (HEPA) filters to remove organic vapors and particulates, and through silica gel to remove moisture. A Scanning Mobility Particle Sizer (SMPS; Model 3080/3078, TSI, St. Paul, Minnesota) was used to measure particle size distributions before and during experiments.

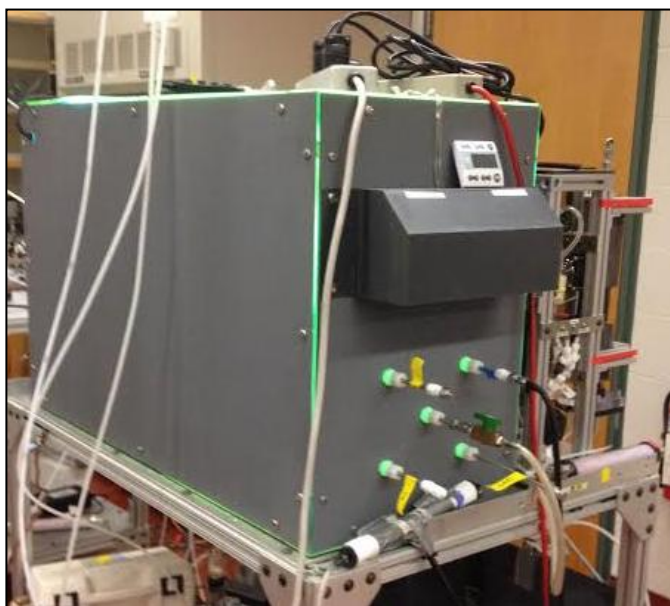
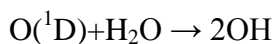
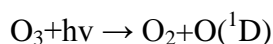


Figure 2-2: Photo-Oxidation Reaction Chamber.

D₅ vapor was generating by passing clean, dry air with a flow rate of ~700 cpm (cm³/min) over the surface of D₅ fluid (CAS No.541-02-6, Gelest, Morrisville, Pennsylvania) in a gently heated gas flask bubbler (Flow 1 in Figure 2-1). Ozone was generated by passing clean air around a mercury lamp (Model No.81-1025-01, BHK Inc., Ontario, California) and the ozone concentration was monitored with a Model 49i O₃ Analyzer (Thermo Fisher Scientific Inc., Waltham, MA). The gas flow of D₅ was sent into the PC along with additional 100cpm flow of 15-20 ppmv ozone and 240cpm flow of water vapor, which was created by bubbling air through deionized water (Flow 2 in Figure 2-1). These flows yielded a nominal residence time of 40 min in the PC. Once the gas flows, ozone

concentration and relative humidity were stabilized, reaction was initiated by irradiating the chamber with UV lamps to generate OH from ozone and water:



The hydroxyl radical concentration used in these experiments was estimated with a method introduced elsewhere²⁰ by sending a known concentration (5ppm) of SO₂ into PC, along with ozone and water vapor. After turning on the UV lamps, OH will react with SO₂ to produce H₂SO₄ with a second order rate constant of $9.0 \times 10^{-13} \text{ cm}^3 \text{ molecule}^{-1} \text{ s}^{-1}$. The OH concentration is estimated by:

$$\frac{d[\text{H}_2\text{SO}_4]}{dt} = k'[\text{OH}]$$

where the change of H₂SO₄ concentration with time is determined from the change of aerosol mass with time (measured by SMPS) and k' is the second order rate constant multiplied by SO₂ concentration (5ppm). For the experiments performed in this study, the OH mixing ratio for these experiments was estimated to be $\sim 1.5 \times 10^8 \text{ molecules cm}^{-3}$. Particulate matter in the air flow exiting the PC was collected at a flow rate of $\sim 2 \text{ lpm}$ for 20-24 hrs onto a Teflon coated, glass fiber filter (GF/D, CAT No.1823-025, Whatman, GE Healthcare, Piscataway, NJ) for chemical analysis. Under the conditions used in this study, the secondary aerosol mass concentration was $\sim 60 \mu\text{g/m}^3$, more than one hundred times larger than the background concentration. Generally, 0.3 to 0.5 mg of aerosol was collected in each experiment for analysis. In all experiments, chamber, filter and solution blanks were collected prior to the injections of reactants to identify and eliminate any artifacts.

After particle collection, the filter was sonicated for one hour with $\sim 8 \text{ ml}$ acetonitrile (ACN) (CAS No. 75-05-8, Fisher Scientific, Pittsburgh, Pennsylvania) and the resulting solution was filtered through a polyvinylidenedifluoride (PVDF) filter (CAT No. 6747-2504, GE Healthcare, Piscataway, NJ). The filtered solution was then concentrated nearly to dryness ($< 0.5 \text{ ml}$) with a Speed Vac

Concentrator (Model SC110A, Thermo Scientific, Waltham, Massachusetts).

Finally, the sample was reconstituted to 1 mg/ml with acetonitrile (ACN).

Reconstitution with methanol or ACN/H₂O 50/50 by volume gave similar mass spectrometry results.

A few experiments were performed by bubbling air through a solution of D₄ rather than D₅. All other conditions for the experiment remained the same. The D₄ concentration in the chamber for these experiments was not estimated, though the aerosol mass loading was similar to the D₅ oxidation experiments.

2.2.2 Mass Spectrometer

High resolution electrospray mass spectra (ESI-MS) in both positive and negative ion modes were obtained with a Q-Exactive Hybrid Quadrupole-Orbitrap Mass Spectrometer (Thermo Scientific, Waltham, Massachusetts) equipped with a heated electrospray ionization source (HESI). Samples were injected at a flow rate of 0.5 μ L/min with a spray voltage of 3.5 kV and a temperature of 250 °C. Mass spectra were obtained over the range 50-950 m/z with a nominal mass resolving power of 70000. Typically, data were acquired for 1 min with ~60 spectra averaged. For ESI-MS/MS experiments, a quadrupole mass filter isolated each chosen precursor, with subsequent analysis using collision induced dissociation (CID) with the collision energy adjusted between 10 and 30 eV depending on the precursor ion.

Samples were also analyzed by GC-MS with a Waters GCT Premier high-resolution time-of-flight mass spectrometer with a scan range of 50-950 m/z coupled to an Agilent 7890A gas chromatograph. Ionization was performed by 70eV EI with a source temperature of 180 °C. Chromatographic separation was performed with an Agilent HP-5 column using a 3 μ L injection volume and an injection port temperature of 280 °C.

Four separate experiments of D₅ oxidation were performed under the conditions given above, and only those ions which were detected by ESI-MS in all

four experiments are discussed below. These ions represented ~85% of the total number of ions detected. Ions that were detected in fewer than four experiments generally had very low signal intensities, which may have inhibited detection in some experiments and/or may have compromised accurate m/z measurement.

2.3 Molecular Characterization of D₅-Oxidized Products

2.3.1 High Resolution Mass Spectra Interpretation

Figure 2-3 shows mass spectra of D₅-derived secondary aerosol averaged from the four replicate experiments in the positive and negative modes respectively. Both monomer and dimer products are observed. Aerosol formation was also studied under lower mass loading condition by injecting a smaller amount of gas phase D₅ into chamber. Figure 2-4 shows ESI mass spectra of aerosol generated from low and high mass loading conditions. 75% of total peaks are observed in both spectra, indicating that the effect of mass loading on the types of extractable products may be small. The monomer signal intensity appeared to increase relative to the dimer signal intensity when the mass loading was decreased, though more work is needed to explore this dependence thoroughly (see Chapter 3).

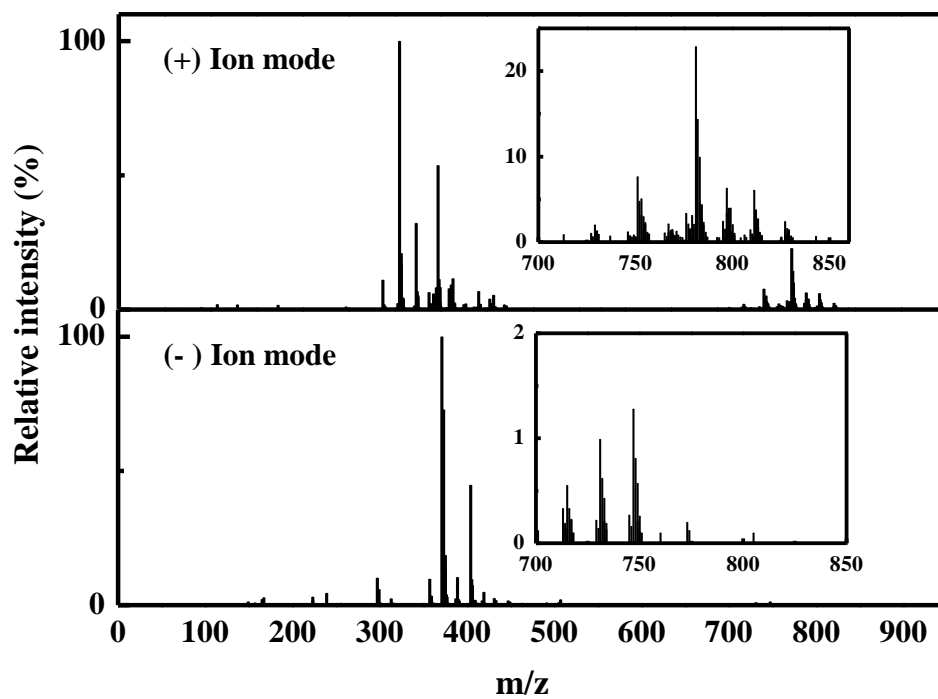


Figure 2-3: Representative ESI mass spectra of secondary aerosol from D₅ oxidation.

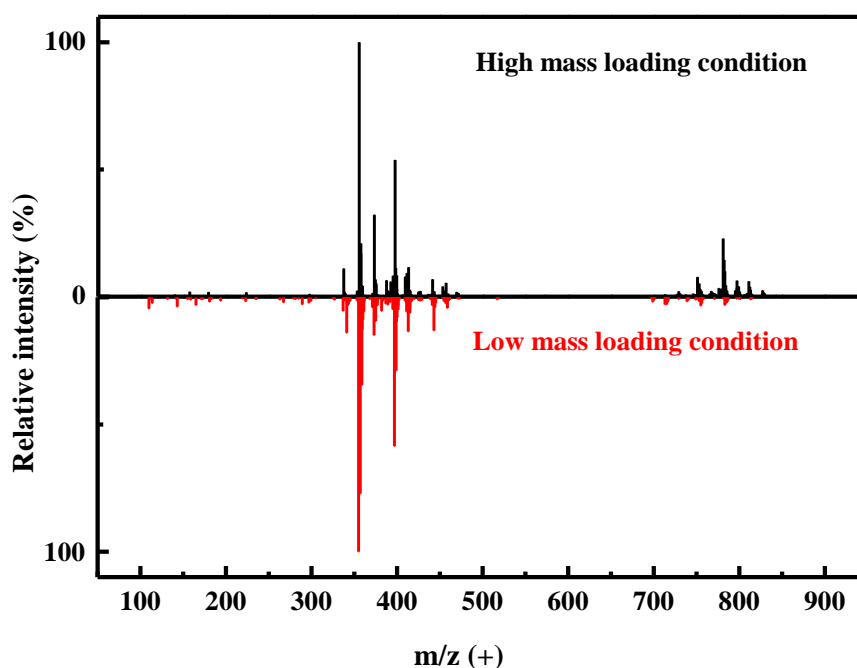


Figure 2-4: Representative ESI mass spectra in the positive ion mode of D_5 -derived aerosol generated under conditions giving high ($60 \mu\text{g}/\text{m}^3$) vs. low ($\sim 6 \mu\text{g}/\text{m}^3$) mass loading.

Ions observed in all four experiments were further characterized in the following way. First, background peaks from the PC and filter were removed from consideration, as were peaks with $<0.5\%$ (positive spectrum) and 0.1% (negative spectrum) relative intensity. This left a total of 190 (positive spectrum) and 233 (negative spectrum) peaks between 50 and 950 m/z . Chemical formulas with theoretical m/z values within ± 5 ppm of the measured m/z values were determined with the mass spectrometer software (Xcalibur). Reasonable formulas were selected based on the following general criteria: a) $C_{0-10}H_{1-30}O_{1-20}Si_{1-5}$ for monomers and $C_{10-20}H_{30-60}O_{10-30}Si_{5-10}$ for dimers, b) up to 1 Na atom for peaks in the positive ion spectrum, and c) H/C atomic ratio between 2.7 and 3.8.

Of the original 190 peaks in the positive spectrum, 154 peaks (81%) were assigned a reasonable single formula based on the above criteria. Of the original

233 peaks in the negative spectrum, 203 peaks (87%) were assigned a single, reasonable formula. The average mass difference between measured and theoretical m/z for peak assignments was 1.28 ppm. The majority of the assigned peaks in the positive ion spectrum (72%) contained one Na atom. Additionally, there was no evidence for multiply charged peaks. Only 30 peaks from the positive spectra and 26 peaks from the negative spectra could not be assigned a reasonable formula, and their relative intensities were generally $< 1\%$. Assigned peaks are given in Appendix A of this thesis. The mass weighted signal intensity fractions (MIF)²² of these ions (defined below in Section 2.3.1.2) showed that the average O/Si atomic ratio increased from 1 in D₅ to ~ 1.3 in the oxidized aerosol while the C/Si atomic ratio decreased from 2 to ~ 1.7 under the experimental conditions used in this study.

Peak assignments from the positive and negative ion spectra were combined, and redundancies due to charge (assuming $M+H^+$, $M+Na^+$, $M-H^-$) and isotopic substitution were removed, giving 135 unique molecular formulas for the (neutral) products. The products were divided into three types: fragmented or ring-opened products, unsaturated products and saturated substituted products. Ring-opened products were defined as those where the siloxane ring had to be broken, i.e. silicon numbers of 1-4 (monomers) or 6-9 (dimers); representative examples are $C_8H_{24}O_4Si_4$ and $C_{10}H_{32}O_8Si_6$. Unsaturated products were defined as those having silicon numbers of 5 (monomers) or 10 (dimers) but with an H/C atomic ratio less than 3, indicating the presence of unsaturated functional group(s); representative examples are $C_9H_{26}O_8Si_5$ and $C_{18}H_{52}O_{12}Si_{10}$. Saturated, substituted products were defined as those having silicon numbers of 5 (monomers) or 10 (dimers), but $H/C \geq 3$ and $O/Si > 1$; representative examples are $C_9H_{28}O_7Si_5$ and $C_{18}H_{54}O_{11}Si_{10}$. Under the conditions of these experiments, more than 95% of the total mass weighted signal intensity was encompassed by ring-opened and saturated products as shown in Table 2-1. Therefore, only these two product types are discussed below.

		Ring-Opened	Saturated	Unsaturated
Positive	# of products	11	49	13
	MIF (%)	31	66	3
Negative	# of products	52	30	22
	MIF (%)	20	79	1

Table 2-1: Number and Mass-Intensity Weighted Fraction, MIF (%), of ring-opened, saturated and unsaturated products of D₅ oxidation in the positive and negative ion modes, respectively.

2.3.1.1 Ring-Opened Products of D₅

A total of 58 neutral ring-opened products were assigned. The molecular formulas suggest the presence of both cyclic and linear siloxane structures with different numbers of subunits, e.g. D₂, D₃, D₄, L₂, L₃, L₄ (D=cyclic; L=linear) with various fragmentations and substitutions e.g. loss of a CH₃ group, substitution of an OH group for a CH₃ group, etc. as shown in Table 2-2. Figure 2-5 gives the positive ESI mass spectrum of pure D₅ as a control. Several fragmentation peaks are observed, some examples being 355.069 m/z assigned as (CH₃)₉(OSi)₅⁺ and 297.082 m/z assigned as (CH₃)₈(OSi)₄H⁺. It is likely that oxidation products of D₅ will also fragment during ESI analysis, making it difficult to distinguish whether or not the ring-opened products observed in this work are the result of photooxidation or an ESI artifact.

	2 Slioxane subunits	3 Slioxane subunits	4 Slioxane subunits	5 Slioxane subunits
Cyclic	(CH ₃) ₄ (OSi) ₂	(CH ₃) ₆ (OSi) ₃	(CH ₃) ₈ (OSi) ₄	(CH ₃) ₉ (OSi) ₅
	(CH ₃) ₃ (OH)(OSi) ₂	(CH ₃) ₅ (OH)(OSi) ₃	(CH ₃) ₇ (OH)(OSi) ₄	(CH ₃) ₈ (OH)(OSi) ₅
		(CH ₃) ₅ (CH ₂ OH)(OSi) ₃	(CH ₃) ₇ (CH ₂ OH)(OSi) ₄	
Linear			(CH ₃) ₆ O(OSi) ₄	
	(CH ₃) ₅ (OH)OSi ₂	(CH ₃) ₆ (OH) ₂ O ₂ Si ₃	(CH ₃) ₈ (OH) ₂ O ₃ Si ₄	N/A

Table 2-2: Several ring-opened products in D₅-derived secondary aerosol. Molecular formulas are written based on likely structures (linear, cyclic) and functional groups. However, it should be noted that these structures have not been confirmed by e.g. MS/MS analysis.

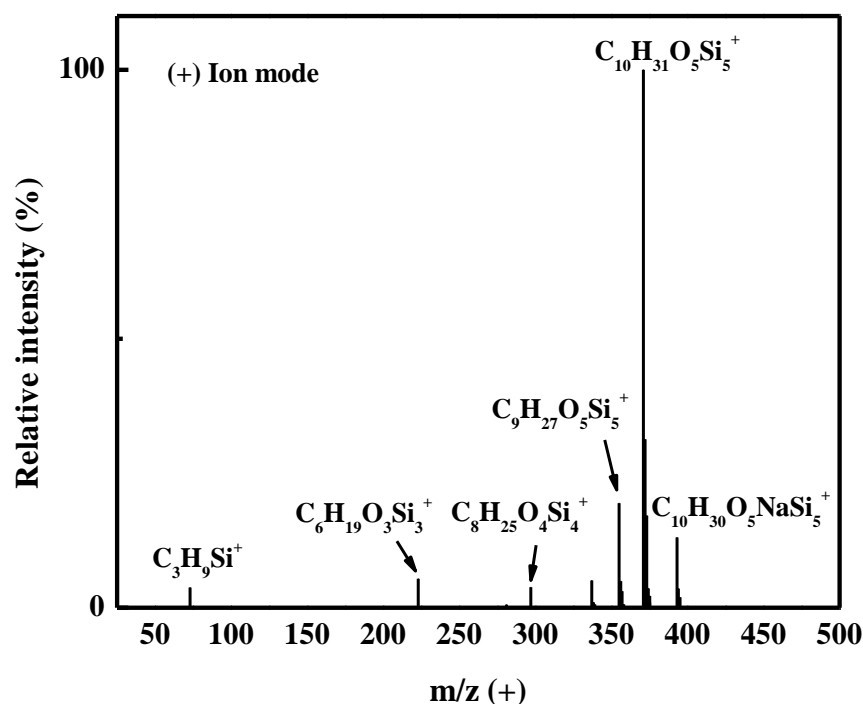


Figure 2-5: Positive ESI mass spectrum of pure D₅ in ACN with a concentration of 100 µg/ml.

2.3.1.2 Saturated Oxidation Products of D₅

The mass-weighted signal intensity fraction (MIF) of an individual peak (i) is given by:

$$MIF_i = \frac{\left(\frac{m}{z}\right)_i I_i}{\sum_i \left(\frac{m}{z}\right)_i I_i}$$

where $(m/z)_i$ is the mass to charge ratio of peak i, I_i is the signal intensity of the peak and the summation is over all assigned peaks. The MIF takes into account that higher intensity and/or higher mass ions tend to represent a greater portion of the total sample mass²². Under the experimental conditions of this study, saturated products represent the majority of the MIF (~70%). Relative to D₅ and its dimer, these products contain higher amounts of oxygen and lower amounts of

carbon and hydrogen. Figure 2-6 provides a graphical summary of these formulas as a function of carbon to silicon (C/Si) and oxygen to silicon (O/Si) atomic ratios. The change in O/Si and C/Si ratios between the D₅ reactant and its oxidation products indicate the types of reactions that take place²³. For example, substituting a CH₂OH group for a CH₃ group increases the O/Si ratio while the C/Si ratio remains constant, i.e. oxidizing (CH₃)₁₀(SiO)₅ to produce (CH₃)_{10-x}(CH₂OH)_x(SiO)₅. Substituting an OH group for a CH₃ group decreases C/Si ratio and increases O/Si ratio, i.e. oxidizing (CH₃)₁₀(SiO)₅ to produce (CH₃)_{10-y}(OH)_y(SiO)₅. For monomers, the assigned product formulas indicate various combinations of OH and CH₂OH substitution with up to 6 CH₃ groups replaced (Fig. 2-6a). The same types of substitutions are observed for dimers (Fig. 2-6b), but with the additional complication that the two monomers in a dimer can be linked with several species i.e. O, CH₂ and CH₂CH₂.

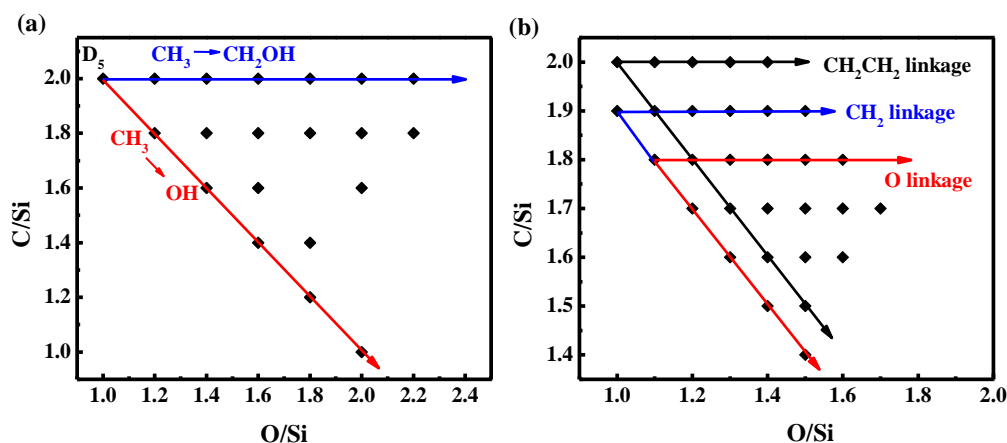


Figure 2-6: Plots of C/Si versus O/Si for saturated products of D₅ oxidation in the monomer (a) and dimer (b) regions. Each dot represents an assigned molecular formula of a saturated oxidation product. The arrows in the monomer plot extend from unoxidized D₅ and represent the two types of substitution that can occur. The arrows in the dimer plot take into account difference possible linkages between monomers.

2.3.2 High Resolution MS/MS Spectra Interpretation

2.3.2.1 OH Substitution of a CH₃ group

Figure 2-7a and 2-7b show ESI-MS/MS spectra of the C₉H₂₈O₆Si₅ neutral product in positive and negative ion modes, which is considered to have one OH substitution for a CH₃ group. The positive spectrum in Figure 2-7a shows the dissociation of the precursor at 373.080 m/z(+) which is assigned as C₉H₂₉O₆Si₅⁺, with -2.43 ppm mass accuracy, while the negative spectrum in Figure 2-7b shows the dissociation of the precursor at 371.066 m/z(-) which is assigned as C₉H₂₇O₆Si₅⁻ with mass accuracy -1.06 ppm. The first neutral loss in positive spectrum is H₂O (C₉H₂₉O₆Si₅⁺ to C₉H₂₇O₅Si₅⁺), while the corresponding loss in the negative spectrum is CH₄ (C₉H₂₇O₆Si₅⁻ to C₈H₂₃O₆Si₅⁻). These products are consistent with protonation of the OH group in the positive spectrum and deprotonation of the OH group in the negative spectrum. Other diagnostic ions are protonated and deprotonated trimethyl silanol, [Si(CH₃)₃OH+H⁺] and [Si(CH₃)₃O⁻] respectively, neutral loss of Si(CH₃)₄, and a series of

protonated/deprotonated products corresponding to successive loss of siloxane subunits e.g. loss of $C_4H_{12}O_2Si_2$ or $C_6H_{18}O_3Si_3$.

It should be noted that a nearby precursor ion is observed in the positive mass spectrum at 373.043 m/z(+), which is assigned as the unsaturated product $C_8H_{25}O_7Si_5^+$ (-2.17 ppm). While this ion could lead to some of the products in Figure 2-7a, several product ions including the first neutral loss cannot be explained by its molecular formula (precursor has fewer carbon atoms than product). Furthermore, when the collision energy is increased from 10eV to 30eV, the product ion signal intensities increase substantially. At the same time, the normalized intensity of the precursor of interest 373.080 m/z(+) decreases by almost a factor of 6 (1.8×10^6 to 3.4×10^5), while the normalized intensity for the “impurity” precursor at 373.043 m/z(+) hardly changes at all (8.0×10^5 to 6.5×10^5). Taken together, the inconsistency of several product ions with the “impurity” precursor and the disparities in signal intensity suggest that the OH substituted product at 373.080 m/z(+) is the main contributor to the spectrum in Figure 2-7a and 2-7b products observed in this work are the result of photooxidation or an ESI artifact.

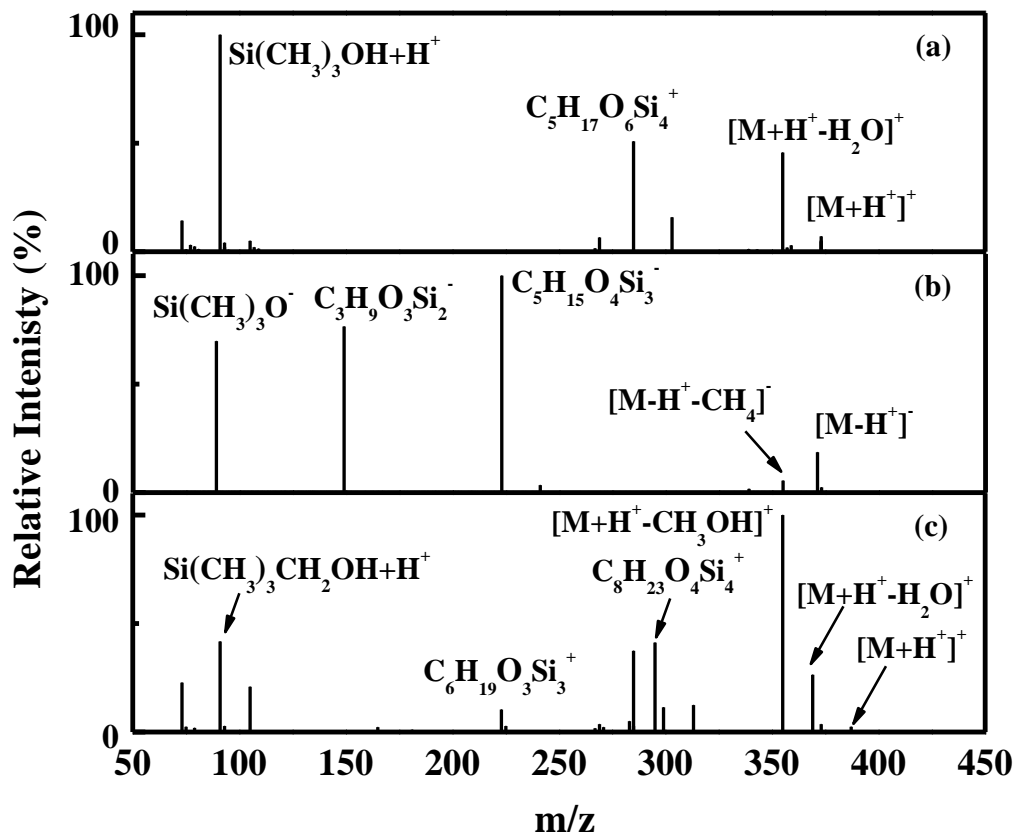


Figure 2-7: Product ion spectra for isolation of a) 373 m/z(+), b) 371 m/z(-) and c) 387 m/z(+). These precursors correspond to the oxidation product of D_5 having one OH substitution for a CH_3 group and D_5 having one CH_2OH substitution for a CH_3 group.

2.3.2.2 CH_2OH Substitution of a CH_3 Group

Figure 2-7c shows the product ion mass spectrum for the 387.098 m/z(+) precursor $\text{C}_{10}\text{H}_{31}\text{O}_6\text{Si}_5^+$ (+0.22 ppm) which corresponds to one CH_2OH substitution for a CH_3 group. The first neutral loss is H_2O , consistent with protonation of the OH functionality. The second and more intense neutral loss is 355.069 m/z(+) ($\text{C}_9\text{H}_{27}\text{O}_5\text{Si}_5^+$, 2.92 ppm), which corresponds to the loss of CH_3OH from the precursor. Another diagnostic ion is $\text{C}_4\text{H}_{13}\text{OSi}^+$, which corresponds to protonated trimethylsilyl-methanol.

2.3.2.3 Dimer Linkages by O and CH_2

Figure 2-8a shows the product ion spectrum of the 727.140 m/z(+) precursor assigned as $\text{C}_{18}\text{H}_{55}\text{O}_{11}\text{Si}_{10}^+$ (-3.47 ppm), while Figure 2-8b shows an

expansion of the product ion spectrum between 350 and 380 m/z(+). Two dimer linkages are possible for the precursor molecular formula. One is linkage by an O atom with all side groups as CH₃ (Figure 2-9a) and the other by a CH₂ group with one side group as OH and the remaining as CH₃ (Figure 2-9b). The two C₉ product ions labeled in black in Figure 8a cannot distinguish between the two linkages since they are expected products of both structures as shown in Figure 2-9a and b. However, insight can be gained from other product ions in the spectrum. The first fragmentation from this precursor (C₁₇H₅₁O₁₁Si₁₀⁺, -1.90 ppm) corresponds to a neutral loss of CH₄ while no H₂O loss is detected (Figure 2-8a). When compared with the neutral losses in Figure 2-7a and 2-7c, this observation suggests that very few precursors have an OH group and, therefore, the two siloxane rings are linked by an O atom in most dimers. However, the expansion in Figure 2-8b shows the presence of very low intensity fragment ions that are consistent with a CH₂ linkage. In particular, the C₁₀H₂₉O₅Si₅⁺ product ion cannot be obtained from a dimer linked by an O atom (see structures in Figure 2-9a and b). Taken together, there is strong evidence that both O and CH₂ linkages exist, though products unique to the O linkage have much greater intensity than those unique to the CH₂ linkage.

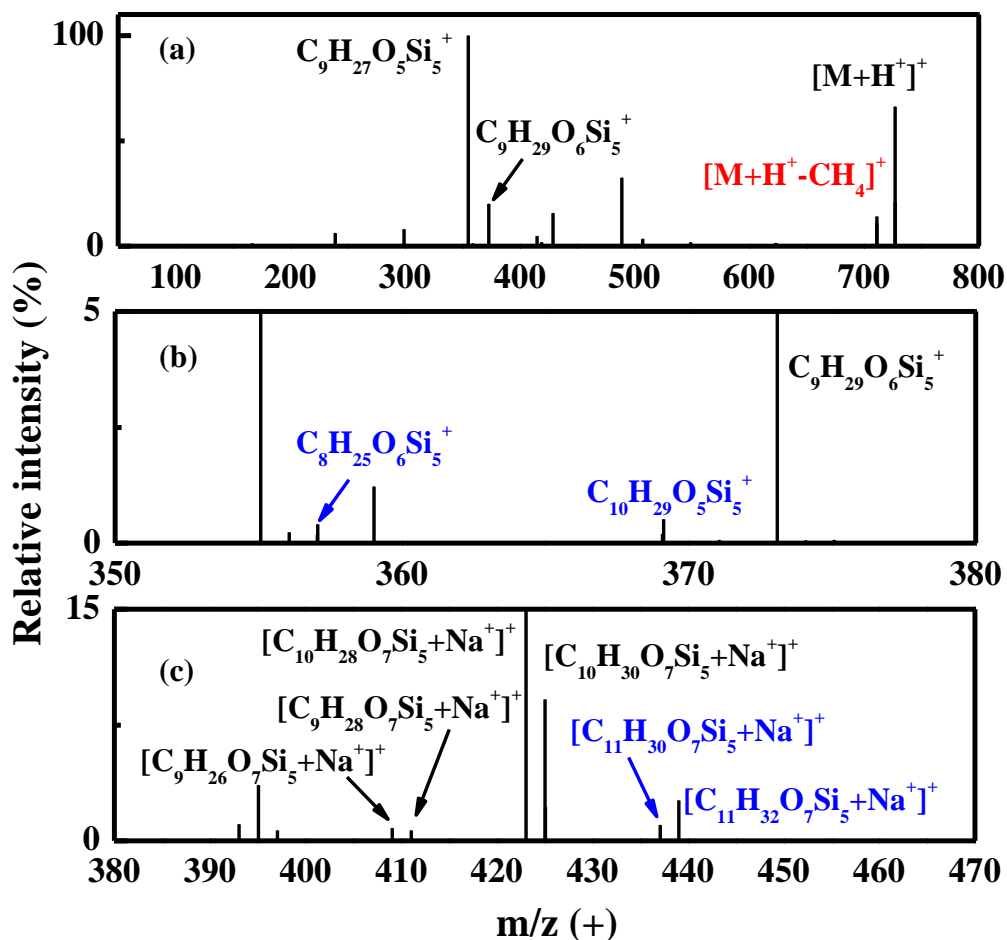
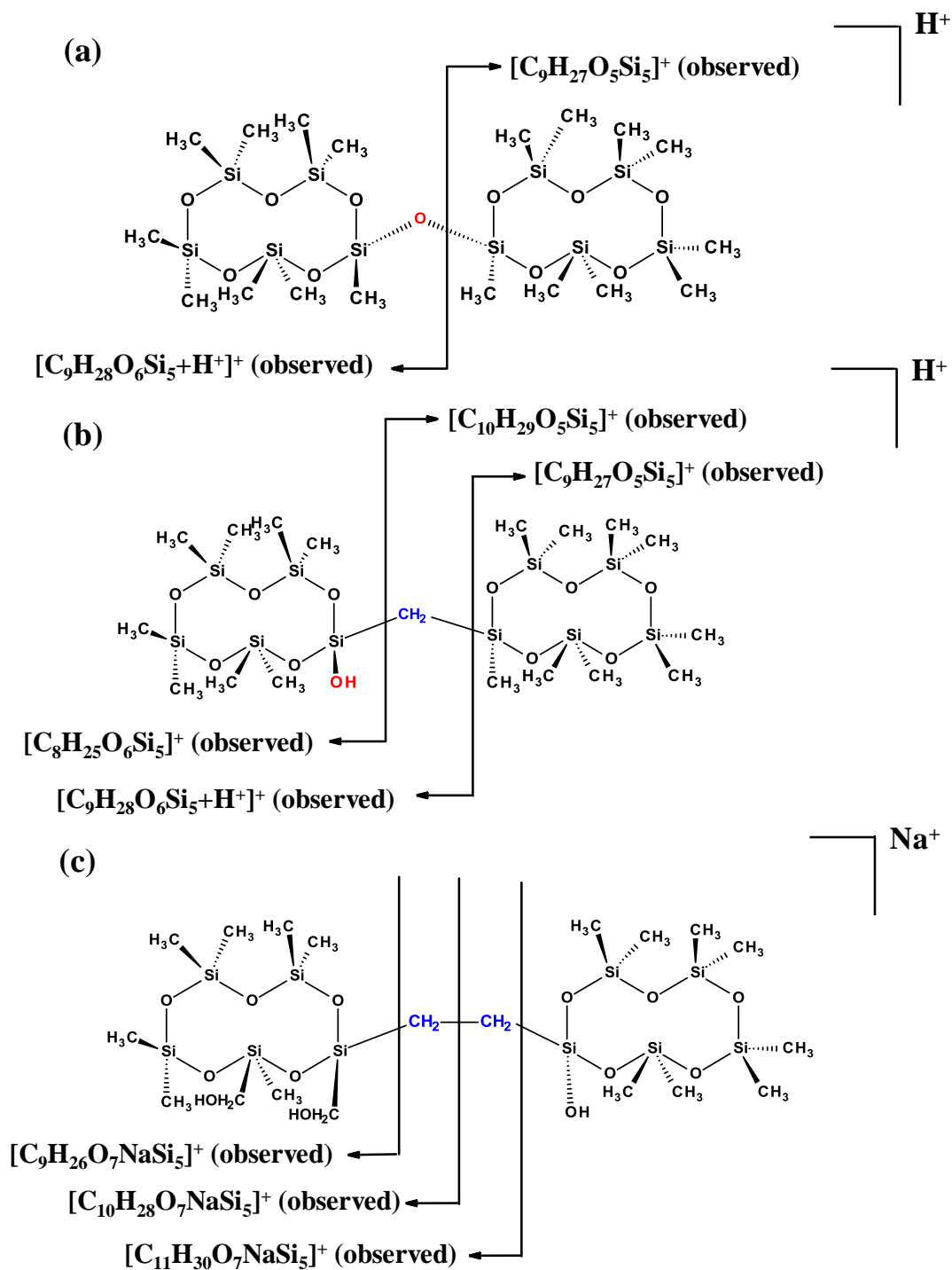


Figure 2-8: Product ion spectrum of 727 m/z(+). a) Complete product ion spectrum. b) An expansion of 350 to 380 m/z(+). Peaks corresponding to an O linkage are marked with red. Peaks corresponding with a CH_2 linkage are marked with blue. Peaks consistent with both are marked in black. c) Expansion of the product ion spectrum of 795 m/z(+) between 380 and 470 m/z(+). Peaks corresponding with a CH_2CH_2 linkage are marked with blue.

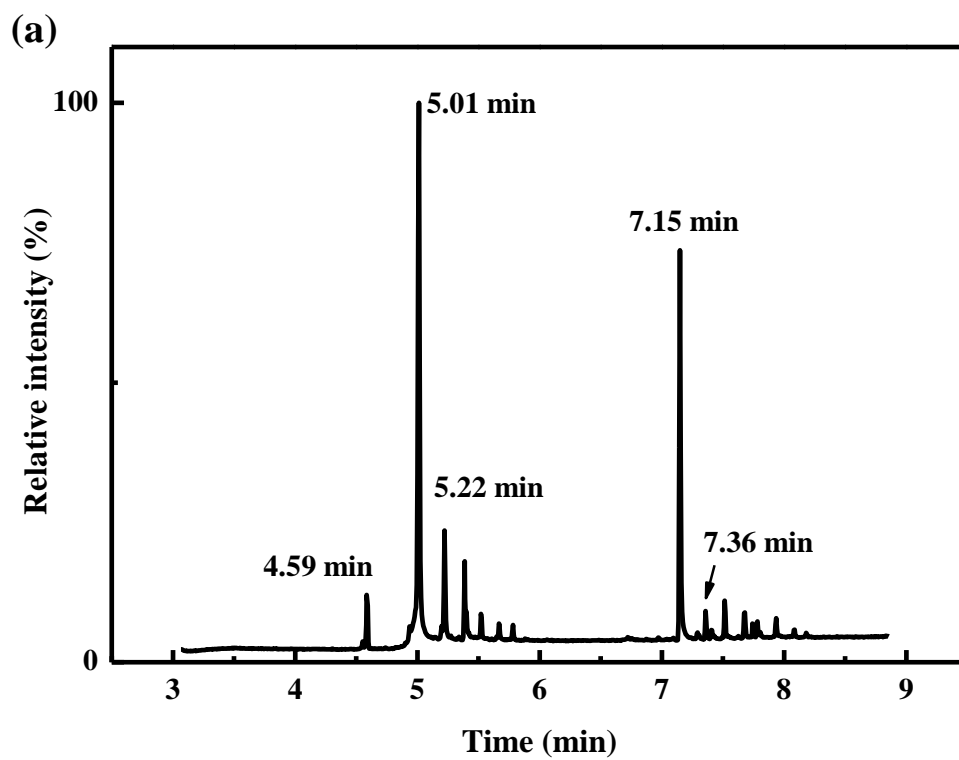


2.3.2.4 Dimer Linkage by CH₂CH₂

A CH₂CH₂ linked dimer has been discussed previously as a product of D₄ oxidation¹⁹. Here, there are many precursors having formulas consistent with a CH₂CH₂ linkage, but it is very difficult in to distinguish by MS/MS a structure having a CH₂ linkage with a CH₂OH substitution from one having a CH₂CH₂ linkage with an OH substitution. Nonetheless, one precursor at 795.128 m/z(+) assigned as C₁₉H₅₆O₁₃Si₁₀Na⁺ with (-3.18 ppm) provides clear evidence for a CH₂CH₂ linkage. This precursor must have either a CH₂ linkage with 3 CH₂OH substitutions or a CH₂CH₂ linkage with 2 CH₂OH substitutions and 1 OH substitution. The key product ion shown in Figure 2-8c is C₁₁H₃₀O₇Si₅Na⁺ (-1.12 ppm), which can only be formed from a precursor having a CH₂CH₂ linkage as illustrated by the structure in Figure 2-9c.

2.4 Comparison to Previous Work

High resolution GC-MS analysis is performed to study the major building blocks of D₅-derived aerosol. These data provide the opportunity to check consistency with ESI MS/MS analysis and compare with previous work. The gas chromatogram obtained is shown in Figure 2-10a. Similar to the study of Sommerlade¹⁹, GC-MS confirms that major components of D₅-derived secondary aerosol are D₅ (presumably partitioned to the particle phase and/or bound within dimers), and an oxidation product corresponding to one OH substitution for CH₃ as shown in Figure 2-10b. Our GC-MS results and those of Sommerlade provide evidence for a CH₂OH substitution product and the presence of dimers (O and CH₂ linked dimers) (Figure 2-10c), which is consistent with ESI-MS results, though the full range of products observed with ESI cannot be characterized by GC-MS.



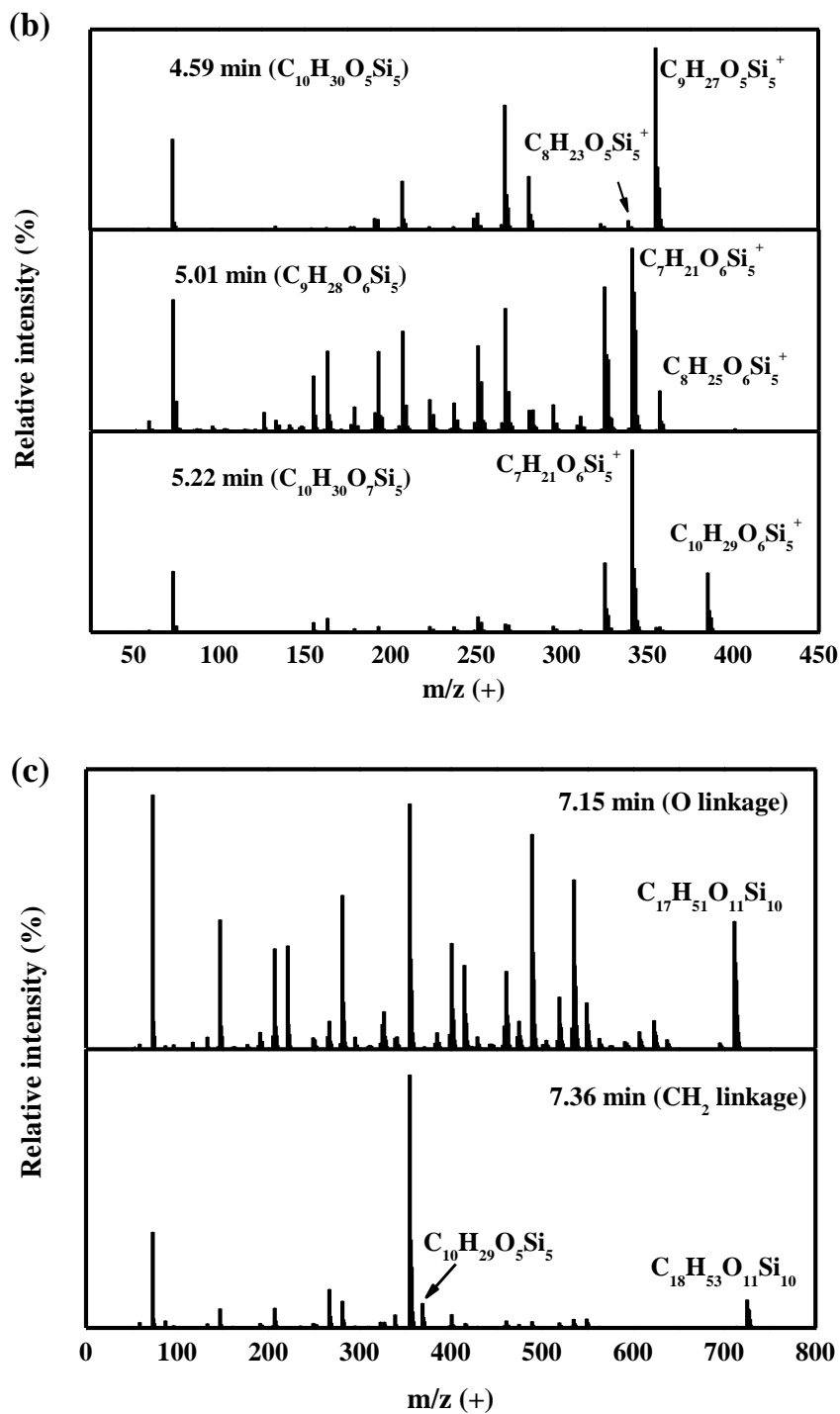


Figure 2-10: a) GC-MS total ion chromatogram of D_5 -derived aerosol. b) EI mass spectra of three peaks in the chromatogram corresponding to D_5 , OH substituted D_5 and CH_2OH substituted D_5 . The EI mass spectra match library spectra for these compounds. c) EI mass spectra of what appear to be peaks corresponding to O and CH_2 linked dimers.

The major products characterized in this work can be explained by OH abstraction of a hydrogen atom from D₅ as the initial step. Figure 2-11 shows possible formation pathways for several of these products. Formation of the OH substitution product is similar to the reaction sequence proposed by Atkinson²⁴. Note that formation of a multiply substituted product does not necessarily require multiple OH abstractions, since an auto-oxidation process based on internal hydrogen rearrangements²⁵ could lead to several substitutions. Figure 2-11 also shows a possible way that a dimer can be produced in the gas phase, while the results discussed in Chapter 3 suggest that dimers are only formed in the particle phase. Ring-opened products could be produced in the gas phase – particularly those that appear to contribute to nucleation (> 5 Si atoms).²⁶

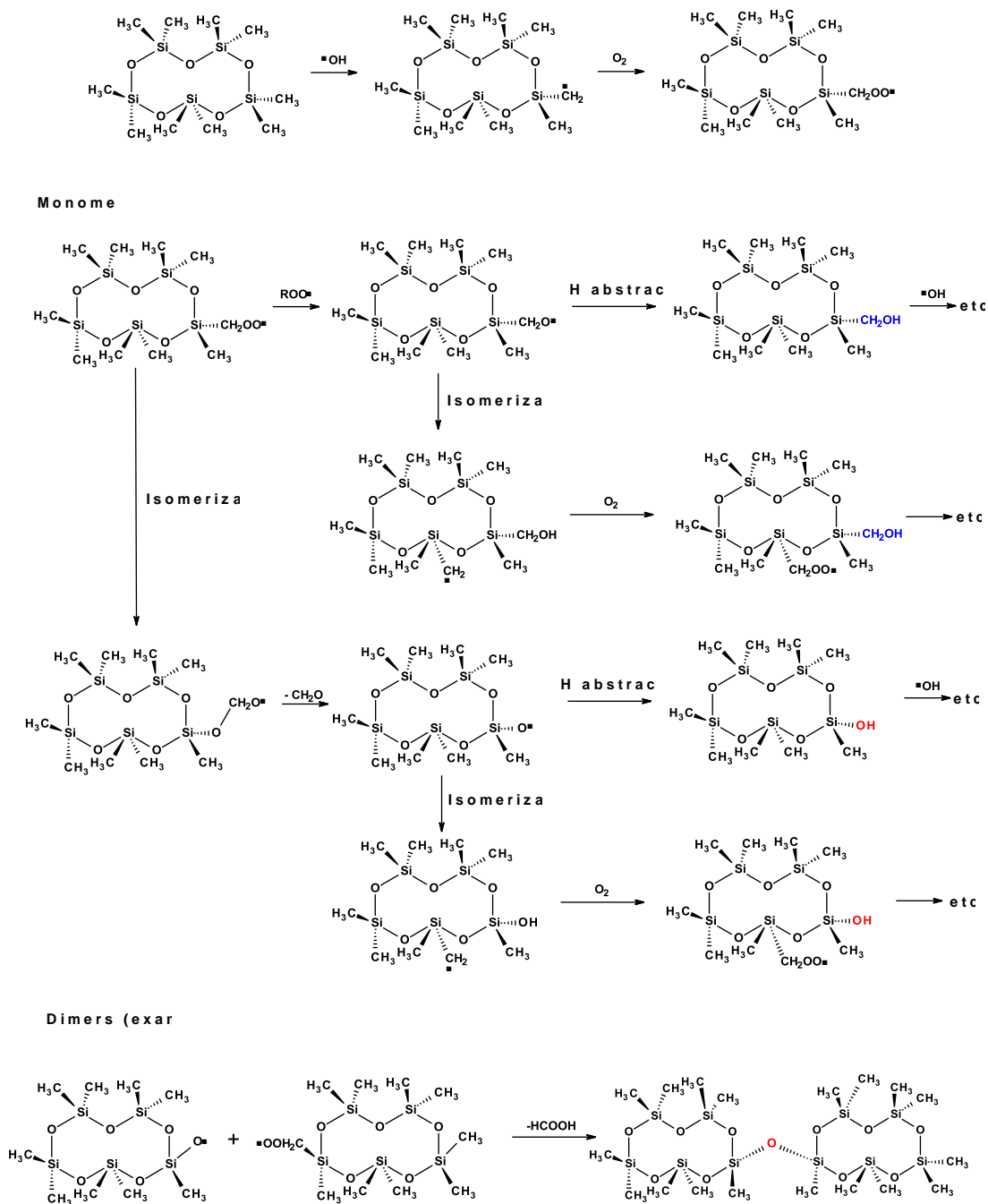


Figure 2-11: Possible pathways for product formation from OH oxidation of D₅.

2.5 D₄-derived Secondary Aerosol

Secondary aerosol derived from OH oxidation of D₄ (C₈H₂₄O₄Si₄) was briefly studied for comparison to D₅-derived aerosol. Representative ESI-MS spectra of D₄-derived aerosol were shown in Figure 2-12. The ESI-MS spectra for

D₄-derived aerosol showed many more peaks than D₅-derived aerosol, especially in the dimer and trimer regions. By applying the analysis procedure as discussed previously for D₅, of the original 736 peaks in the positive spectrum, 671 peaks (91%) were assigned a reasonable, single formula. Of the original 455 peaks in the negative spectrum, 409 peaks (90%) were assigned a single, reasonable formula. The average mass difference between measured and theoretical m/z for peak assignments was 2.56 ppm. After removing redundancies due to charge (assuming MH⁺, MNa⁺, M-H⁻) and isotopic substitution, 529 unique molecular formulas for the (neutral) products were obtained, which could be subdivided into ring-opened, unsaturated and saturated products. About 96 % of the total products were ring-opened or saturated, but more ring-opened products were observed for D₄-derived aerosol than D₅-derived aerosol. MIF analysis showed the O/Si ratio increased from 1 in D₄ to ~1.48 in the oxidized aerosol while the C/Si ratio decreased from 2 to ~ 1.56 for the conditions used in this study.

Saturated products are shown graphically in Figure 2-13 where C/Si vs. O/Si is plotted for each observed molecular formula. Both OH and CH₂OH substitutions for CH₃ were identified, and relative to D₅, a greater fraction of the CH₃ groups were found to be oxidized in D₄. Furthermore, monomer products having more than 8 oxygen atoms added to the D₄ molecule were detected, indicating that peroxy groups (CH₂OOH) must also be formed which also consistent with the result published by Sommerlade et al.¹⁹

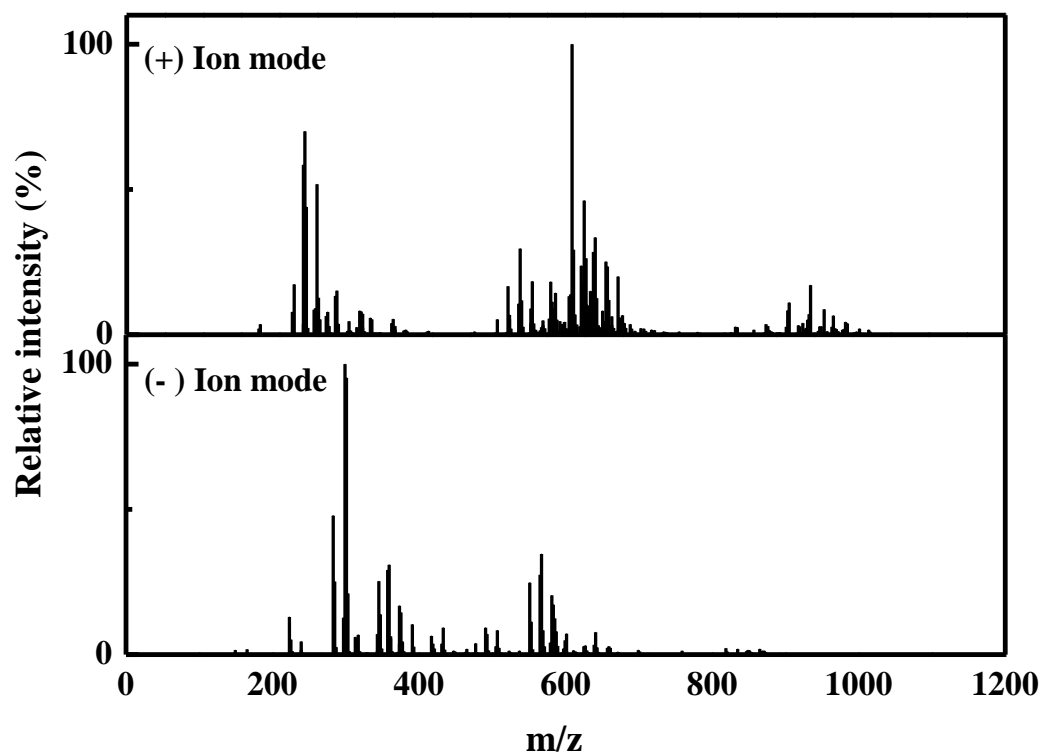


Figure 2-12: Representative ESI mass spectra of secondary aerosol from D_4 oxidation.

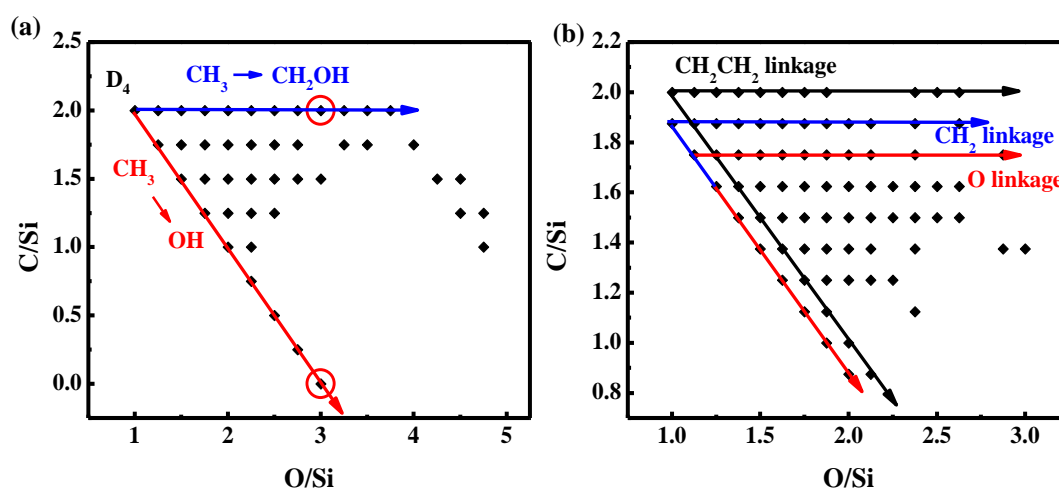


Figure 2-13: Plots of C/Si versus O/Si for saturated products of D₄ oxidation in the a) monomer and b) dimer regions. Each dot represents an assigned molecular formula of a saturated oxidation product. The arrows in the monomer plot extend from unoxidized D₄ and represent the two main types of substitution that occur. The arrows in the dimer plot take into account different possible linkages between monomers. Circles represent monomer products where all eight CH₃ groups have been substituted. Formulas to the right of the circles (same C/Si but higher O/Si) must contain peroxy groups.

2.6 Conclusions

In this chapter, the molecular composition of cVMS-derived secondary aerosol was characterized by high performance mass spectrometry. Based on chemical assignments, the products can be divided into three types: ring-opened products, unsaturated substituted products and saturated substituted products. Ring-opened products arise at least probably in part as artifacts of electrospray ionization. Saturated substituted products exhibit the highest signal intensities. Based on a mass-weighted intensity fraction analysis, gas phase D₅ (O/Si=1, C/Si=2) was oxidized to produce aerosol whose detected products have an average O/Si \approx 1.3 and an average C/Si \approx 1.7 under the conditions studied. Gas phase D₄ was oxidized to produce trimers in addition to monomers and dimers, with the detected products having average O/Si \approx 1.5 and C/Si \approx 1.6 under the conditions studied. ESI-MS/MS analysis of the D₅-derived aerosol provided evidence for

major substitution types along the siloxane ring and the linkages of two siloxane rings to produce dimers. The results showed that OH and CH₂OH substitutions are prevalent, and dimers can be linked by O, CH₂ and CH₂CH₂ groups. D₄-derived aerosol gave evidence for the presence of peroxy groups (CH₂OOH). GC-MS with EI generally confirmed the ESI analysis, though products were incompletely characterized owing to the greater extent of ion fragmentation. The work presented in this chapter was published in [*Journal of The American Society for Mass Spectrometry*](#) by Wu and Johnston in 2016²⁷.

REFERENCES

- (1) Smith, J. N.; Barsanti, K. C.; Friedli, H. R.; Ehn, M.; Kulmala, M.; Collins, D. R.; Scheckman, J. H.; Williams, B. J.; McMurry, P. H. *Proceedings of the National Academy of Sciences of the United States of America* **2010**, *107*, 6634-6639.
- (2) Zhang, R.; Wang, L.; Khalizov, A. F.; Zhao, J.; Zheng, J.; McGraw, R. L.; Molina, L. T. *Proceedings of the National Academy of Sciences of the United States of America* **2009**, *106*, 17650-17654.
- (3) See, S. W.; Balasubramanian, R.; Wang, W. *Journal of Geophysical Research: Atmospheres* **2006**, *111*, n/a-n/a
- (4) Bzdek, B. R.; Johnston, M. V. *Analytical Chemistry* **2010**, *82*, 7871-7878.
- (5) Li, N.; Xia, T.; Nel, A. E. *Free Radical Biology & Medicine* **2008**, *44*, 1689-1699.
- (6) Inoue, K.; Takano, H.; Yanagisawa, R.; Hirano, S.; Kobayashi, T.; Fujitani, Y.; Shimada, A.; Yoshikawa, T. *Toxicology* **2007**, *238*, 99-110.
- (7) Quadros, M. E.; Marr, L. C. *Journal of the Air & Waste Management Association* **2010**, *60*, 770-781.
- (8) Riipinen, I.; Yli-Juuti, T.; Pierce, J. R.; Petaja, T.; Worsnop, D. R.; Kulmala, M.; Donahue, N. M. *Nature Geoscience* **2012**, *5*, 453-458.
- (9) Kroll, J. H.; Seinfeld, J. H. *Atmospheric Environment* **2008**, *42*, 3593-3624.
- (10) Pennington, M. R.; Klems, J. P.; Bzdek, B. R.; Johnston, M. V. *Journal of Geophysical Research: Atmospheres* **2012**, *117*, n/a-n/a.
- (11) Bein, K. J. *Journal of Geophysical Research* **2005**, *110*.
- (12) Wang, S.; Johnston, M. V. *International Journal of Mass Spectrometry* **2006**, *258*, 50-57.
- (13) Ross Pennington, M.; Johnston, M. V. *International Journal of Mass Spectrometry* **2012**, *311*, 64-71.
- (14) Bzdek, B. R.; Horan, A. J.; Pennington, M. R.; Janecek, N. J.; Baek, J.; Stanier, C. O.; Johnston, M. V. *Environmental Science & Technology* **2014**, *48*, 11137-11145.

- (15) Genualdi, S.; Harner, T.; Cheng, Y.; Macleod, M.; Hansen, K. M.; van Egmond, R.; Shoeib, M.; Lee, S. C. *Environmental Science & Technology* **2011**, *45*, 3349-3354.
- (16) Krogseth, I. S.; Kierkegaard, A.; McLachlan, M. S.; Breivik, K.; Hansen, K. M.; Schlabach, M. *Environmental Science & Technology* **2013**, *47*, 502-509.
- (17) Wang, D. G.; Norwood, W.; Alaei, M.; Byer, J. D.; Brimble, S. *Chemosphere* **2013**, *93*, 711-725.
- (18) Atkinson, R. *Environmental Science & Technology* **1991**, *25*, 863-866.
- (19) Sommerlade, R.; Parlar, H.; Wrobel, D.; Kochs, P. *Environmental Science & Technology* **1993**, *27*, 2435-2440.
- (20) Hall, W. A. t.; Pennington, M. R.; Johnston, M. V. *Environmental Science & Technology* **2013**, *47*, 2230-2237.
- (21) Kang, E.; Root, M. J.; Toohey, D. W.; Brune, W. H. *Atmospheric Chemistry and Physics* **2007**, *7*, 5727-5744.
- (22) Hall, W. A.; Johnston, M. V. *Aerosol Science and Technology* **2011**, *45*, 37-45.
- (23) Walser, M. L.; Desyaterik, Y.; Laskin, J.; Laskin, A.; Nizkorodov, S. A. *Physical Chemistry Chemical Physics : PCCP* **2008**, *10*, 1009-1022.
- (24) Atkinson, R.; Tuazon, E. C.; Kwok, E. S. C.; Arey, J.; Aschmann, S. M.; Bridier, I. *Journal of the Chemical Society-Faraday Transactions* **1995**, *91*, 3033-3039.
- (25) Crounse, J. D.; Nielsen, L. B.; Jørgensen, S.; Kjaergaard, H. G.; Wennberg, P. O. *The Journal of Physical Chemistry Letters* **2013**, *4*, 3513-3520.
- (26) Crounse, J. D.; Nielsen, L. B.; Jørgensen, S.; Kjaergaard, H. G.; Wennberg, P. O. *The Journal of Physical Chemistry Letters* **2013**, *4*, 3513-3520.
- (27) Wu, Y.; Johnston, M. V. *Journal of the American Society for Mass Spectrometry* **2016**, *27*, 402-409.

Chapter 3

AEROSOL FORMATION FROM OXIDATION OF VOLATILE CYCLIC METHYL SILOXANE (cVMS) DECAMETHYLPENTASILOXANE

In this chapter, the molecular composition of secondary aerosol obtained from D₅ oxidation is studied both in the presence and absence of ammonium sulfate seed aerosol using high performance mass spectrometry. Systematic changes in the molecular composition with aerosol mass loading are observed and interpreted on the basis of estimated volatilities of the individual molecular products, which give fundamental insight into the pathways¹ involved in secondary aerosol formation. Accretion reactions, specifically those where two semivolatile monomers react in the particle phase to give a nonvolatile dimer, are shown to have a substantial impact on aerosol formation as the aerosol mass loading increases.

3.1 Experimental Section

As discussed in Chapter 2, secondary aerosol was generated in a Photo-oxidation chamber (PC) consisting of a 50L (251 × 251 × 800 mm, WxHxL) rectangular bag composed of a perfluoroalkoxy copolymer (Welch Fluorocarbon, Dover, New Hampshire). To avoid any potential contaminations from the air, a Zero-Air generation system (Model 737, Aadco, Cleves, Ohio) is applied in all experiments. Before each experiment, the PC was still cleaned by exposure to 20 ppmv ozone in the presence of ultraviolet radiation for at least 48 hr and flushed continuously with clean, dry, air for 4-5 days. A Scanning Mobility Particle Sizer (SMPS; Model 3080/3078, TSI, St. Paul, Minnesota) was used to measure particle size distributions.

To better control the amount of precursor sent into the chamber, a syringe pump (Model No. 55-1199, Harvard Apparatus, Holliston, Massachusetts) was

used to replace the gas bubbler used in chapter 2 and to feed precursor fluid (D_5 /MeOH as 1/5 by volume) (CAS No.541-02-6, Gelest, Morrisville, Pennsylvania) at a rate of 0.1 $\mu\text{L}/\text{min}$ into an airflow through a gently heated Teflon fitting. This airflow was then diluted to adjust the initial concentration of gas phase D_5 and a constant flow of the diluted air was sent into the PC. Ozone was generated by passing clean air around a mercury lamp (Model No.81-1025-01, BHK Inc., Ontario, California). The ozone laden air was then bubbled through deionized water and sent into the PC where interaction with ultraviolet radiation produced OH. When combined and sent into the PC, the ozone, D_5 and a third make-up air flow yielded a nominal residence time of 15 min in the PC. Seed particles were generated by atomizing a 5mM ammonium sulfate solution. The particles were then sent through a diffusion drier and entered the PC through a third portion of the makeup air flow. After mixing, the seed aerosol mass concentration in the PC was $1.9 \mu\text{g}/\text{m}^3$. All experiments were performed with low relative humidity (typically 8-10%) and a temperature of 27°C . Table 3-1 summarizes the experiments that were performed, five each seeded and unseeded. Figure 3-1 then shows representative particle size distributions for three aerosol mass loading

Expt. No.	Initial D ₅ conc. (ppbv)	Estimated ΔD_5 conc. (ppbv) ^c	ΔM ($\mu\text{g}/\text{m}^3$) ^d	Volume/Surface Area (nm) ^e
1 ^a	5.4	1.0	1.2 \pm 0.1	7.7 \pm 0.2
2 ^a	8.4	2.2	3.3 \pm 0.2	12.7 \pm 0.4
3 ^a	11.0	2.9	5.6 \pm 0.4	19.5 \pm 0.6
4 ^a	12.4	3.7	8.0 \pm 0.3	21.5 \pm 0.3
5 ^a	13.3	5.0	12.0 \pm 0.6	34.7 \pm 1.6
6 ^b	5.4	1.1	2.3 \pm 0.2	16.1 \pm 0.4
7 ^b	8.1	1.4	3.2 \pm 0.1	21.6 \pm 0.4
8 ^b	8.5	1.7	4.5 \pm 0.3	23.3 \pm 0.5
9 ^b	11.1	2.9	9.6 \pm 0.7	28.9 \pm 0.3
10 ^b	12.4	3.6	12.6 \pm 0.2	31.6 \pm 0.3

a: Unseeded experiments.

b: Seeded experiments (1.9 $\mu\text{g}/\text{m}^3$ ammonium sulfate).

c: Estimated from [OH] concentration.

d: Secondary aerosol mass concentration (seed concentration subtracted from total concentration in experiments 6-10).

e: Volume and surface area of the aerosols were calculated from measured size distributions by SMPS using vendor-supplied software; seed ratio was subtracted from total ratio in experiments 6-10.

Table 3-1: Experimental conditions for secondary aerosol formation from OH oxidation of D₅ with/without seed particles. ΔD_5 is the estimated reacted concentration of gas phase D₅, ΔM is the aerosol mass concentration.

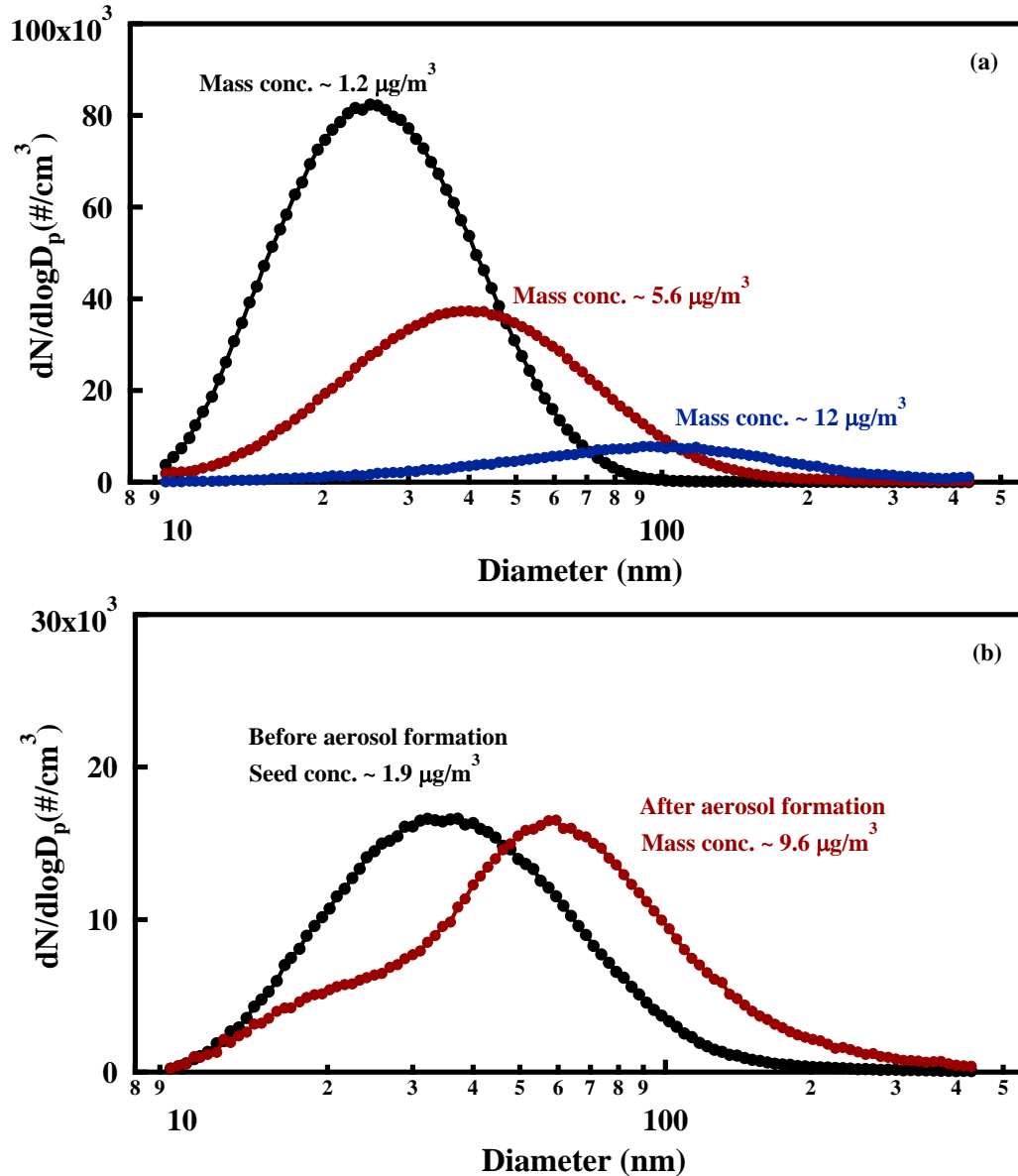


Figure 3-1: a) Number based size distributions from unseeded experiments with secondary mass loadings of 1.2, 5.6 and $12 \mu\text{g}/\text{m}^3$, respectively. b) Number based size distributions from a seeded experiment before and after secondary aerosol formation.

Particulate matter in the air flow exiting the PC was collected at a flow rate of $\sim 2 \text{ L}/\text{min}$ for 20-24 hrs onto a Teflon coated, glass fiber filter (GF/D, CAT No.1823-025, Whatman, GE Healthcare, Piscataway, NJ) for chemical analysis. Generally, $\sim 0.2 \text{ mg}$ of aerosol was collected in each experiment for analysis and four separate filter collections were obtained for each experiment in Table 3-1.

Chamber, filter and solution blanks were collected prior to the injections of reactants to identify and remove artifacts. After particle collection, each filter was sonicated for three hours with 8 ml acetonitrile (ACN)/deionized H₂O 50/50 by volume (CAS No. 75-05-8, Fisher Scientific, Pittsburgh, Pennsylvania) and the resulting solution was filtered through a polyvinylidenedifluoride (PVDF) filter (CAT No. 6747-2504, GE Healthcare, Piscataway, NJ). The filtered solution was then concentrated nearly to dryness (<0.3 ml) with a Speed Vac Concentrator (Model SC110A, Thermo Scientific, Waltham, Massachusetts). Finally, the sample was reconstituted to 1 mg/mL with ACN for off line analysis.

Sample analysis was performed with a Q-Exactive hybrid Quadrupole-Orbitrap mass spectrometer (Thermo Scientific, Waltham, MA) coupled with a heated-electrospray ionization (HESI) probe using a spray voltage of 3.5 kV and capillary temperature of 275 °C. Mass spectra were obtained over the range 100-1200 m/z with a nominal mass resolving power of 70000. Typically, data were acquired for 0.8 min with ~180 spectra averaged. The mass spectra were processed with Xcalibur software supplied with the mass spectrometer using the procedure described in our previous work². Briefly, only those ions that were positively detected in all four filter samples for a given experiment were considered for molecular formula assignment. Assigned peaks represented on average 88% of the total signal intensity in each experiment.

3.2 Aerosol Formation in Unseeded Experiments

Figure 3-2 shows the positive ion mass spectra averaged over replicate samples for three aerosol mass loadings. The ions observed from these samples are very similar to the previous study, discussed in Chapter 2, with a much higher aerosol mass loading (> 60 µg/m³), where accurate mass measurements and MS/MS spectra were used to characterize the molecular products of D₅ oxidation². Similarly, although the mass spectra are complex, molecular products can be divided into three main types according to the chemical assignments. First are

monomer products, defined here as those containing exactly 5 Si atoms, at least 5 O atoms, and a molecular formula (and MS/MS spectra) consistent with one siloxane ring but no other sites of unsaturation. Relative to the D₅ precursor molecule, monomer products contain various combinations of functionalization where CH₃ groups are replaced by OH and/or CH₂OH groups. In Figure 3-2, monomer products are coded red.

Second are dimer products, defined here as those containing exactly 10 Si atoms, at least 10 O atoms, and a molecular formula (and MS/MS spectra) consistent with two siloxane rings but no other sites of unsaturation. Dimers also contain various combinations of functionalization where CH₃ groups are replaced by OH and/or CH₂OH, and the two siloxane rings can be linked by O, CH₂ or CH₂CH₂ groups. In Figure 3-2, dimer products are coded black.

Third are ring-opened products, defined here as those containing neither 5 nor 10 Si atoms. Formation of these products necessarily requires fragmentation of the original D₅ siloxane ring structure. Molecular formulas and MS/MS spectra of these products are consistent with CH₃ replacement by OH and/or CH₂OH, and sometimes indicate an additional site of unsaturation, for example, Si=O. In Figure 3-2, ring-opened products are coded blue.

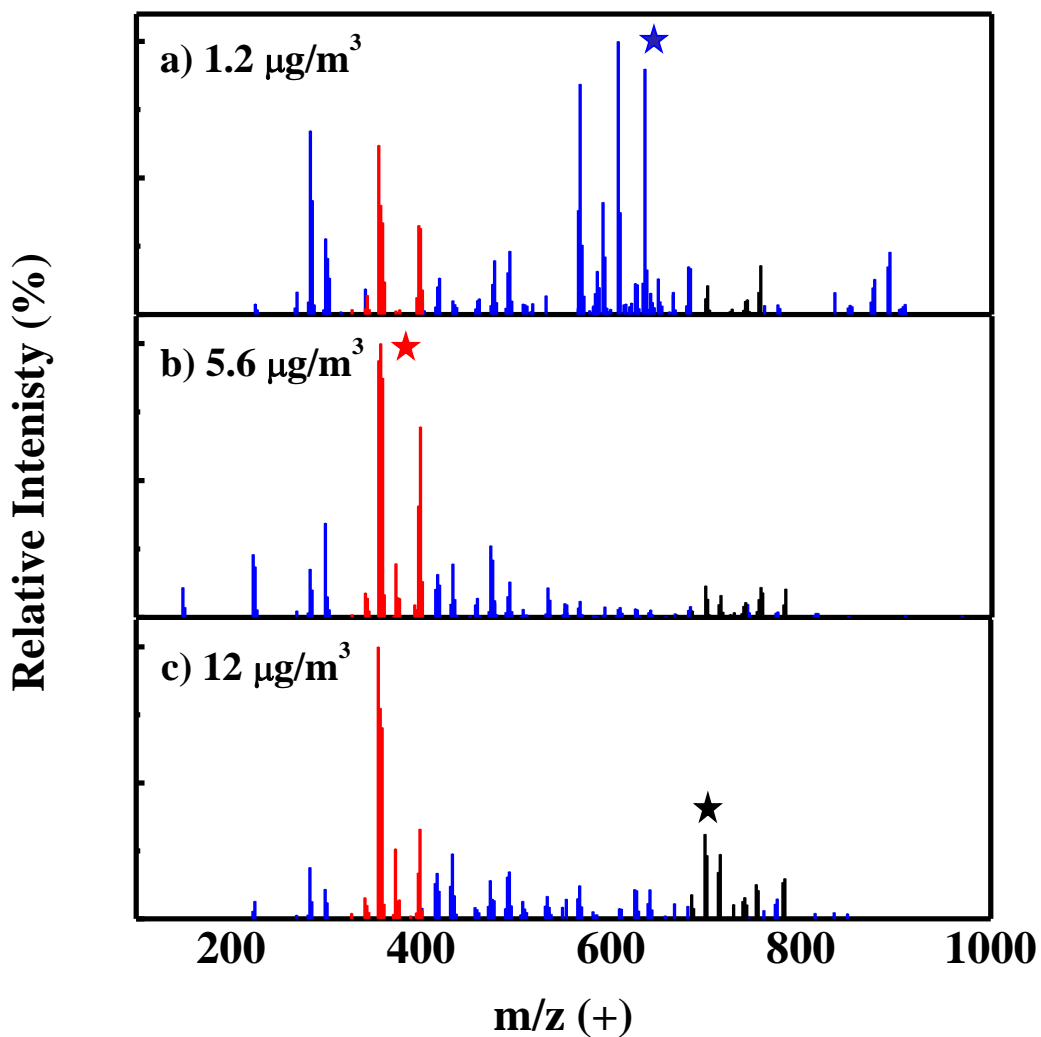


Figure 3-2: ESI mass spectra in positive ion mode of secondary aerosol from D₅ oxidation under various aerosol mass loadings. Ion signal intensities are averaged over four separate measurements from four different samples. Peaks considered as ring opened products are coded blue, dimers are coded black, and monomers are coded red. Candidate structures for starred ions are given in Figure 3-3.

Figure 3-3 shows candidate structures for three prominent ions of each type, which are starred in the mass spectra of Figure 3-2. While not proven, candidate structures are consistent with molecular formulas and MS/MS spectra. Figure 3-4 shows MS/MS spectra for the three starred ions in Figure 3-2. Accurate mass and MS/MS spectra often permit identification of specific

functional groups and dimer linkages, but they generally cannot determine functional group locations².

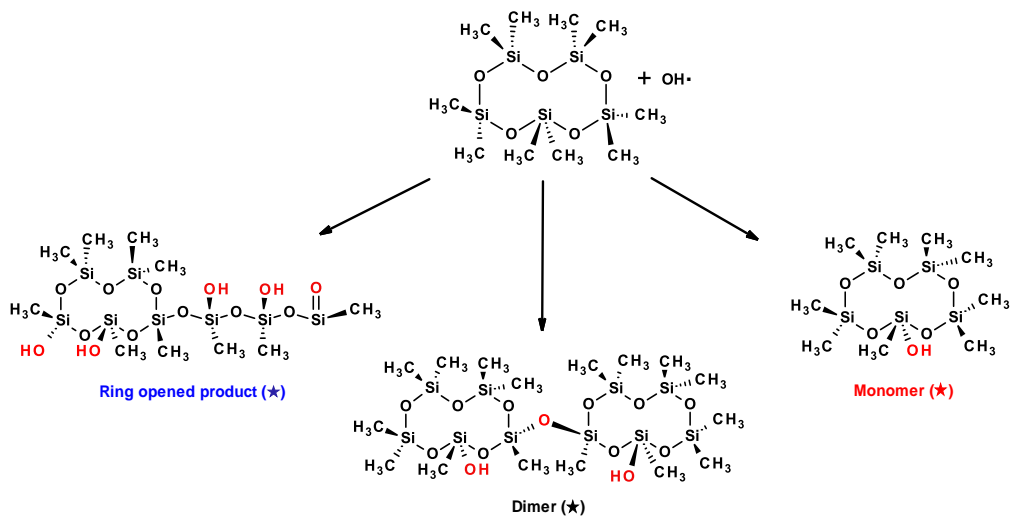


Figure 3-3: Candidate structures for the three types of reaction products found in siloxane secondary aerosol. These structures are consistent with molecular formulas and MS/MS spectra of the starred ions in Figure 3-2.

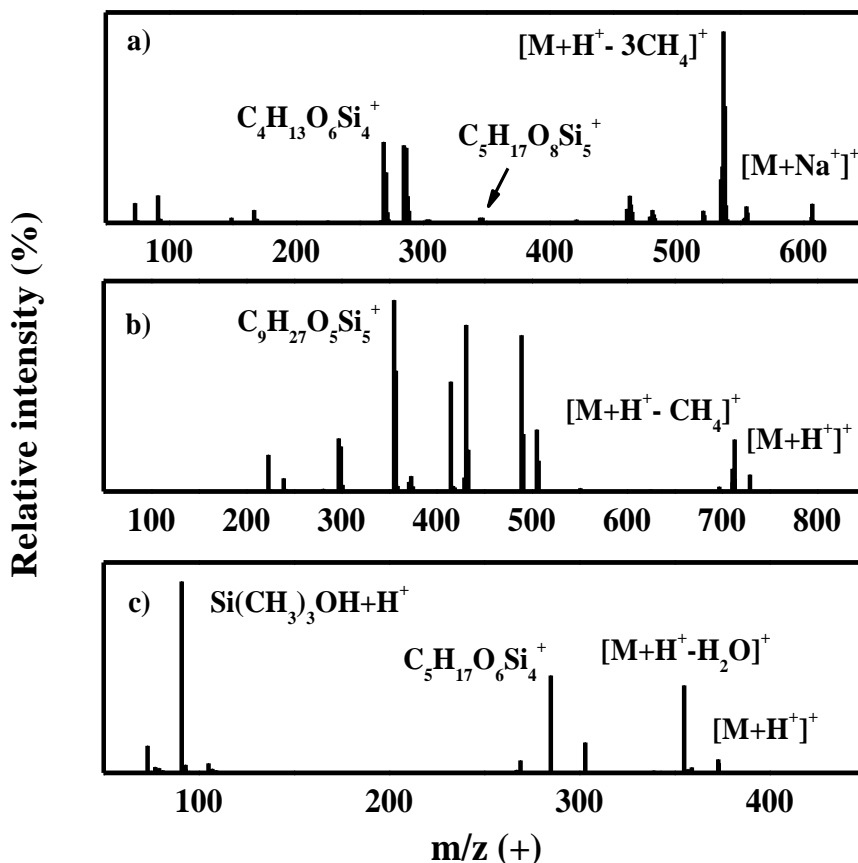


Figure 3-4: Product MS/MS ion spectra for isolation of (a) 607 m/z(+), (b) 729 m/z(+), and (c) 373 m/z(+). These precursors correspond to the three starred ions in Figure 1 and the candidate ring opened product (a), dimer (b) and monomer (c), respectively in Fig 3-3.

In Chapter 2 with a high aerosol mass loading ($> 60 \mu\text{g}/\text{m}^3$)², ring-opened products had very low signal intensities that could be explained in part by molecular decomposition within the ESI source. Therefore, those ring-opened products were discussed only briefly. In contrast, the ring-opened products in Figure 3-2 have very high signal intensities especially at a very low aerosol mass loading that cannot be explained simply by ESI decomposition. Additionally, a control experiment was performed by sonicating 100 $\mu\text{g}/\text{ml}$ D₅ (dissolved in ACN/H₂O 50/50 by volume) for 3 hours under the same experimental condition. Figure 3-5 then shows that the positive ESI mass spectrum obtained after sonication was generally devoid of ring-opened species, indicating that the high

abundance of these products in the filter samples was not from sonochemistry. It should be noted that ring-opened products have been reported previously in plasma polymerization experiments³, so it is not unreasonable to expect they can be formed by OH oxidation.

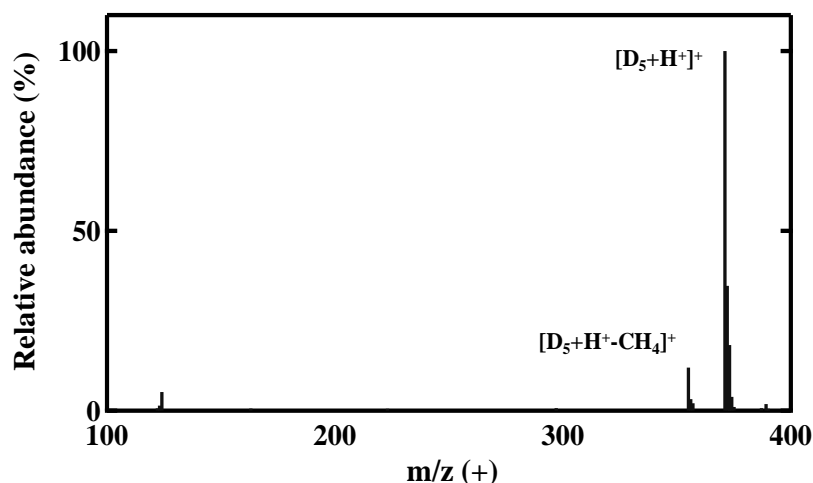


Figure 3-5: Positive ESI mass spectrum of pure D₅ in ACN/H₂O 50/50 by volume with a concentration of 100 µg/ml sonicating for 3 hours.

To understand possible formation mechanisms of different types of products, the total surface area of aerosol (S) and volume (V) is calculated based on the particle number concentration (N_i) in each diameter bin (D_i):

$$S = \sum_i N_i \pi D_i^2, V = \sum_i N_i \frac{\pi D_i^3}{6}$$

As a result, the volume to surface area ratio of the aerosol (V/S) is obtained at different aerosol mass loading conditions (as displayed in Table 3-1). After calculation, the volume to surface area ratio of the unseeded aerosols studied in this work scale approximately linearly with mass loading as shown in Figure 3-6. The mass loading dependence of the three product types are explored further in Figure 3-7a where the ratio of the summed signal intensities of dimers to

ring-opened products is plotted as a function of aerosol volume to surface area ratio.

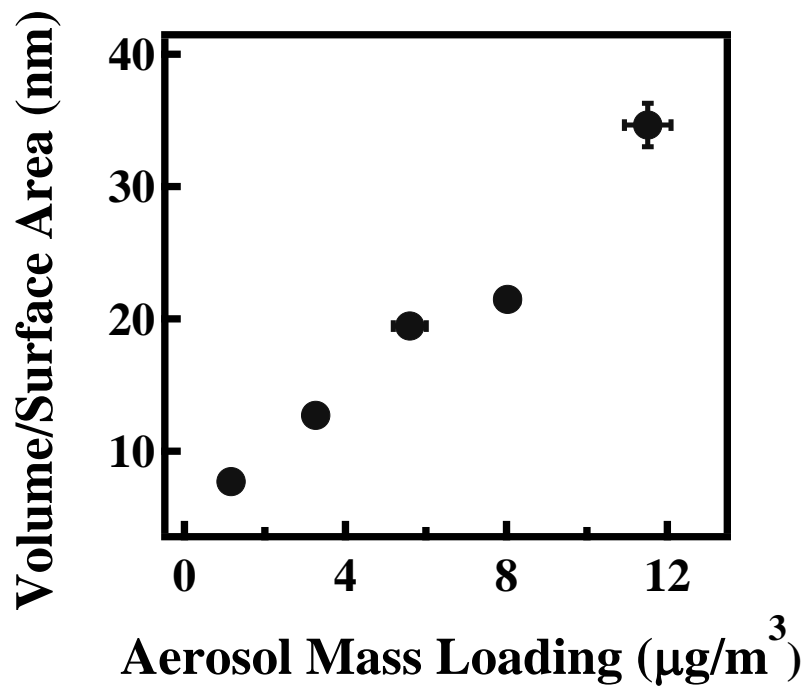


Figure 3-6: Volume-to-surface area ratio vs. mass loading for the unseeded aerosols studied in this work. Error bars represent one standard deviation. Error bars smaller than the symbol are not shown.

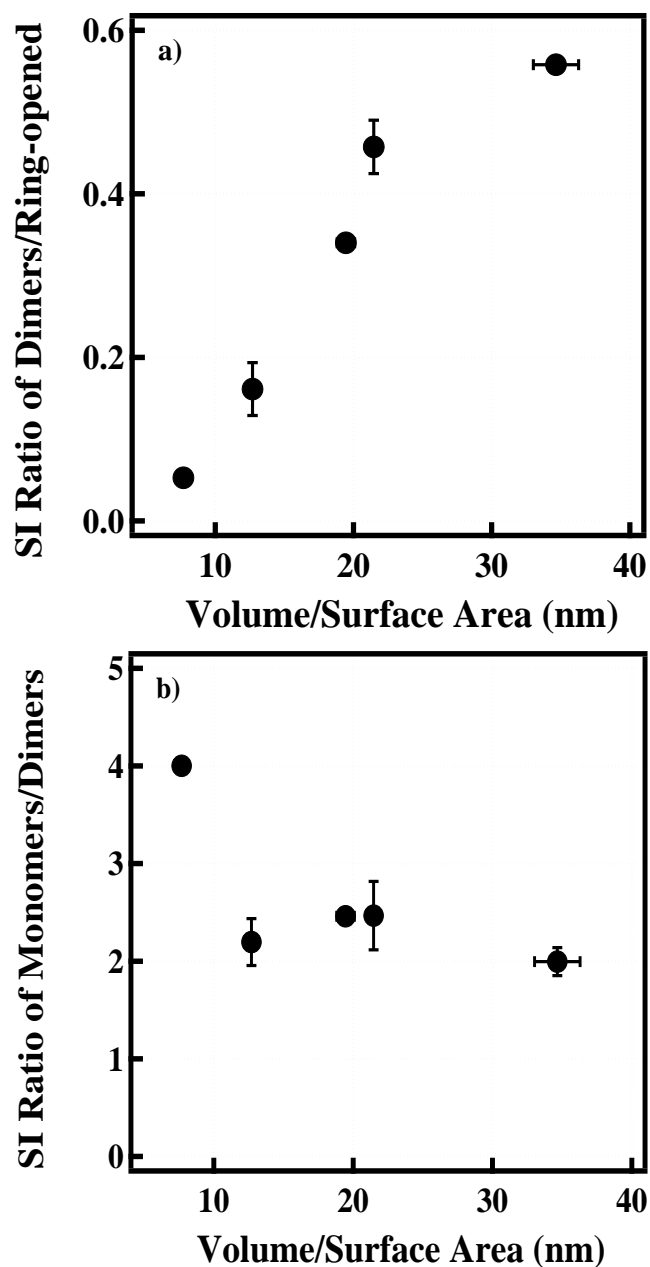


Figure 3-7: Signal intensity ratio of a) dimers to ring-opened products and b) monomers to dimers vs. volume/surface area ratio of the secondary aerosol. Error bars represent one standard deviation. Error bars smaller than the symbols are not shown.

Figure 3-7a shows that the ratio of dimers to ring-opened products increases approximately linearly with increasing volume to surface area ratio. As will be discussed later, all dimers and most ring-opened products are expected to be extremely nonvolatile with predicted saturation concentrations (C^*) that are

orders of magnitude lower than the aerosol mass loadings in these experiments. The approximately linear relationship in Figure 3-7a suggests different formation mechanisms for these two types of products. Ring-opened products appear to be necessary for particle formation and/or early growth since they are most prevalent at low volume to surface area ratio. These species are likely to be formed directly in the gas phase and then condense when they strike the particle surface. It is also possible that ring-opened products are formed directly at the particle surface. In either case, particle growth via ring-opened species is determined by the available surface area.

Chapter 2, performed with a high aerosol mass loading, speculated that dimers were formed in the gas phase². However, the mass loading dependence observed in the current study shows that dimers must be formed by accretion reactions in the particle phase, since they are nonvolatile but strongly represented only in higher mass loadings where the aerosol volume is larger. The possibility of condensed phase formation of oligomers has been reported previously⁴. Dimer linked by O can be produced from the hydrolysis of two OH substituted monomers⁵.

A linear dependence on volume to surface area ratio would be expected for a volume-limited process such as accretion chemistry relative to a surface-limited process such as condensation. The linear relationship in Figure 3-7a is similar to that recently reported by our group for accretion reaction products in biogenic secondary organic aerosol (SOA) as a function of particle size in the 35-110 nm range⁶. Note that the volume to surface area ratio for a particle of diameter d is $2d/3$, making the range of volume to surface area ratios where accretion chemistry becomes important similar for the siloxane secondary aerosol in Figure 3-7a and the biogenic SOA studied previously by another Johnston research group member⁶.

Figure 3-7b shows ratio of monomer to dimer mass-weighted signal intensities. In contrast to ring-opened products, the monomer to dimer ratio is

relatively invariant with volume to surface area ratio as would be expected for a quasi-equilibrium process where monomers react to form dimers. Note that monomer partitioning between the gas and particle phases like accretion chemistry is a volume-limited process. The slight increase in monomers to dimers at the lowest volume to surface area ratio arises from a slight change in the distribution of monomers – compare the mass spectrum in Figure 3-2a to those in 3-2b and 3-2c. As a group, the monomers in Figure 3-2a are less volatile than those in Figures 3-2b and 3-2c based on calculated saturation concentrations of candidate molecular structures (see below).

3.3 Aerosol Formation in Seeded Experiments

SOA formation usually occurs in the presence of background particles that are ubiquitous in the ambient atmosphere. Therefore, many chamber studies have focused on the potential effects of preexisting particles on aerosol formation^{7,8}. In particular, most chamber studies of SOA yields to date have either used no seed at all (i.e., homogeneous nucleation of SOA)⁹, or added ammonium sulfate (AS) seed to provide a surface area for condensation¹⁰.

In this study, secondary aerosol formation in the presence of ammonium sulfate seed was found to give different product distributions than those observed in the unseeded experiments. Figure 3-8 compares the mass spectra of secondary aerosol from seeded and unseeded experiments where the aerosol mass loadings after subtraction of the seed are the same. The main difference between the two is the very low contribution of ring-opened products to the seeded spectrum. In fact, the mass spectra obtained from seeded experiments show no significant change with aerosol mass loading.

These results are consistent with the above conclusions for unseeded aerosol. In seeded experiments, formation and/or growth of new particles is less important since secondary aerosol is able to grow on the preexisting seeds. The volume to surface area ratio of the seed aerosol was 18 nm, which then increased

to as high as 32 nm depending on the amount of secondary aerosol produced. Based on the plot in Figure 3-7a, ring-opened species would be expected to represent only a minor contribution to aerosol mass at such high values of volume to surface area ratio. Once particle formation and early growth has been accomplished (or replaced through the presence of seed particles), secondary aerosol formation proceeds mainly by a combination of monomer partitioning and particle phase accretion reactions to produce dimers.

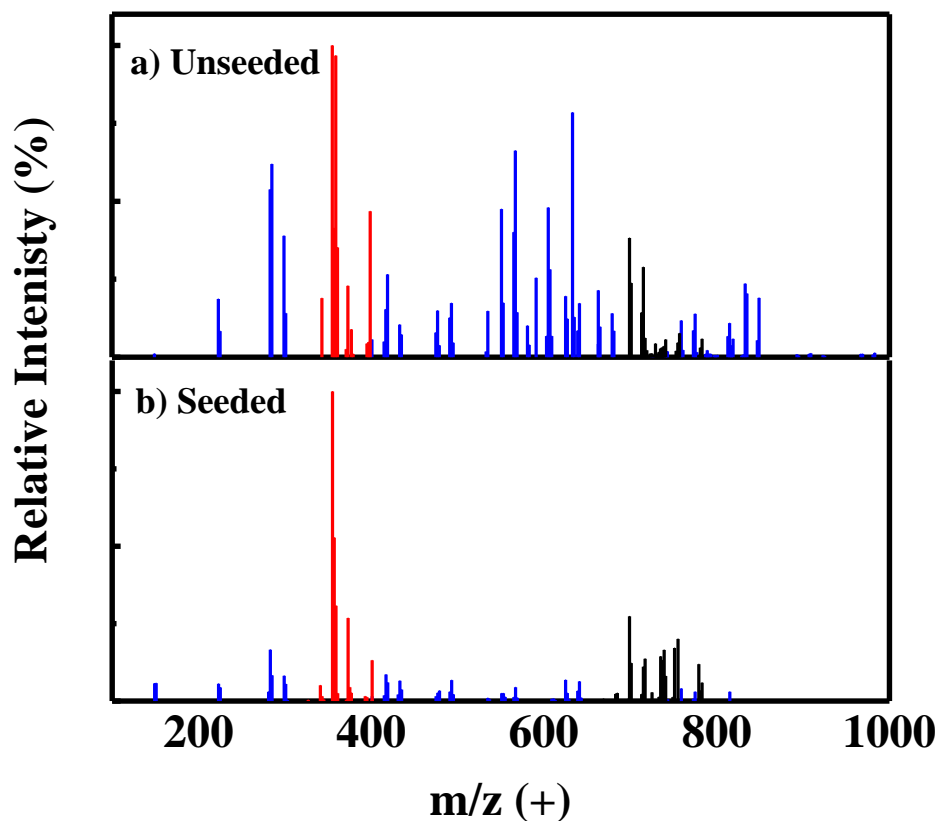


Figure 3-8: ESI mass spectra in positive ion mode for a) unseeded and b) seeded aerosol produced by OH oxidation of D₅ under conditions that give similar mass loadings (after subtraction of seed aerosol) of ~3 μg/m³. Ion signal intensities are averaged over four separate measurements from four different samples. Peaks considered as ring opened products are coded blue, dimers are coded black, and monomers are coded red.

3.4 Product Volatility Estimation

The difference in composition between the seeded and unseeded aerosols in Figure 3-8 is further examined on the basis of molecular volatility as given by the saturation concentration (C^*) which is numerically the vapor pressure of the compound in units of μg/m³. Measuring or estimating values of C^* for individual molecular components is important since in combination with the aerosol mass loading it determines the fraction of that component that exists in the gas vs. particle phase at equilibrium^{10, 11}. Specifically, the fraction F of a semi-volatile compound in the particle phase can be expressed in terms of C^* :

$$F = \frac{P}{G + P} = \frac{MK_p}{1 + MK_p} = \frac{1}{1 + C^*/M}$$

As the amount of absorbing material (M) increases, compounds of higher volatility (larger C^* , smaller K_p) will partition increasingly into the particle phase. When $C^*=M$, half of the semivolatile mass resides in the particle phase. If $M \gg C^*$, essentially all of the semivolatile species is in the particle phase ($F \approx 1$)¹².

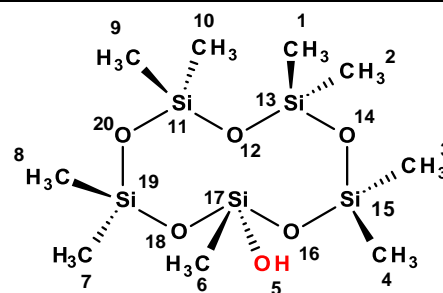
Several volatility estimation methods have been reported in the literature with varying degrees of complexity¹³⁻¹⁵. The method introduced by Nannoolal et al. is most relevant to the current study since it considers group contributions involving silicon^{15, 16}. Beginning with a candidate molecular structure, the method calculates a normal boiling point based on the sum of group contributions ($\sum N_i C_i$), a group interaction term (GI) and finally the vapor pressure (saturation concentration) by using following equations:

$$T_b = \frac{\sum N_i C_i}{n^a + b} + c \quad (a = 0.6583, b = 1.6868, c = 84.3395)$$

$$dB = \left(\sum N_i C_i + GI \right) - 0.176055$$

$$\log (p/\text{atm}) = (4.1012 + dB) \left(\frac{T_{rb}-1}{T_{rb}-1/\varepsilon} \right)$$

To clarify how the method applied, Table 3-2 represented an example of the estimations of boiling point and saturation vapor concentration of one OH substituted D₅ (C₉H₂₈O₆Si₅). According to the method introduced by Nannoolal et al., group contributed from carbon is the CH₃ not connected to N, O, F and Cl; group contributed from oxygen represents the OH connected to Si which has four non-hydrogen neighbors and the -O- connected to two neighbors which are Si; group contributed from silicon is the Si attached to two carbon and Si attached to one carbon. OH-O interaction is also considered to estimate the final value.



Number of atoms: 20, formula: C₉H₂₈O₆Si₅.

Group	Frequency	Contribution (K)	Total
-CH ₃	9	177.3066	1595.7594
-OH	1	349.9409	349.9409
Si-O-Si	5	146.4836	732.4180
H ₃ C-Si-CH ₃	4	282.0181	1128.0724
H ₃ C-Si-OH	1	207.9312	207.9312
Interactions	Frequency	Contribution (K)	Total
OH-O	10/20	435.0923	217.5462
Sum			4231.6681

$$T_b = \frac{4231.6681}{20^{0.6583} + 1.6868} + 84.3395 = 561.28\text{K}$$

Group	Frequency	Contribution (dB)	Total
-CH ₃	9	0.0133	0.1197
-OH	1	0.7194	0.7194
Si-O-Si	5	0.1085	0.5425
H ₃ C-Si-CH ₃	4	-0.0474	-0.1896
H ₃ C-Si-OH	1	-0.0666	-0.0666
Sum			1.1257
Correction	Frequency	Contribution (dB)	Total
OH-O	10/20	-0.7995	-0.3998

$$\text{dB} = 1.1257 - 0.3998/20 - 0.176055 = 0.9297$$

$$P^S = [10^{(4.1012 + 0.9297)((299.15/561.28) - 1)/((299.15/561.28) - 1/8)}] = 0.0012 \text{ kPa};$$

$$\log C^* = 4.42 \mu\text{g}/\text{m}^3.$$

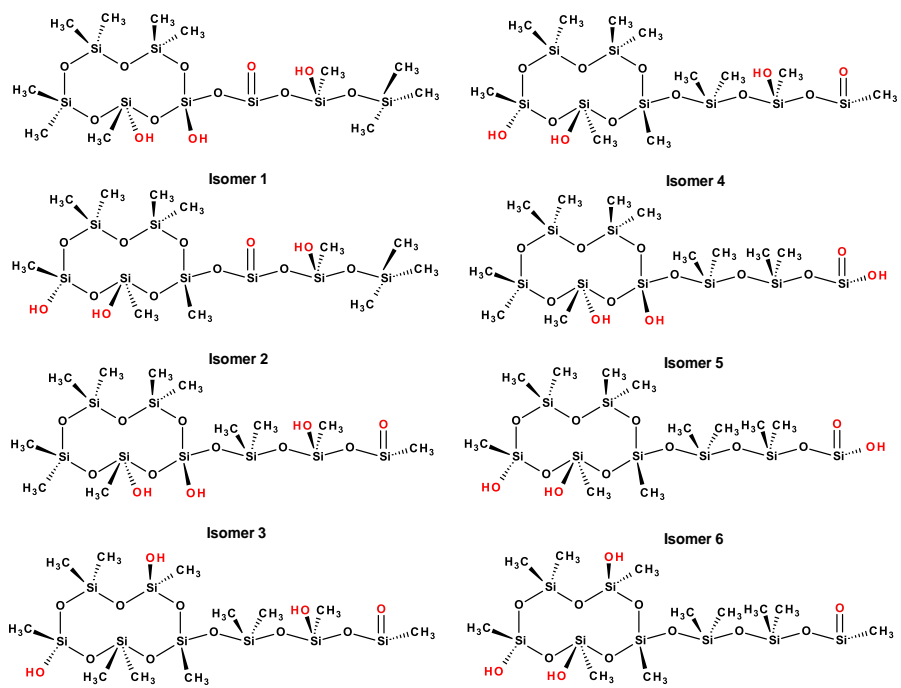
Table 3-2: Estimation of boiling point and volatility at 299.15K of one OH substituted D₅ (C₉H₂₈O₆Si₅).

To confirm the validity of this method in this study, this approach was tested by comparing measured and calculated boiling points and saturation concentrations for cyclic siloxanes D₃ to D₇ first. The results, shown in Table 3-3, demonstrate agreement between measured and calculated C* within a factor of 5 or less. To further test the method, I took the molecular formula for the

ring-opened product in Figure 3-3 and calculated C* values for eight candidate structures including the one shown in Figure 3-3. The results, shown in Table 3-4, give predicted C* values within a factor of 2-4 of each other. The relatively close agreement for different candidate structures arises in large part from similar Si-O scaffolding and only minor perturbation due to type and location of functional groups. Applying this method to candidate structures for all molecular products leads values spanning many orders of magnitude in C*, whereas the uncertainty associated with any individual prediction is likely to be much less than one order of magnitude. A complete list of molecular formulas and predicted C* values is given in Appendix B. A summary plot of O/Si ratio of the molecular formula vs. log C* is shown in Figure 3-9. All dimers and most ring-opened products are relatively nonvolatile, having predicted log C* values below -2. Most monomers are semivolatile or volatile, though a few can be considered nonvolatile.

Siloxane	Boiling point (K)		logC* (saturation conc., $\mu\text{g}/\text{m}^3$)	
	Measured	Calculated	Measured	Calculated
D ₃	404.15	428.80	7.63	7.75
D ₄	448.15	481.32	7.22	6.82
D ₅	483.15	525.66	6.60	5.95
D ₆	518.15	556.78	5.73	5.28
D ₇	609.15	591.91	4.78	4.45

Table 3-3: Estimation of boiling point and volatility at 299.15K of various siloxanes.



Isomer 7		Isomer 8	
Isomer	logC*	Isomer	logC*
1	-5.65	5	-5.98
2	-5.35	6	-5.68
3	-5.68	7	-5.38
4	-5.38	8	-5.36

Table 3-4: Estimation of volatility at 299.15K for candidate isomers of the ring opened product ($C_{11}H_{36}O_{12}Si_8$).

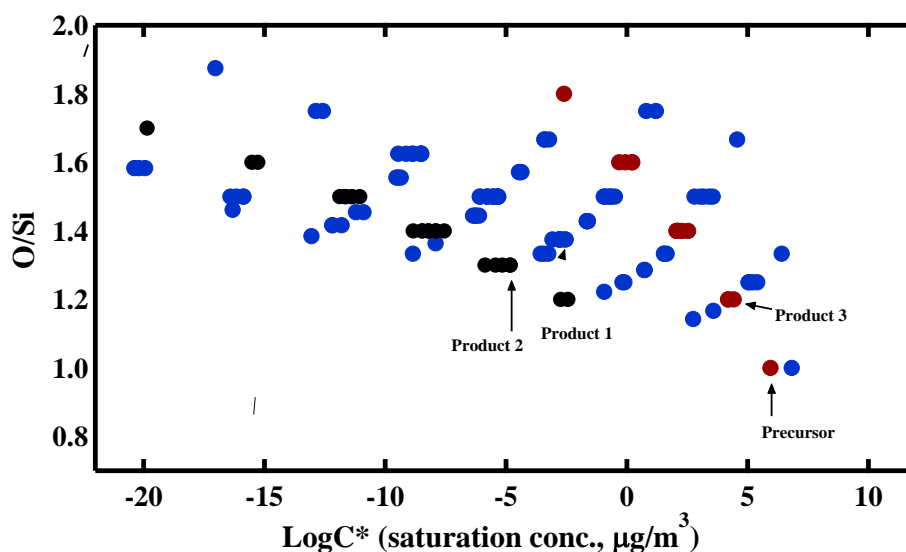


Figure 3-9: O/Si ratio and estimated C^* values for molecular formulas assigned from siloxane secondary aerosol. This figure summarizes the data in Appendix B. Ring opened products are coded blue; dimers are coded black; monomers are coded red.

Figure 3-9 summarizes the mass spectra in Figure 3-8 using a volatility basis set representation^{12, 18}, which normally involves a plot of aerosol mass concentration (or mass fraction) vs. $\log C^*$. In Figure 3-10, the mass-weighted signal intensity is used as a surrogate for mass fraction (discussed in Chapter 2)¹⁸. I find for the mass spectrometer used in this study that ESI detection efficiencies for different cyclic siloxanes can vary by up to a factor of 3. A smaller variation is likely for linear polydimethyl siloxanes since ESI has been shown to be able to accurately determine average molecular weights for polymeric samples^{20, 21}.

Figure 3-10 provides insight into the contributions of different volatility species to seeded vs. unseeded aerosol. Figure 3-10a shows that the majority of nonvolatile matter ($\log C^* < -2$) in unseeded aerosol consists of ring-opened products with a minor contribution from dimers, while the opposite is true for seeded aerosol in Figure 3-10b. This observation is not surprising since ring-opened species are needed for particle formation and/or early growth in an unseeded experiment but not in the presence of seeds. The fraction of

intermediate volatility monomers is higher in the seeded experiment, which suggests that dimer formation in the particle phase is at least partially reversible. However, it is not clear from the experiments performed whether such decomposition would have occurred during the sample preparation process or in the reactor itself when the aerosol was formed. If reversibility occurred on the timescale of aerosol formation, then the higher fraction of intermediate volatility monomers in Figure 3-10b would suggest that they can be trapped within the particle phase owing to hindered diffusion²²⁻²⁴ and/or phase separation²⁵⁻²⁸.

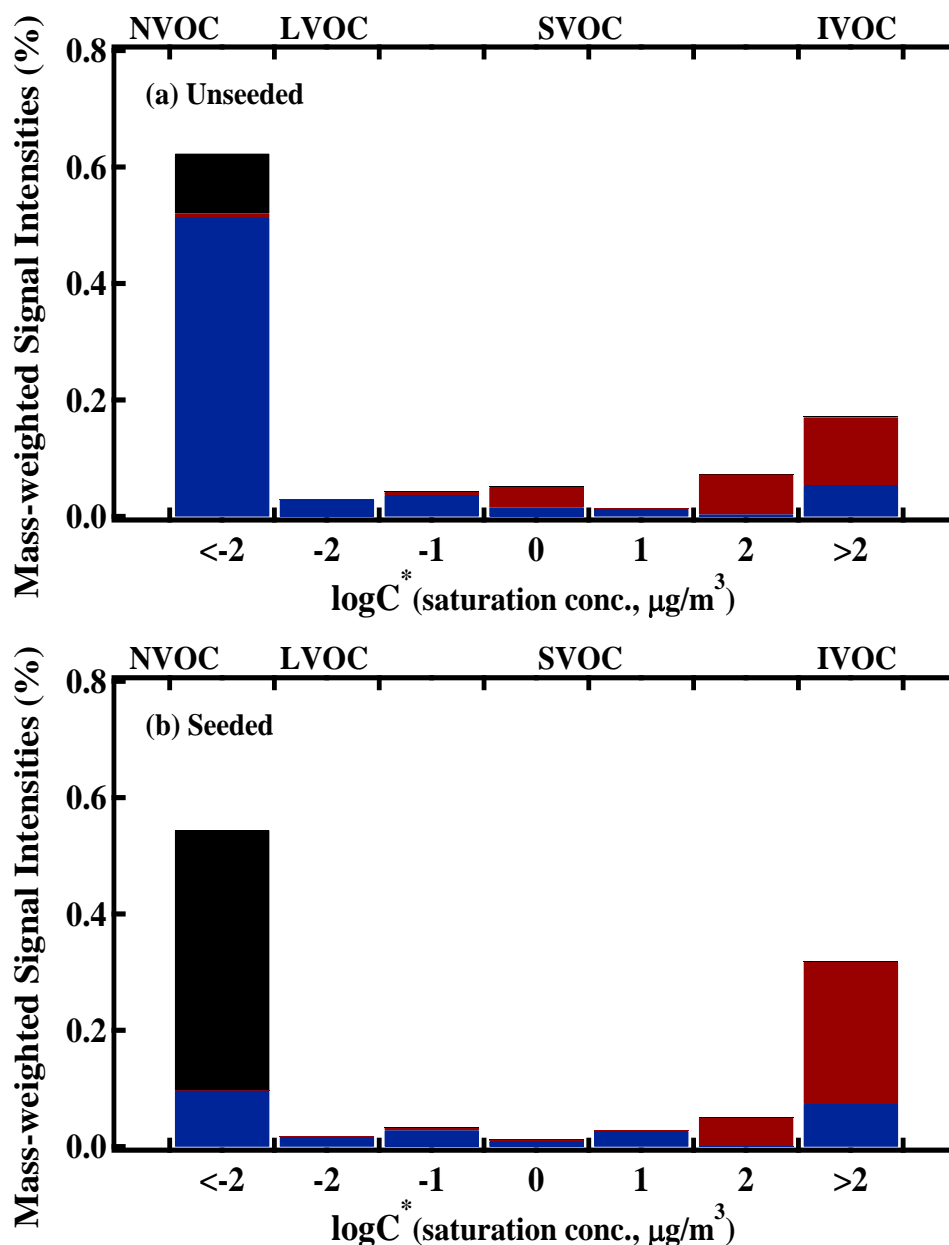


Figure 3-10: Mass-weighted signal intensities summed over the three types of ions in a) unseeded and b) seeded aerosols vs. $\log C^*$ for candidate structures that correspond to individual ions. These plots are for assigned ions in the mass spectra of Figures 3-8a and 3-8b, respectively. Ring-opened products are coded blue, dimers are coded black, and monomers are coded red.

3.5 Aerosol Yield and Atmospheric Implication

Efforts to represent aerosol formation in ambient conditions have been based on using experimentally determined fractional aerosol mass yields^{29,30}. The aerosol mass yield (Y) is defined as the fraction of a reactive organic gas mass that is converted into aerosol mass, and has been estimated for SOA produced in

laboratory environmental chambers by various researchers over the last 30 years²⁹,
³⁰. Substantial progress has been then made in understanding reaction mechanisms and the factors that influence aerosol yields and chemical compositions. For example, aerosol yields appear to have a complex dependence on precursor concentration³¹, temperature³², relative humidity³³. In typical chamber experiments, a range of initial precursor concentration is employed in order to determine aerosol yields as a function of mass concentration of particles generated³¹. Chamber experiments are conducted over a range of initial VOC concentrations, affording a view of the full spectrum of oxidation products and thereby facilitating the formulation of chemical mechanisms.

In this work, aerosol mass yield could be determined by calculating the ratio of aerosol mass concentration M (in $\mu\text{g}/\text{m}^3$) to the amount of precursor (P) reacted ΔD_5 (in $\mu\text{g}/\text{m}^3$) at the end of each experiment:

$$Y = \frac{M}{\Delta D_5}$$

Gas vapor D_5 reacts with OH radical with a second order rate constant of $2.6 \times 10^{-12} \text{ cm}^3 \text{ molecule}^{-1} \text{ s}^{-1}$ ³⁴. Here, the amount of reacted D_5 in these experiments could be then estimated by using the flowing equation:

$$\frac{d[D_5]}{dt} = -k' [D_5]$$

where k' is the second order rate constant multiplied by OH concentration and t is considered as the residence time (15min) in the chamber. As shown in Table 3-1, for the unseeded experiments performed in this study, the reacted D_5 concentration could be varied from ~ 1 to 5ppbv. Generally, aerosol formation was observed immediately after the addition of the second reactant in the presence of UV. The time-dependence of the aerosol number and mass concentrations are given in Figure 3-11 showing that there was a very fast increase in number concentration followed by a gradual decrease throughout the experiments. This observation was consistent with an initial nucleation step to produce a burst of

nano-particles, followed by the coagulation of those particles resulting in an increase in mean diameter along with a corresponding decrease in the number concentration³⁴. Particle wall loss was also studied to correct the aerosol mass concentration, however, no significant wall loss was observed probably due to the smaller surface area to volume ratio of photo-oxidation chamber designed in this experiment ($\sim 18\text{nm}^{-1}$) compared to the Potential Aerosol Mass reactor (PAM) which is also identical in Figure 3-11³⁶.

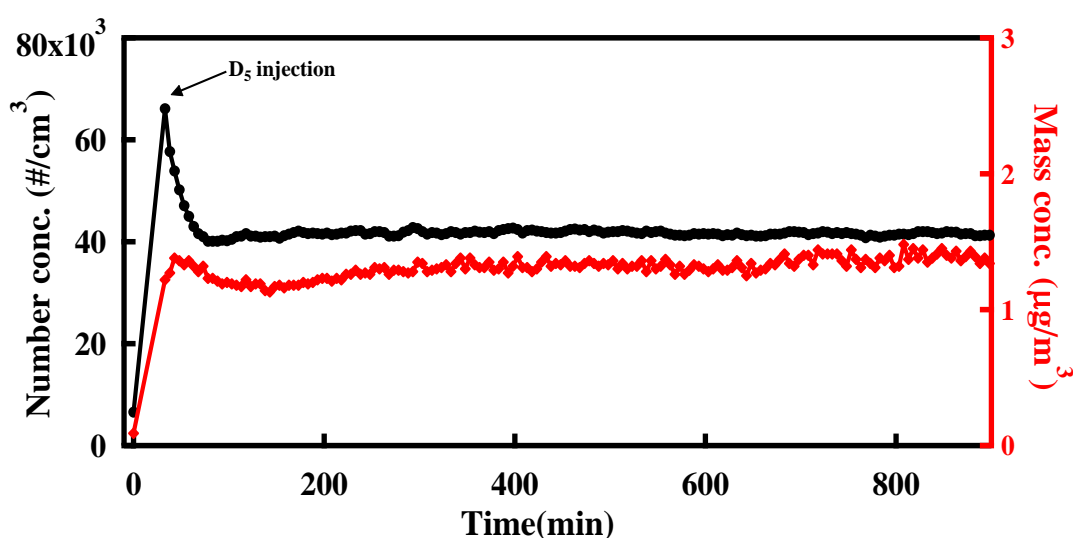


Figure 3-11: Plot of number and mass concentration as a function of time after reaction was initiated.

Figure 3-12 shows plots of aerosol yield and aerosol mass concentration against reacted D_5 mass concentration, respectively, for unseeded experiments. Both of aerosol mass concentration and yield were reacted mass concentration dependent. Aerosol mass concentration increased as a function of increasing reacted D_5 concentration, suggesting that aerosol formation is due to oxidation of gas-phase species and then leading to subsequent condensation or further oxidation of initial products³⁷. Aerosol yield increased with reacted mass loading as well, ranging from ~ 0.08 to 0.15 . At an initial stage, there was a rapid increase in aerosol yield representing the condensation of the lowest volatility

products. The yield curve then showed a slight reduction in the slope as a function of increasing reacted mass concentration reaching at a final value as 0.15. This suggested the partitioning of more volatile species as aerosol organic volume increases, due to continued gas phase reactions or to the larger concentration of the volatile products³⁷. However, I caution that these values for aerosol yields are *not* based on direct measurement of the change in D₅ concentration, but calculated from the OH mixing ratio which itself was estimated from a different set of measurements whose error was difficult to assess.

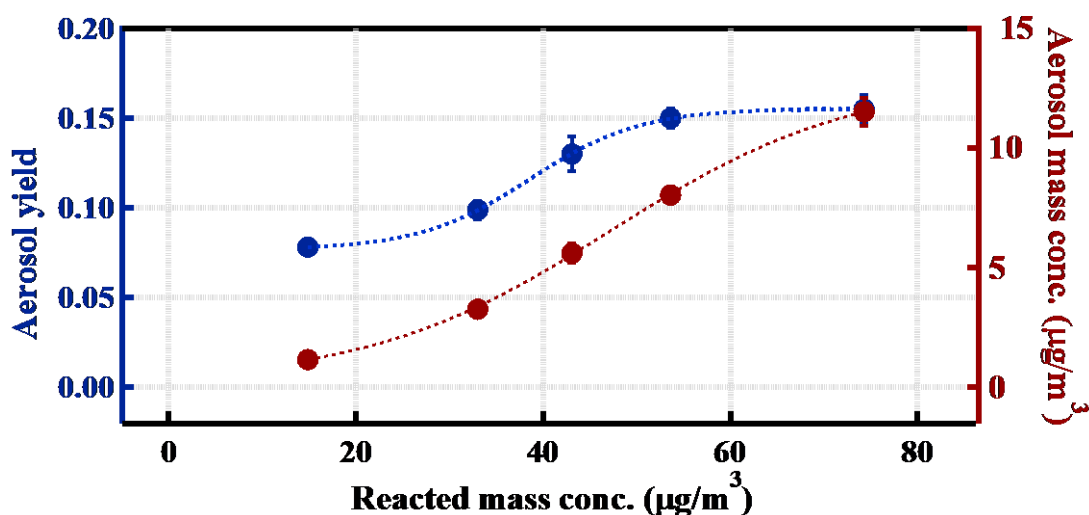


Figure 3-12: Plot of aerosol yield and aerosol mass concentration versus reacted mass concentration. These data are for unseeded experiments.

The first basic model of SOA formation can be represented by the SOA formation of two products (one semi-volatile and one non-volatile product), which is introduced by Odum et al.³⁷, Donahue et al. then modified this model in terms of volatility of several products which will be applied in this study¹². Therefore, the yields can also be further described by a volatility basis set model and applied to fit the experimental SOA yields to reproduce chamber data:

$$Y = \sum_i \alpha_j \left(1 + \frac{10^{-j}}{M_o}\right)^{-1}$$

where α_j is the mass-based gas-phase stoichiometric fraction for semi-volatile species j , M_o is the aerosol mass concentration. In this study, the mass of aerosol in bin j is obtained by optimal fitting to the experimental SOA yield data by a three product model (NVOC, SVOC and IVOC). Figure 3-13 shows the plot of aerosol yield as a function of aerosol mass concentration. By applying the parameters shown in Table 3-5, the model can be fitted to the experimental data with R^2 value as 0.997. α_j , additionally, represents the mass yield of a product in the aerosol phase. As a result, the product with C^* as $100 \mu\text{g}/\text{m}^3$ shows the highest mass yield compared to the products with lower volatility.

α_1	α_2	α_3	$C^*_1(\mu\text{g}/\text{m}^3)$	$C^*_2(\mu\text{g}/\text{m}^3)$	$C^*_3(\mu\text{g}/\text{m}^3)$
0.02	0.09	0.53	0.01	1	100

Table 3-5: Empirical parameters for three products model describing the particle mass yield of aerosol produced from unseeded experiments.

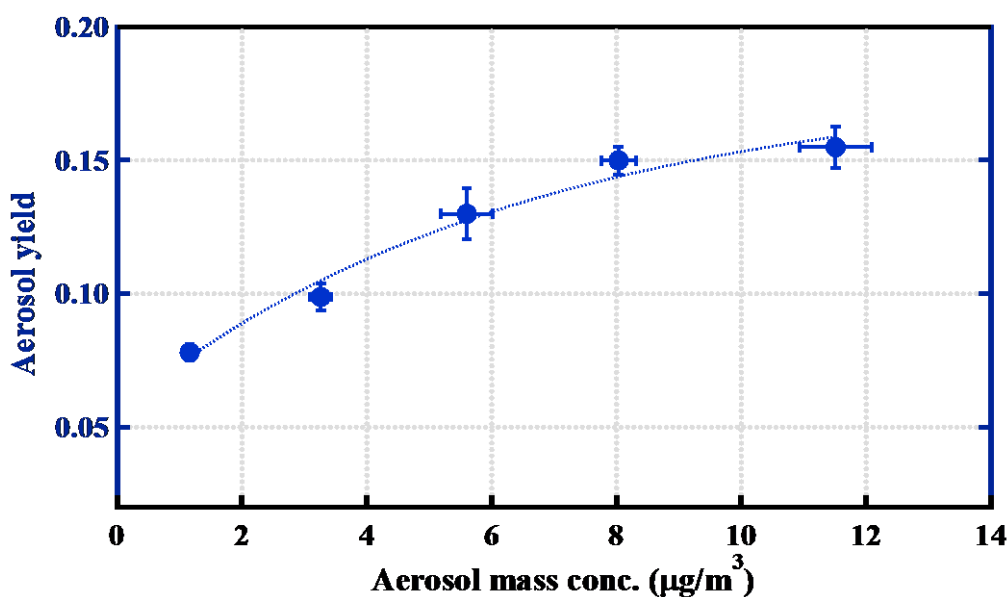


Figure 3-13: Plot of aerosol yield versus aerosol mass concentration. These data are for unseeded experiments. The dashed line represents the volatility basis set model fit.

Adding seed particles had the effect of significantly increasing the aerosol yield. For example, the unseeded experiment in Figure 3-1a had identical

reaction conditions to the seeded experiment in Figure 3-8b, yet the secondary aerosol mass concentration was a factor of 2 greater for the seeded experiment. The higher aerosol yield in the seeded experiment is likely a reflection on the kinetics of aerosol formation. In the unseeded experiment, particle formation was slow since it relied on formation of ring-opened species that represented a small fraction of the D₅ oxidation product yield. The consequence of slow particle formation would be a significant amount of time needed to reach a volume to surface area ratio that became favorable for dimer formation. In contrast, the aerosol volume to surface area ratio reached a favorable level much faster in the presence of seed particles, enhancing the formation of dimers through accretion chemistry and hence the amount of secondary aerosol produced within the residence time of the reactor. The higher aerosol yields of the seeded experiments may also reflect a smaller impact due to vapor wall loss than in the unseeded experiments.

3.6 Morphology of D₅-derived Aerosol

In the past a few years, a Thermophoretic Nanoparticle Sampler (TPS) has been designed and used to collect nanoparticles onto a standard STEM (scanning transmission electron microscope) grid^{38, 39}. After collection, nanoparticles on STEM grid are analyzed with an electron microscope and the resultant data used to determine the characteristics of aerosol sampled. Through the collaboration with Justin Krasnomowitz (Johnston research group) and RJ Lee Group Inc (Monroeville, Pennsylvania), aerosol produced from chamber reaction of D₅ in the absence and presence of seed were collected by TPS for ~30min respectively, particles were deposited on removable electron microscopy grid which caused by the temperature gradient within the sampler (110°C of hot plate and 25°C of cold plate). The elements observed in unseeded aerosol include C, O and Si while seeded aerosol contains C, O, Si, N and S indicating the ammonium sulfate seed particles are coated on the outside of D₅-derived liquid-like matter which enables

the formation of dimer in the particle phase. This result also provides confirmation of a spherical geometry for calculating aerosol surface area. However, additional data should be obtained under a wider range of experimental conditions, especially atmospheric relevant conditions.

3.7 Conclusion

This chapter shows that condensation, partitioning and particle phase chemistry (in this case accretion reactions) all contribute to secondary aerosol formation by gas phase D₅ oxidation. Condensation appears to be driven mainly by the formation of ring-opened products in the gas phase, though a few monomer oxidation products are also nonvolatile. Partitioning is dominated by monomer oxidation products, most of which are semivolatile. Dimers are nonvolatile but formed mainly by accretion reactions within the particle phase.

Future experiments should focus on accurate and precise measurements of aerosol yield. Since aerosol formation from D₅ oxidation is strongly influenced by accretion reactions, work is also needed to study this chemistry under a wider range of experimental conditions and particle phase morphologies that might be encountered in ambient aerosol. The work presented in this chapter was published in *Environmental Science and Technology* by Wu and Johnston in 2017⁴⁰

REFERENCES

- (1) Kroll, J. H.; Seinfeld, J. H. *Atmospheric Environment* **2008**, *42*, 3593-3624.
- (2) Wu, Y.; Johnston, M. V. *Journal of the American Society for Mass Spectrometry* **2016**, *27*, 402-409.
- (3) Fouquet, T.; Petersen, J.; Bomfim, J. A. S.; Bour, J.; Ziarelli, F.; Ruch, D.; Charles, L. *International Journal of Mass Spectrometry* **2012**, *313*, 58-67.
- (4) Cypryk, M.; Apeloig, Y. *Organometallics* **2002**, *21*, 2165-2175.
- (5) Rucker, C.; Kummerer, K. *Chemical Reviews* **2015**, *115*, 466-524.
- (6) Tu, P.; Johnston, M. V. *Atmospheric Chemistry and Physics* **2017**, *17*, 7593-7603.
- (7) Meyer, N. K.; Duplissy, J.; Gysel, M.; Metzger, A.; Dommen, J.; Weingartner, E.; Alfarra, M. R.; Prevot, A. S. H.; Fletcher, C.; Good, N.; McFiggans, G.; Jonsson, A. M.; Hallquist, M.; Baltensperger, U.; Ristovski, Z. D. *Atmospheric Chemistry and Physics* **2009**, *9*, 721-732.
- (8) Volkamer, R.; Ziemann, P. J.; Molina, M. J. *Atmospheric Chemistry and Physics* **2009**, *9*, 1907-1928.
- (9) Pathak, R. K.; Stanier, C. O.; Donahue, N. M.; Pandis, S. N. *Journal of Geophysical Research* **2007**, *112*.
- (10) Lambe, A. T.; Chhabra, P. S.; Onasch, T. B.; Brune, W. H.; Hunter, J. F.; Kroll, J. H.; Cummings, M. J.; Brogan, J. F.; Parmar, Y.; Worsnop, D. R.; Kolb, C. E.; Davidovits, P. *Atmospheric Chemistry and Physics* **2015**, *15*, 3063-3075.
- (11) Donahue, N. M.; Robinson, A. L.; Trump, E. R.; Riipinen, I.; Kroll, J. H. *Topics in Current Chemistry* **2014**, *339*, 97-143.
- (12) Donahue, N. M.; Robinson, A. L.; Stanier, C. O.; Pandis, S. N. *Environmental Science & Technology* **2006**, *40*, 2635-2643.
- (13) Chan, M. N.; Chan, A. W. H.; Chhabra, P. S.; Surratt, J. D.; Seinfeld, J. H. *Atmospheric Chemistry and Physics* **2009**, *9*, 5669-5680.
- (14) Donahue, N. M.; Epstein, S. A.; Pandis, S. N.; Robinson, A. L. *Atmospheric Chemistry and Physics* **2011**, *11*, 3303-3318.
- (15) Donahue, N. M.; Kroll, J. H.; Pandis, S. N.; Robinson, A. L. *Atmospheric Chemistry and Physics* **2012**, *12*, 615-634.

- (16) Nannoolal, Y.; Rarey, J.; Ramjugernath, D. *Fluid Phase Equilibria* **2007**, *252*, 1-27.
- (17) Nannoolal, Y.; Rarey, J.; Ramjugernath, D.; Cordes, W. *Fluid Phase Equilibria* **2004**, *226*, 45-63.
- (18) Robinson, A. L.; Donahue, N. M.; Shrivastava, M. K.; Weitkamp, E. A.; Sage, A. M.; Grieshop, A. P.; Lane, T. E.; Pierce, J. R.; Pandis, S. N. *Science* **2007**, *315*, 1259-1262.
- (19) Hall, W. A.; Johnston, M. V. *Aerosol Science and Technology* **2011**, *45*, 37-45.
- (20) Yan, W. Y.; Gardella, J. A.; Wood, T. D. *Journal of the American Society for Mass Spectrometry* **2002**, *13*, 914-920.
- (21) Liu, X. M.; Maziarz, E. P.; Heiler, D. J.; Grobe, G. L. *Journal of the American Society for Mass Spectrometry* **2003**, *14*, 195-202.
- (22) Faulhaber, A. E.; Thomas, B. M.; Jimenez, J. L.; Jayne, J. T.; Worsnop, D. R.; Ziemann, P. J. *Atmospheric Measurement Techniques* **2009**, *2*, 15-31.
- (23) Grayson, J. W.; Zhang, Y.; Mutzel, A.; Renbaum-Wolff, L.; Böge, O.; Kamal, S.; Herrmann, H.; Martin, S. T.; Bertram, A. K. *Atmospheric Chemistry and Physics* **2016**, *16*, 6027-6040.
- (24) Renbaum-Wolff, L.; Grayson, J. W.; Bateman, A. P.; Kuwata, M.; Sellier, M.; Murray, B. J.; Shilling, J. E.; Martin, S. T.; Bertram, A. K. *Proceedings of the National Academy of Sciences of the United States of America* **2013**, *110*, 8014-8019.
- (25) Laskina, O.; Morris, H. S.; Grandquist, J. R.; Qin, Z.; Stone, E. A.; Tivanski, A. V.; Grassian, V. H. *The Journal of Physical Chemistry. A* **2015**, *119*, 4489-4497.
- (26) Veghte, D. P.; Altaf, M. B.; Freedman, M. A. *Journal of the American Chemical Society* **2013**, *135*, 16046-16049.
- (27) Virtanen, A.; Kannosto, J.; Kuuluvainen, H.; Arffman, A.; Joutsensaari, J.; Saukko, E.; Hao, L.; Yli-Pirilä P.; Tiitta, P.; Holopainen, J. K.; Keskinen, J.; Worsnop, D. R.; Smith, J. N.; Laaksonen, A. *Atmospheric Chemistry and Physics* **2011**, *11*, 8759-8766.
- (28) Werner, J.; Dalirian, M.; Walz, M. M.; Ekholm, V.; Wideqvist, U.; Lowe, S. J.; Ohrwall, G.; Persson, I.; Riipinen, I.; Bjorneholm, O. *Environmental Science & Technology* **2016**, *50*, 7434-7442.
- (29) Hao, L. Q.; Romakkaniemi, S.; Yli-Pirilä P.; Joutsensaari, J.; Kortelainen, A.; Kroll, J. H.; Miettinen, P.; Vaattovaara, P.; Tiitta, P.; Jaatinen, A.; Kajos,

- M. K.; Holopainen, J. K.; Heijari, J.; Rinne, J.; Kulmala, M.; Worsnop, D. R.; Smith, J. N.; Laaksonen, A. *Atmospheric Chemistry and Physics* **2011**, *11*, 1367-1378.
- (30) Shilling, J. E.; Chen, Q.; King, S. M.; Rosenoern, T.; Kroll, J. H.; Worsnop, D. R.; McKinney, K. A.; Martin, S. T. *Atmospheric Chemistry and Physics* **2008**, *8*, 2073-2088.
- (31) Alfarra, M. R.; Hamilton, J. F.; Wyche, K. P.; Good, N.; Ward, M. W.; Carr, T.; Barley, M. H.; Monks, P. S.; Jenkin, M. E.; Lewis, A. C.; McFiggans, G. B. *Atmospheric Chemistry and Physics* **2012**, *12*, 6417-6436.
- (32) Clark, C. H.; Kacarab, M.; Nakao, S.; Asa-Awuku, A.; Sato, K.; Cocker, D. R., 3rd *Environmental Science & Technology* **2016**, *50*, 5564-5571.
- (33) Healy, R. M.; Temime, B.; Kuprovskite, K.; Wenger, J. C. *Environmental Science & Technology* **2009**, *43*, 1884-1889.
- (34) Safron, A.; Strandell, M.; Kierkegaard, A.; Macleod, M. *International Journal of Chemical Kinetics* **2015**, *47*, 420-428.
- (35) Coeur-Tourneur, C.; Tomas, A.; Guilloteau, A.; Henry, F.; Ledoux, F.; Visez, N.; Riffault, V.; Wenger, J. C.; Bedjanian, Y. *Atmospheric Environment* **2009**, *43*, 2360-2365.
- (36) Lambe, A. T.; Ahern, A. T.; Williams, L. R.; Slowik, J. G.; Wong, J. P. S.; Abbatt, J. P. D.; Brune, W. H.; Ng, N. L.; Wright, J. P.; Croasdale, D. R.; Worsnop, D. R.; Davidovits, P.; Onasch, T. B. *Atmospheric Measurement Techniques* **2011**, *4*, 445-461.
- (37) Odum, J. R.; Hoffmann, T.; Bowman, F.; Collins, D.; Flagan, R. C.; Seinfeld, J. H. *Environmental Science & Technology* **1996**, *30*, 2580-2585.
- (38) Leith, D.; Miller-Lionberg, D.; Casuccio, G.; Lersch, T.; Lentz, H.; Marchese, A.; Volckens, J. *Aerosol Science and Technology* **2013**, *48*, 81-89.
- (39) Sawvel, E. J.; Willis, R.; West, R. R.; Casuccio, G. S.; Norris, G.; Kumar, N.; Hammond, D.; Peters, T. M. *Atmospheric Environment* **2015**, *105*, 61-69.
- (40) Wu, Y.; Johnston, M. V. *Environmental Science & Technology* **2017**, *51*, 4445-4451

Chapter 4

SECONDARY AEROSOL FORMATION FROM OXIDATION OF DECAMETHYLOENTASILXOANE MIXED WITH β -PINENE

4.1 SOA from Biogenic and Anthropogenic Sources

It has been discussed in chapter 1 that volatile organic compounds (VOCs) are emitted into atmosphere from anthropogenic and biogenic sources. Anthropogenic VOC sources comprise organics such as alkanes, alkenes, aromatics and siloxanes, while biogenic sources include organics such as isoprene, monoterpenes and sesquiterpenes¹. The investigation of key physical and chemical processes during SOA formation in the atmosphere is complicated by the large number of species involved and their generally low concentrations. Globally, the production of biogenic SOA (BSOA) dominates over the anthropogenic (ASOA) with estimated fluxes of 88 and 10 TgC per year, respectively². As discussed by Hallquist et al. (2009)³ there are large uncertainties, but all global estimates indicate the production of BSOA to be significantly larger than ASOA (Spracklen et al., 2011; Kanakidou et al., 2005; Heald et al., 2010; Goldstein and Galbally, 2007)⁴⁻⁷. The formation of ASOA and BSOA could be influenced by each other. In some locations, ASOA can supersede BSOA². In several field observations, SOA has been attributed to originate from both biogenic and anthropogenic sources, and it seems that anthropogenic activities enhance BSOA abundance^{8,9}.

Several studies have stressed the potential of anthropogenic-biogenic interactions to be important for SOA formation^{4,10}. There are several potential ways of interactions, both directly by gas-particle chemistry and physics, and indirectly by anthropogenic influence on the emission rates of biogenic VOCs². Hildebrandt et al. found that anthropogenic-biogenic SOA derived from mixtures

of AVOC and BVOC can be treated as ideal mixtures¹¹. The yields can be parameterized applying the assumption of a common organic phase for partitioning¹¹. In the atmosphere there are a number of interesting issues regarding SOA formation from mixed air masses where typical anthropogenic precursors behave differently compared to biogenic precursors¹¹.

Reaction chambers can be used to produce controlled atmospheres to investigate a range of physical phenomena from the formation of gas-phase reaction products to the partitioning of semi-volatile compounds between the gas and particle phase¹². Such experiments can be useful in understanding the chemical and physical parameters that control the formation of secondary organic aerosols. A number of reaction chamber studies have investigated gas-particle partitioning of products of photochemical reactions involving anthropogenic as well as biogenic precursors¹². Much of the effort has been directed toward quantifying the aerosol formation potential (aerosol yield) of small aromatic and natural hydrocarbon compounds both in the absence and presence of seed aerosol particles¹³. Other studies have attempted to identify the molecular composition of the oxidation products of anthropogenic and biogenic precursors, mainly aromatic and monoterpene compounds, and have offered detailed reaction mechanisms for the formation of various chemical species¹². However, relatively little effort has been made to study the influence of BSOA on ASOA, and the effect is still not well understood.

Aerosol formation products and mechanisms from OH oxidation of D₅ which is a certain type of ASOA has been discussed in detail at the molecular level in Chapters 2 and 3. Although there is a potential to produce siloxane-derived aerosol in ambient air, aerosol formation is complicated due to a low concentration of the D₅ precursor and relatively higher abundance of biogenic SOA under atmospherically relevant conditions. As a result, in this chapter, a mass spectrometric study of secondary organic aerosols formed from the

photo-oxidation of mixed D₅ and β-pinene precursors in the photo-oxidation chamber will be investigated.

4.2 Aerosol Generation from Photo-oxidation of D₅ and β-pinene

The experimental setup for generating secondary aerosol was identical to that discussed in Section 3.2. Similarly, before each experiment, the PC was cleaned by exposure to 20 ppmv ozone in the presence of ultraviolet radiation for at least 48 hr and flushed continuously with clean, dry, air for 4-5 days obtained from a Zero-Air generation system (Model 737, Aadco, Cleves, Ohio). A Scanning Mobility Particle Sizer (SMPS; Model 3080/3078, TSI, St. Paul, Minnesota) was used to measure particle size distributions.

To better control the amount of precursor sent into the chamber, a syringe pump (Model No. 55-1199, Harvard Apparatus, Holliston, Massachusetts) was used to feed precursor fluid at a rate of 0.1 μL/min into an air flow through a gently heated Teflon fitting. D₅/methanol solution was mixed with β-pinene (CAS No. 18172-67-3, Sigma-Aldrich, Louis, Missouri) to a volume ratio of 1/5/0.25 (D₅/methanol/β-pinene). This airflow was then diluted to adjust the initial concentration of precursor and a constant flow of the diluted air was sent into the PC. Ozone was generated by passing clean air around a mercury lamp (Model No.81-1025-01, BHK Inc., Ontario, California). The ozone laden air was then bubbled through deionized water and sent into the PC where interaction with ultraviolet radiation produced OH. Another make up air flow was added and adjusted to maintain the same residence time at 15 min in the PC. All experiments were performed with low relative humidity (typically 8-10%) and a temperature of 27 °C. Table 4-1 summarizes four experiments that were performed in the absence of seed aerosol. Particulate matter in the air flow exiting the PC was collected and analyzed with the same procedures discussed in Chapter 3. Mass analysis was performed by direct infusion ESI on a Q-Exactive

hybrid Quadrupole-Orbitrap mass spectrometer with full scan MS and MS/MS modes.

Expt. No.	Initial precursor conc. (ppbv) ^a		Estimated reacted precursor conc. (ppbv) ^b		ΔM ($\mu\text{g}/\text{m}^3$) ^c	Volume/Surface Area (nm) ^d
	D ₅	β -pinene	D ₅	β -pinene		
1	5.2	1.3	0.9	1.3	1.0 \pm 0.2	13.1 \pm 0.8
2	5.4	1.4	1.1	1.4	2.1 \pm 0.1	13.8 \pm 0.3
3	7.7	1.9	1.9	1.9	4.9 \pm 1.2	18.0 \pm 0.9
4	10.7	2.7	2.8	2.7	10.2 \pm 1.2	26.7 \pm 1.3

a: D₅ and β -pinene initial precursor concentration.

b: D₅ and β -pinene reacted precursor concentration which estimated from [OH] concentration. [OH]: 1.5×10^8 molecules cm^{-3} ; [O₃]: 6.0×10^8 molecules cm^{-3}

c: Secondary aerosol mass concentration.

d: Volume and surface area of the aerosols were calculated from measured number size distributions by SMPS.

Table 4-1: Experimental conditions for secondary aerosol formation from OH oxidation of D₅ and β -pinene. ΔM is the aerosol mass concentration.

4.3 Chemical Composition of Aerosol Formation in Mixed System

4.3.1 Molecular Characterization of Mixed Aerosol

Figure 4-1 shows the representative positive ion mass spectra averaged over replicate samples for four aerosol mass loadings. Molecular products can be divided into three main types according to formula assignment from high resolution mass analysis. First are β -pinene SOA products coded as red; second are D₅-derived products coded as blue. Third are “mixed products”, defined as products arising from a combination of β -pinene and D₅ oxidation coded as black. Specifically, the mixed products contain silicon, but are not observed as products from either D₅ or β -pinene oxidation alone, for example m/z 299.111 assigned as $\text{C}_{11}\text{H}_{24}\text{O}_4\text{NaSi}_2^+$. Typically, only one or two silicon atoms were observed within

the mixed product formulas. More details of mixed products will be discussed later in this chapter. It has been reported that the rate constant of gas phase β -pinene and D₅ with OH radical to be $\sim 7.9 \times 10^{-11}$, and 2.6×10^{-12} cm³ molecule⁻¹ s⁻¹ respectively^{14,15}. And the rate constant¹⁶ of ozonolysis of gas phase β -pinene was reported to be $\sim 2.1 \times 10^{-17}$ cm³ molecule⁻¹ s⁻¹, estimated reacted concentration from ozonolysis is calculated to be negligible compared to OH oxidation. Therefore, as shown in Table 4-1, almost 100% of β -pinene was reacted while only $\sim 20\%$ of D₅ reacted with OH radical. As shown in Figure 4-1, β -pinene SOA represents more than 85% of overall mass weighted signal intensity of total observed products no matter how the aerosol mass loading varies, while D₅-derived aerosol consists of about 5% of the signal intensity, and the rest (about 10%) is attributed to mixed products. One possible reason is D₅ products are diluted within the particle phase (mostly β -pinene SOA), and therefore there is much less oligomerization.

In this chapter, I will mainly focus on D₅-derived reaction products under various aerosol mass loadings (blue ions in Figure 4-1). For consistency with Chapter 3, when I make plots of D₅ products, as shown Figure 4-2a, I will revert to the color coding in Chapter 3 where monomer products are coded red, dimer products are coded black and ring-opened products are coded blue.

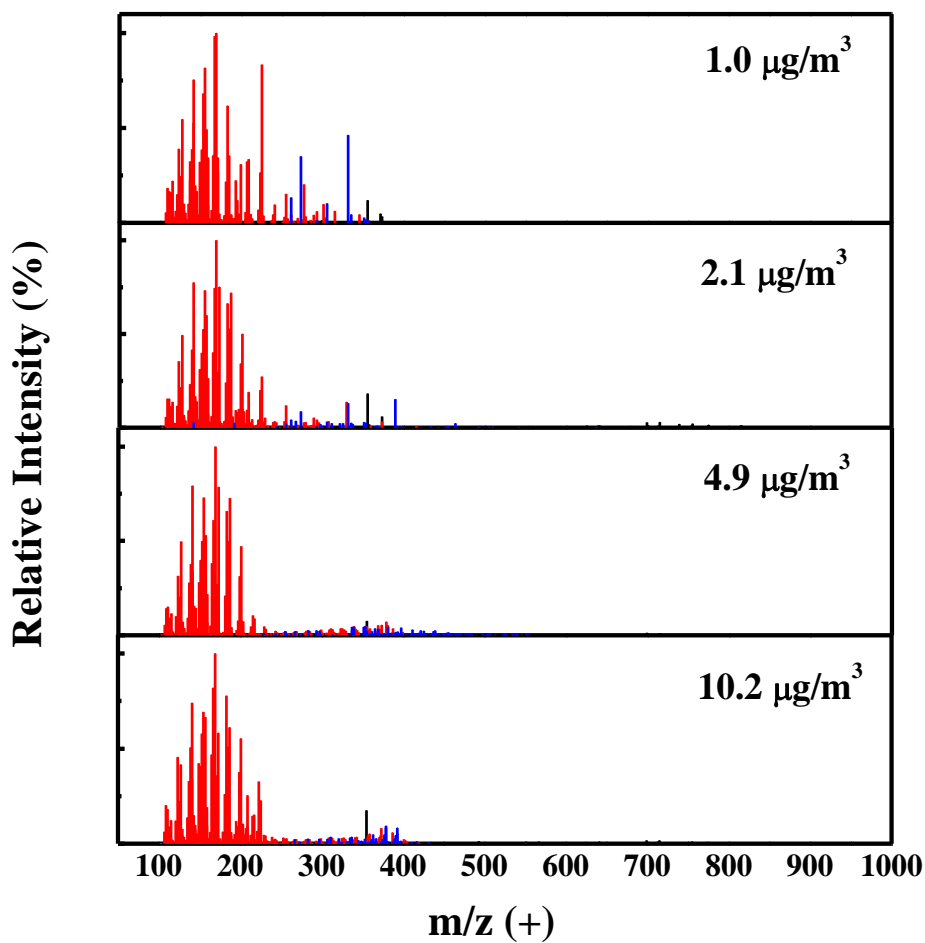


Figure 4-1: ESI mass spectra in positive ion mode of secondary aerosol from mixed D_5 and β -pinene oxidation under various aerosol mass loadings. Ion signal intensities are averaged over four separate measurements from four different samples. Peaks considered D_5 -derived aerosol are coded blue, β -pinene SOA are coded red, and mixed products are coded black. Note that the color coding in this figure is different from that in Chapter 3 and for most Figures that follow in Chapter 4.

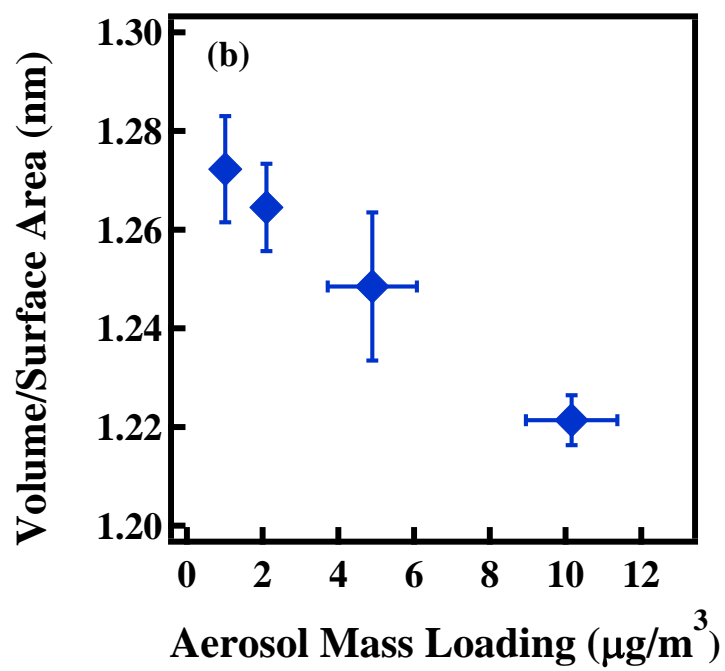
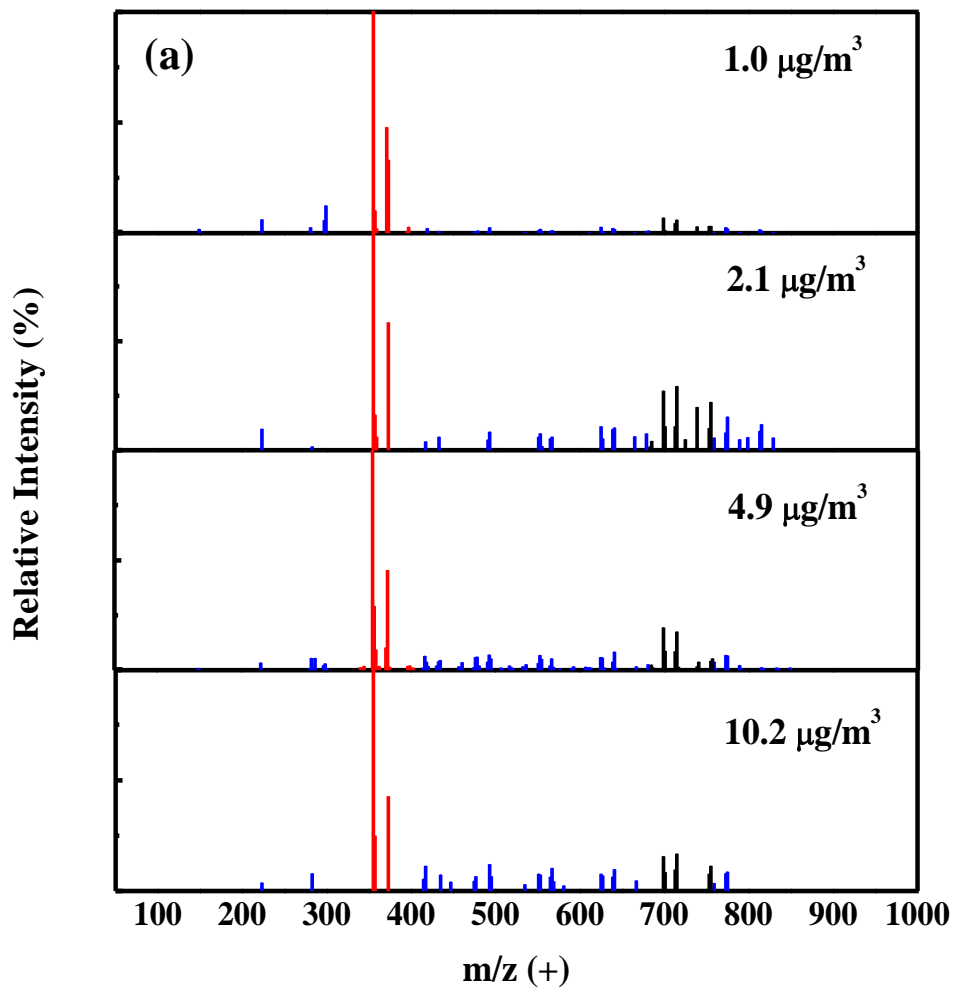


Figure 4-2: a) ESI mass spectra in positive ion mode of oxidation products of D₅ observed in secondary aerosol from the mixed precursor experiments. Ion signal intensities are averaged over four separate measurements from four different samples. Peaks considered as ring opened products are coded blue, dimers are coded black, and monomers are coded red. The relative abundance is ranged from 0 to 15%; b) Plot of average O/Si as a function of aerosol mass loadings.

4.3.2 Chemical Composition of Mixed Aerosol

The mass weighted signal intensity fractions (MIF)¹⁷ analysis is used to calculate the average O/Si and C/Si ratios of aerosol produced under various mass loadings for all experiments (unseeded, seeded and mixed). Figure 4-2b represents the plot of average O/Si as function of aerosol mass loadings. The effect of aerosol mass loading on the chemical composition as shown by e.g. Shilling et al. (2009), is very pronounced¹⁸. Apparently, with increase mass concentration less oxidized (more volatile) compounds tend to partition to the particle phase which generally give lower O/Si ratio as described¹⁸. Figure 4-3 shows the chemical composition of D₅-derived aerosol as O/Si and C/Si ratios plotted against each other. For similar aerosol mass loadings, the mixed aerosol is the least oxidized, the unseeded aerosol is the most oxidized, and the seeded aerosol is overlapped in between. The relative contribution of ring opened species, monomers and dimers were analyzed respectively for different experimental conditions. Particularly in the mixed aerosol, a much higher amount of monomers was observed. It is not surprising because the β -pinene SOA matrix with larger volume would promote the partitioning of those semi-volatile monomers, finally resulting in much higher O/Si elemental ratio. Additionally, the black dashed line shown in Figure 4-3 indicates OH substitutions on siloxane, red dashed line is the CH₂OH substitutions and average elemental composition under various experimental conditions. Both of OH and CH₂OH substitutions influence the deviation of the experimental data from the dashed lines. Specifically, average O/Si (~1.2) of mixed aerosol suggests one OH substitution, while average O/Si (~1.4) of single aerosol suggests two OH substitutions. It is also consistent with the fact that the one OH substituted siloxane tends to partition between the particle and gas phases, while the two OH substituted siloxane is nonvolatile and found in the particle phase only¹⁹.

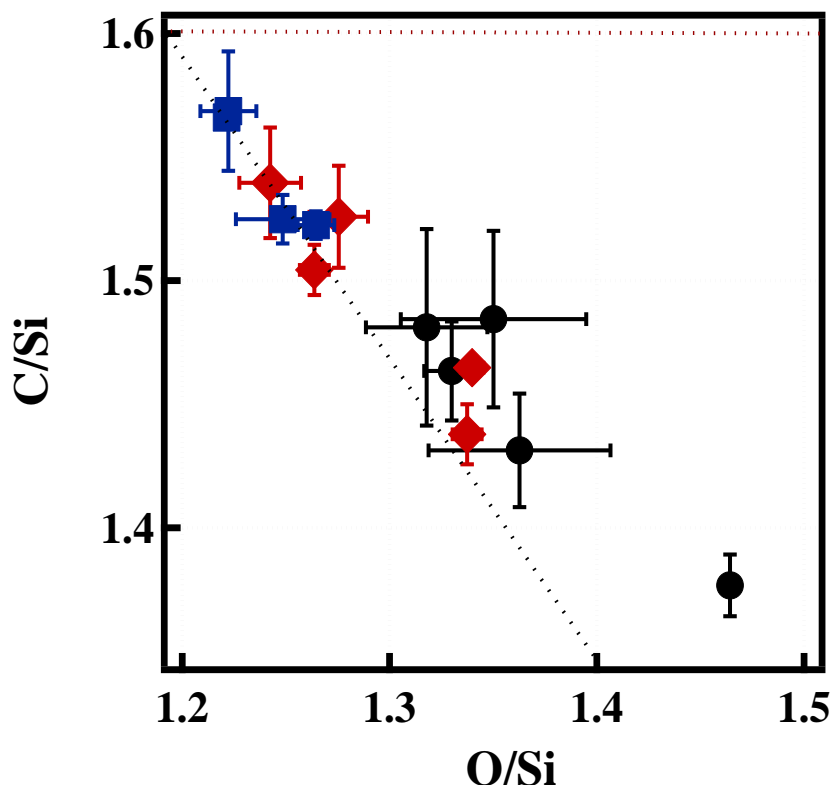


Figure 4-3: Plot of C/Si versus O/Si showing chemical composition of unseeded (black), seeded (red) and mixed (blue) experiments. The black dashed line represents OH substitutions on siloxane ($\text{CH}_3 \rightarrow \text{OH}$); the red dashed line represents CH_2OH substitutions on siloxane ($\text{CH}_3 \rightarrow \text{CH}_2\text{OH}$).

4.4 Aerosol Formation from of Mixed Conditions

4.4.1 Aerosol Yield Expression

Aerosol yield of the precursor mixture is calculated from the total reacted precursor mass concentration:

$$Y = \frac{M}{\Delta\beta\text{-pinene} + \Delta D_5}$$

As a result, aerosol yields are compared for mixed and single siloxane experiments and shown in Figure 4-4. Figure 4-1 shows that most of the products detected are from β -pinene oxidation. However, elemental composition derived from Nano Aerosol Mass spectrometer (discussed in Section 2.1) needs to be confirmed, to eliminate any possibilities that electrospray is more sensitive to β -pinene products. Generally, for β -pinene and D_5 experiment the yield is consistently lower than single D_5 experiment indicating that β -pinene suppresses

aerosol growth by D₅ oxidation. To investigate the deviations from the yield, I compared the aerosol size distributions in the different experiments by plotting the volume to surface area ratio as a function of aerosol mass loading in Figure 4-5. At relatively lower mass concentrations, mixed aerosol represents a higher volume to surface area ratio indicating large size of the particles, and a lower volume to surface area ratio at higher aerosol mass loadings indicating smaller size of the particles. This suggests that nucleation is suppressed by β -pinene (fewer number of particles for a given aerosol mass). Also, the two plots cross suggesting that growth by D₅ oxidation is more efficient than in the mixed case. To form particles, a sufficient concentration of low volatility products must be formed. β -pinene on the other hand produces much less low volatility material that is able to induce nucleation¹⁹. The effect of β -pinene SOA on mixtures can be explained from the reactor dynamics. The concentration of nucleating vapours from D₅ may therefore initially be suppressed due to β -pinene consumption of OH, even though the integral OH-exposure was not influenced. With a slower initial production and consequent lower concentrations, these vapors will be more likely to condense on existing particles rather than forming nucleation clusters. This will lower the total number concentration exiting the reactor while SOA mass is kept constant if the integrated OH exposure is not changed²⁰. The yields are also affected by the fate of the low volatility organic compounds (LVOCs) that are produced by precursor oxidation. These LVOCs can react with OH, stick to the walls, exit the reactor or condense onto particles.

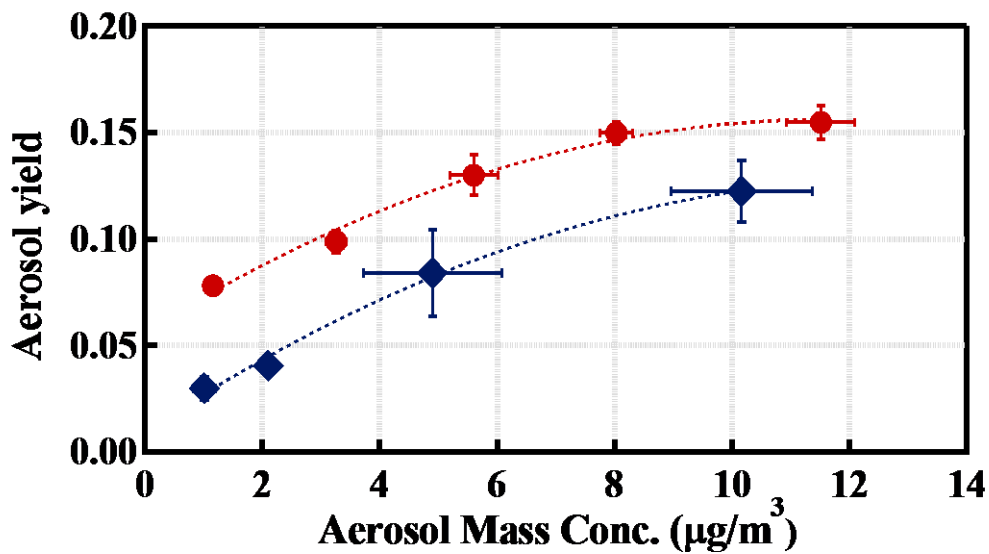


Figure 4-4: Plot of aerosol yield versus aerosol mass concentration of single siloxane experiment (red) and mixed experiment (blue) respectively.

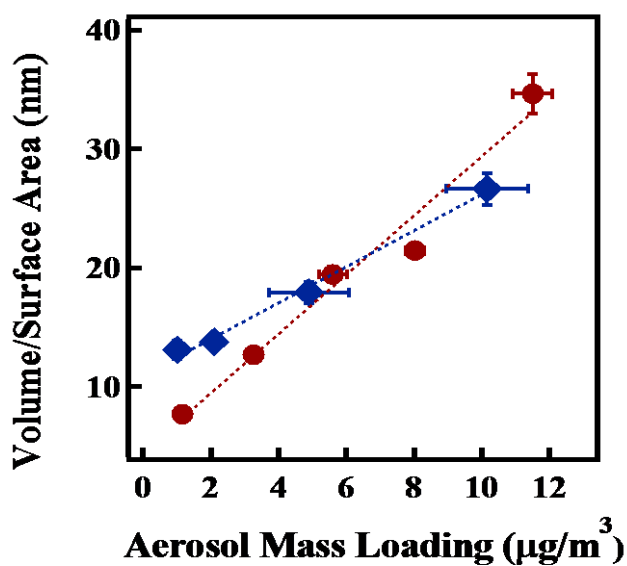


Figure 4-5: Volume-to-surface area ratio vs. mass loading for the single siloxane experiments (red) and mixed experiments (blue) studied in this work. Error bars represent one standard deviation. Error bars smaller than the symbol are not shown.

Figure 4-6a then shows the ratio of the summed signal intensities of dimers to ring-opened products plotted as a function of aerosol volume to surface area ratio. The relationship is approximately linear, and the mixed aerosol shows a higher

ratio compared to the single siloxane aerosol, suggesting the formation of dimers is more favored in the mixed oxidation system. This is not surprising the aerosol produced by β -pinene oxidation could serve as the condensed phase volume needed to promote the particle phase reaction (dimerization) of D_5 oxidation products. Figure 4-6b shows ratio of the summed signal intensities of monomers to dimers as a function of particle volume to surface area ratio. The signal intensity ratio is much higher in mixed oxidation system especially at very high aerosol mass loadings, which is consistent with the fact that D_5 -derived aerosol consists of monomers as the highest portion. This is also confirmed with the discussion in Section 4.3.2, because most of the aerosol is from β -pinene resulting in larger aerosol volume that monomers can partition into. In contrast, in the unseeded experiments, the aerosol volume is entirely siloxane derived. Therefore, it would be expected a higher fraction of monomers in the mixed experiment than in the unseeded experiment.

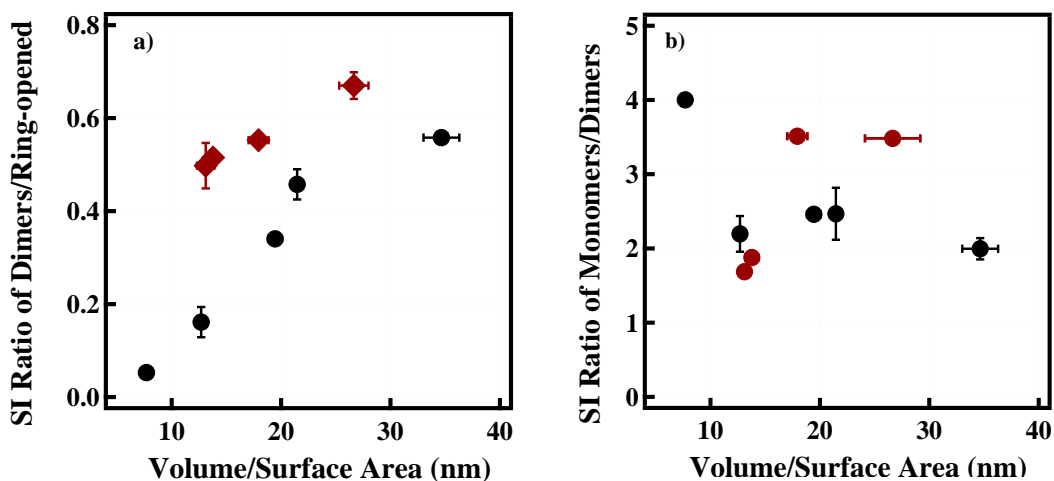


Figure 4-6: Signal intensity ratio of a) dimers to ring-opened products and b) monomers to dimers vs. volume/surface area ratio of the secondary aerosol. Unseeded aerosol coded black and mixed aerosol coded red. Error bars represent one standard deviation. Error bars smaller than the symbols are not shown

4.4.2 Product Volatility Estimation

Figure 4-7 then provides insight into the contributions of different volatility species to aerosol produced under different experimental conditions (a-unseeded, b-seeded and c-mixed). More non-volatile matters are observed in unseeded aerosol and since partitioning of SVOC and IVOC increases in seeded and mixed aerosol. Figure 4-7a shows that the majority of nonvolatile matter ($\log C^* < -2$) in unseeded aerosol consists of ring-opened products with a minor contribution from dimers, while more dimers are observed in the seeded and mixed aerosol which is shown in Figure 4-7b, c. This observation is not surprising since ring-opened species are needed for particle formation and/or early growth in an unseeded experiment but not in the presence of seeds or β -pinene SOA. The fraction of intermediate volatility monomers is highest in the mixed experiment, which mainly consists of monomers, suggesting that monomers tend to partition more into those non-siloxane volumes.

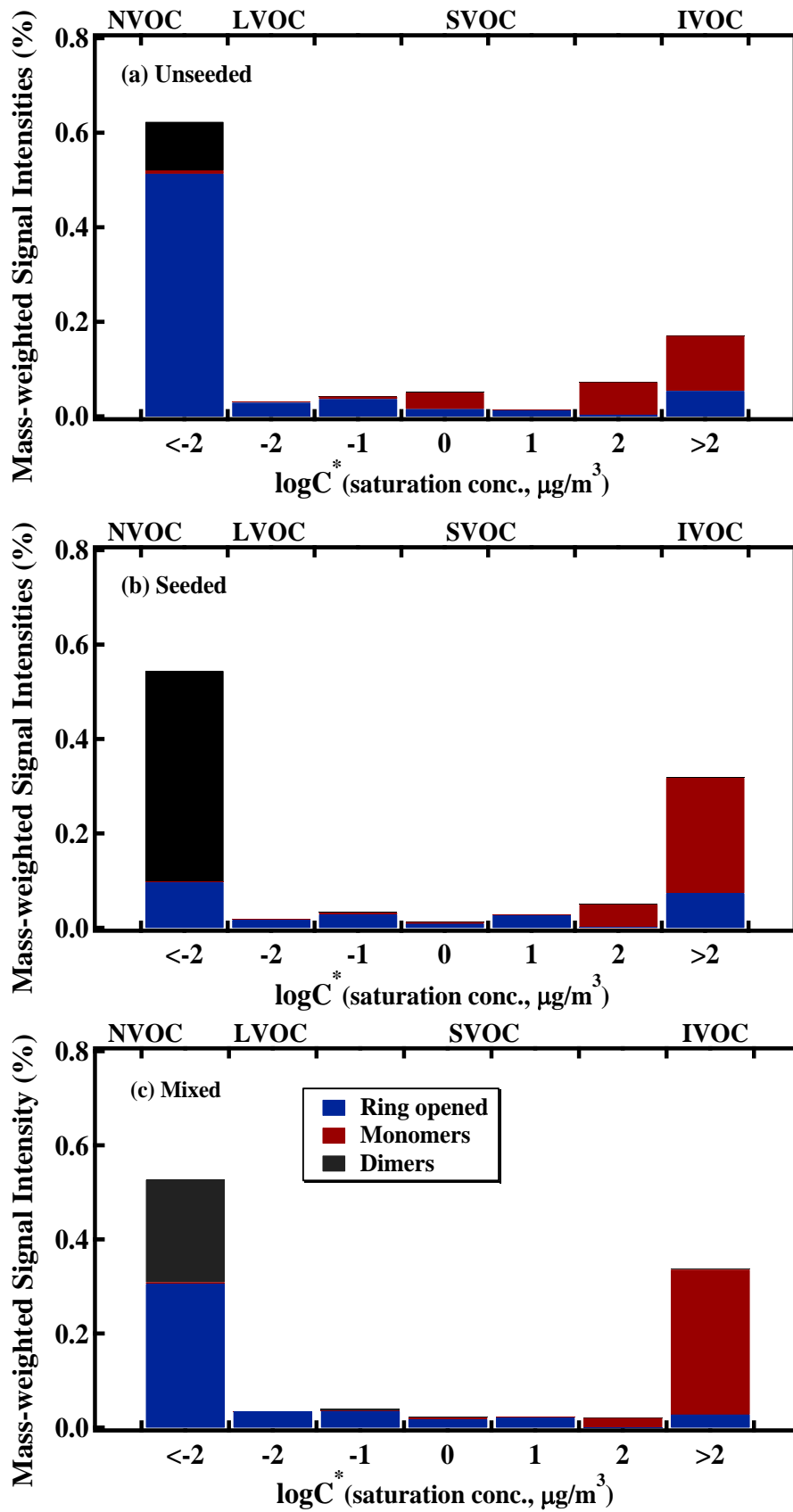


Figure 4-7: Mass-weighted signal intensities summed over the three types of ions in a) unseeded, b) seeded and c) mixed aerosols vs. $\log C^*$ for candidate structures that correspond to individual ions. These plots are for assigned ions in the mass spectra of Figure 3-6a, b and Figure 4-2c, respectively. Ring-opened products are coded blue, dimers are coded black, and monomers are coded red.

4.4.3 Chemically Resolved Partitioning

A view of chemically-resolved gas-particle partitioning can be obtained from the high resolution mass spectra. A volatile basis-set model would be used to parameterize the empirical formulas of those basis-set products normalized to one silicon atom¹⁷. Basically, the empirical formulas $(O/Si)_i$ and $(C/Si)_i$ of the basis-set products i are related to $(O/Si)_j$ and $(C/Si)_j$ measured at each aerosol mass loading j by applying following equations,

$$(O/Si)_j = \frac{\sum_i f_{i,j} \lambda_i (O/Si)_i}{\sum_i f_{i,j} \lambda_i}, (C/Si)_j = \frac{\sum_i f_{i,j} \lambda_i (C/Si)_i}{\sum_i f_{i,j} \lambda_i}, (H/Si)_j = \frac{\sum_i f_{i,j} \lambda_i (H/Si)_i}{\sum_i f_{i,j} \lambda_i}$$

where λ_i is the silicon molinity, defined as the moles of silicon of product i per kilogram of product i . In the case of siloxane-derived aerosol of composition $C_x H_y O_z Si_f$ and no other elements, we could express

$\lambda_i = 1000 / [28 + 16(O/Si)_i + 12(C/Si)_i + (H/Si)_i]$. The mass fraction $f_{i,j}$ is then obtained from the basis-set parameterization of aerosol yield. The particle phase partial mass yield $\xi_{i,j}$ at loading C_j is given by $\xi_{i,j} = \alpha_i (1 + C^*_i / C_j)^{-1}$, where C^*_i belongs to $[10^{-2}, 10^{-1}, 10^0, 10^1 \dots \mu\text{g}/\text{m}^3]$ and α_i is the aerosol mass yield of product i ¹⁷. As a result, at each mass loading C_j , the relative concentration of product i in the particle phase on a mass fraction basis as follows: $f_{i,j} = \xi_{i,j} (\sum_{i=1}^4 \xi_{i,j})^{-1}$. According to the estimated volatility distribution (See Chapter 3), C^* is chosen as 0.01, 1 and 100 $\mu\text{g}/\text{m}^3$ respectively representing one NVOC, SVOC and IVOC. Eventually, the empirical formulas of basis-set products are shown in Table 4-2 for unseeded and mixed aerosol respectively.

	C* _i (μg/m ³)	α _i		(O/Si) _i		(C/Si) _i		Formulas	
		Unseeded	Mixed	Unseeded	Mixed	Unseeded	Mixed	Unseeded	Mixed
Product 1	0.01	0.02	0.01	1.70	1.34	1.30	1.30	C _{1.3} O _{1.7} Si	C _{1.3} O _{1.3} Si
Product 2	1	0.09	0.01	1.40	1.34	1.40	1.31	C _{1.4} O _{1.4} Si	C _{1.3} O _{1.3} Si
Product 3	100	0.53	1.07	1.13	1.20	1.69	1.54	C _{1.7} O _{1.1} Si	C _{1.5} O _{1.2} Si

Table 4-2: Three model products *i* describing the partitioning of D₅-derived aerosol molecules between the gas and particle phases. Shown are the mass yield α_{*i*}, the decadal volatility C*_{*i*} (μg/m³), the atomic ratios (O/Si)_{*i*} and (C/Si)_{*i*}, and the corresponding empirical formulas on a one-silicon basis.

After comparison, product 1 is much more highly oxidized in unseeded aerosol considering to be NVOC; both of product 2 (SVOC) and product 3 (IVOC) show similar chemical compositions. According to the molecular characterization and estimated volatility results, in unseeded aerosol, three empirical products are thought to be C₁₃H₄₄O₁₆Si₁₀, C₁₀H₃₀O₁₁Si₈ and C₉H₂₈O₆Si₅; while in mixed aerosol, three empirical products are thought to be C₁₄H₄₂O₁₃Si₁₀, C₁₀H₃₀O₁₁Si₈ and C₉H₂₈O₆Si₅. Additionally, chemical composition of mixed aerosol is mainly dominated by product 3 which presents a greatly highest mass yield relative to the rest of the other two. This is also consisted with the fact that no obvious aerosol mass loading dependent relationship is observed in mixed aerosol.

4.5 MS/MS Analysis for Structure Identification of ‘Mixed Products’

As mentioned in section 4.3, besides β-pinene SOA and D₅-derived aerosol, a third type of mixed products is observed in mixed oxidation condition as well. Figure 4-8 shows the average representative mass spectra of mixed products at various aerosol mass loadings. In order to understand the aerosol formation mechanism in the mixed oxidation system, chemical structure of mixed products is studied by performing MS/MS experiments.

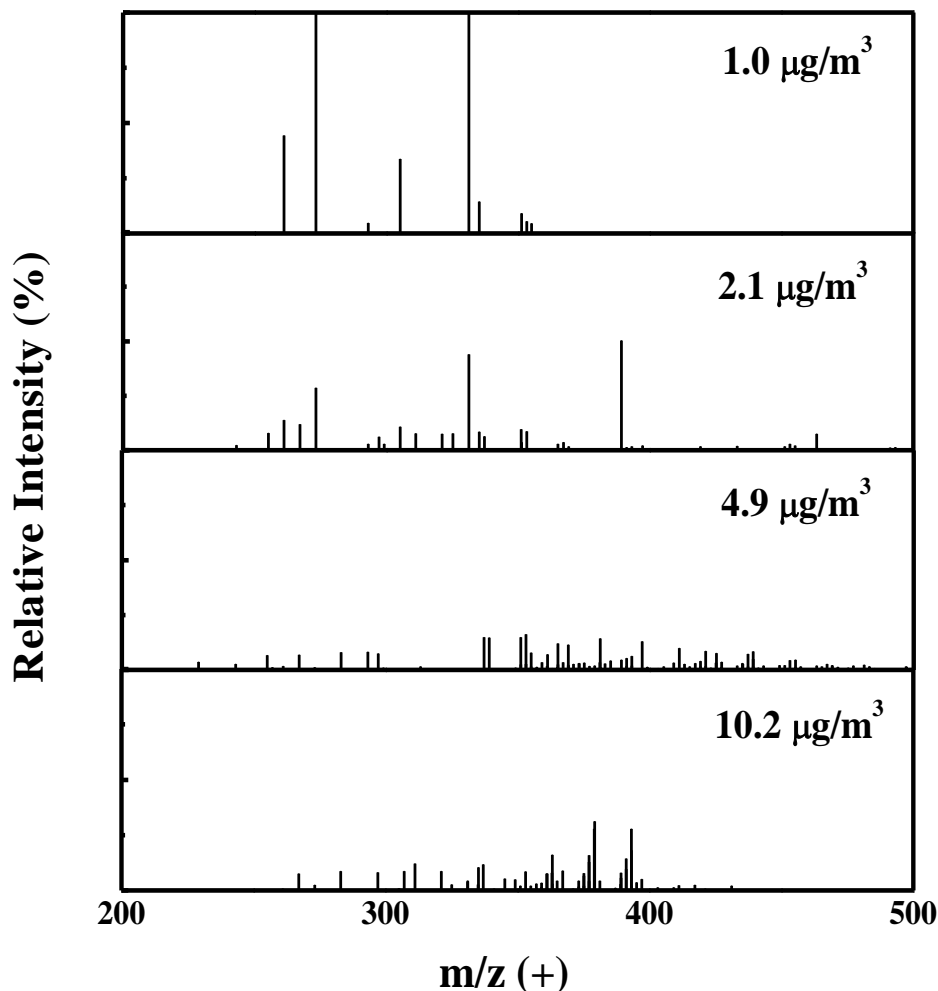


Figure 4-8: ESI mass spectra in positive ion mode of mixed products. Ion signal intensities are averaged over four separate measurements from four different samples. The relative abundance is ranged from 0 to 30%.

Figure 4-9 shows ESI-MS/MS spectra of the $C_{11}H_{24}O_4Si_2$ neutral product in positive ion mode, which is considered as combination of β -pinene (structure shown in Figure 4-9) SOA and D_5 -derived aerosol building blocks. This precursor was chosen not only because of relatively higher signal intensity, but also because the formula contains smaller number of Si, which rules out more complexity. Based on the chemical composition of D_5 -derived aerosol building block, which more likely to be a ring-opened species with/without OH substitutions on it. And after subtracting the composition of siloxane, the rest would be considered as β -pinene SOA building block. As shown in Figure 4-9a, H_2O is observed as neutral loss for twice suggesting that there are at least two

O-containing functional groups (especially -OH). There are multiple combinations and one possible representative structure is shown in Figure 4-9b especially fragment ions, $C_7H_{11}O^+$ and $C_4H_{12}O_3Si_2^+$ are observed (Figure 4-9a); No mixed products were observed containing oligomers produced from either β -pinene or D_5 . It indicates that the oligomerization of β -pinene and D_5 are different and not comparable with each other.

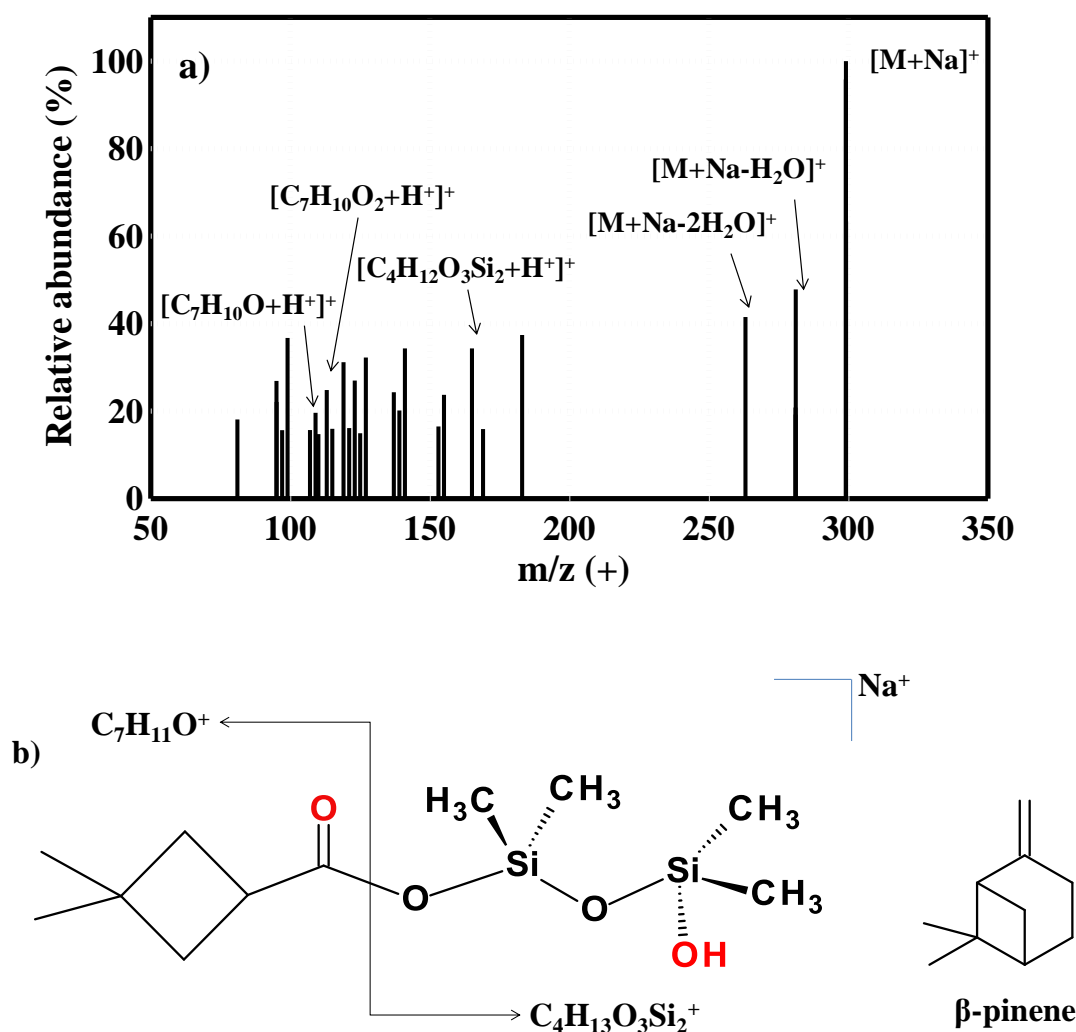


Figure 4-9: Product ion spectrum of 299 m/z (+). a) Complete product ion spectrum. b) Representative chemical structure of isolated precursor and β -pinene.

4.6 Conclusions

This chapter discussed a set of mixed OH oxidation experiments in a photo-oxidation chamber, using β -pinene (biogenic) and D₅ (anthropogenic) as precursors. The SOA mass yields and chemical compositions from single D₅ experiments are compared even though no correction was made for wall losses. For two component mixtures containing D₅ and β -pinene, respectively, the aerosol yields are slightly lower than the single D₅ experiment indicating the formation of D₅-derived aerosol is superseded by β -pinene SOA due to aerosol dynamics.

The main products produced in mixed condition are from β -pinene oxidation representing ~80% of mass weighted intensity fraction. Chemical compositions of D₅-derived aerosol were characterized in terms of elemental ratios, especially O/Si and C/Si, by high-resolution mass spectrometry. The results showed that aerosol generated from mixtures was much less oxidized than unseeded aerosol. That is because a much higher amount of volatile monomers tend to partition to the particle phase in the presence of large β -pinene SOA matrix.

The elemental ratios were also studied on a molecule by molecule base and accurately parameterized by a three-product basis set of decadal volatility (0.01, 1, 100 $\mu\text{g}/\text{m}^3$). Those employing products having empirical formulas of C₁₃H₄₄O₁₆Si₁₀, C₁₀H₃₀O₁₁Si₈ and C₉H₂₈O₆Si₅ in unseeded aerosol; while in mixed aerosol, three empirical products are thought to be C₁₄H₄₂O₁₃Si₁₀, C₁₀H₃₀O₁₁Si₈ and C₉H₂₈O₆Si₅. It is not surprising because β -pinene SOA would be generated first serving as seed particles to promote the partitioning of more semi-volatile products. The role as seed of β -pinene SOA with higher volume to surface area ratio is also convinced by the product volatility estimation showing that more dimers were observed. Finally mixed products were analyzed by high-resolution MS/MS which confirms that those mixed products consist of D₅ and β -pinene SOA fragments. No oligomers consisting of intact D₅ and β -pinene

monomers were observed among mixed products suggested that the condensed phase oligomerization of D₅ and β-pinene oxidation products are not compatible.

REFERENCES

- (1) Baltensperger, U.; Kalberer, M.; Dommen, J.; Paulsen, D.; Alfarra, M. R.; Coe, H.; Fisseha, R.; Gascho, A.; Gysel, M.; Nyeki, S.; Sax, M.; Steinbacher, M.; Prevot, A. S. H.; Sjögren, S.; Weingartner, E.; Zenobi, R. *Faraday Discussions* **2005**, *130*, 265.
- (2) Emanuelsson, E. U.; Hallquist, M.; Kristensen, K.; Glasius, M.; Bohn, B.; Fuchs, H.; Kammer, B.; Kiendler-Scharr, A.; Nehr, S.; Rubach, F.; Tillmann, R.; Wahner, A.; Wu, H. C.; Mentel, T. F. *Atmospheric Chemistry and Physics* **2013**, *13*, 2837-2855.
- (3) Hallquist, M.; Wenger, J. C.; Baltensperger, U.; Rudich, Y.; Simpson, D.; Claeys, M.; Dommen, J.; Donahue, N. M.; George, C.; Goldstein, A. H.; Hamilton, J. F.; Herrmann, H.; Hoffmann, T.; Iinuma, Y.; Jang, M.; Jenkin, M. E.; Jimenez, J. L.; Kiendler-Scharr, A.; Maenhaut, W.; McFiggans, G.; Mentel, T. F.; Monod, A.; Prevot, A. S. H.; Seinfeld, J. H.; Surratt, J. D.; Szmigielski, R.; Wildt, J. *Atmospheric Chemistry and Physics* **2009**, *9*, 5155-5236.
- (4) Spracklen, D. V.; Jimenez, J. L.; Carslaw, K. S.; Worsnop, D. R.; Evans, M. J.; Mann, G. W.; Zhang, Q.; Canagaratna, M. R.; Allan, J.; Coe, H.; McFiggans, G.; Rap, A.; Forster, P. *Atmospheric Chemistry and Physics* **2011**, *11*, 12109-12136.
- (5) Kanakidou, M.; Seinfeld, J. H.; Pandis, S. N.; Barnes, I.; Dentener, F. J.; Facchini, M. C.; Van Dingenen, R.; Ervens, B.; Nenes, A.; Nielsen, C. J.; Swietlicki, E.; Putaud, J. P.; Balkanski, Y.; Fuzzi, S.; Horth, J.; Moortgat, G. K.; Winterhalter, R.; Myhre, C. E. L.; Tsigaridis, K.; Vignati, E.; Stephanou, E. G.; Wilson, J. *Atmospheric Chemistry and Physics* **2005**, *5*, 1053-1123.
- (6) Heald, C. L.; Kroll, J. H.; Jimenez, J. L.; Docherty, K. S.; DeCarlo, P. F.; Aiken, A. C.; Chen, Q.; Martin, S. T.; Farmer, D. K.; Artaxo, P. *Geophysical Research Letters* **2010**, *37*.
- (7) Goldstein, A. H.; Galbally, I. E. *Environmental Science & Technology* **2007**, *41*, 1514-1521.
- (8) Aiken, A. C.; Salcedo, D.; Cubison, M. J.; Huffman, J. A.; DeCarlo, P. F.; Ulbrich, I. M.; Docherty, K. S.; Sueper, D.; Kimmel, J. R.; Worsnop, D. R.; Trimborn, A.; Northway, M.; Stone, E. A.; Schauer, J. J.; Volkamer, R. M.; Fortner, E.; de Foy, B.; Wang, J.; Laskin, A.; Shutthanandan, V.; Zheng, J.; Zhang, R.; Gaffney, J.; Marley, N. A.; Paredes-Miranda, G.; Arnott, W. P.; Molina, L. T.; Sosa, G.; Jimenez, J. L. *Atmospheric Chemistry and Physics* **2009**, *9*, 6633-6653.

- (9) Carlton, A. G.; Pinder, R. W.; Bhave, P. V.; Pouliot, G. A. *Environmental Science & Technology* **2010**, *44*, 3376-3380.
- (10) Hoyle, C. R.; Boy, M.; Donahue, N. M.; Fry, J. L.; Glasius, M.; Guenther, A.; Hallar, A. G.; Huff Hartz, K.; Petters, M. D.; Petäjä, T.; Rosenoern, T.; Sullivan, A. P. *Atmospheric Chemistry and Physics* **2011**, *11*, 321-343.
- (11) Hildebrandt, L.; Henry, K. M.; Kroll, J. H.; Worsnop, D. R.; Pandis, S. N.; Donahue, N. M. *Environmental Science & Technology* **2011**, *45*, 6329-6335.
- (12) Alfarra, M. R.; Paulsen, D.; Gysel, M.; Garforth, A. A.; Dommen, J.; Prevot, A. S. H.; Worsnop, D. R.; Baltensperger, U.; Coe, H. *Atmospheric Chemistry and Physics* **2006**, *6*, 5279-5293.
- (13) Odum, J. R.; Hoffmann, T.; Bowman, F.; Collins, D.; Flagan, R. C.; Seinfeld, J. H. *Environmental Science & Technology* **1996**, *30*, 2580-2585.
- (14) Safron, A.; Strandell, M.; Kierkegaard, A.; Macleod, M. *International Journal of Chemical Kinetics* **2015**, *47*, 420-428.
- (15) Atkinson, R.; Aschmann, S. M.; Pitts, J. N. *International Journal of Chemical Kinetics* **1986**, *18*, 287-299.
- (16) Atkinson, R.; Winer, A. M.; Pitts, J. N. *Atmospheric Environment* **1982**, *16*, 1017-1020.
- (17) Hall, W. A.; Johnston, M. V. *Aerosol Science and Technology* **2011**, *45*, 37-45.
- (18) Shilling, J. E.; Chen, Q.; King, S. M.; Rosenoern, T.; Kroll, J. H.; Worsnop, D. R.; DeCarlo, P. F.; Aiken, A. C.; Sueper, D.; Jimenez, J. L.; Martin, S. T. *Atmospheric Chemistry and Physics* **2009**, *9*, 771-782.
- (19) Trostl, J.; Chuang, W. K.; Gordon, H.; Heinritzi, M.; Yan, C.; Molteni, U.; Ahlm, L.; Frege, C.; Bianchi, F.; Wagner, R.; Simon, M.; Lehtipalo, K.; Williamson, C.; Craven, J. S.; Duplissy, J.; Adamov, A.; Almeida, J.; Bernhammer, A. K.; Breitenlechner, M.; Brilke, S.; Dias, A.; Ehrhart, S.; Flagan, R. C.; Franchin, A.; Fuchs, C.; Guida, R.; Gysel, M.; Hansel, A.; Hoyle, C. R.; Jokinen, T.; Junninen, H.; Kangasluoma, J.; Keskinen, H.; Kim, J.; Krapf, M.; Kurten, A.; Laaksonen, A.; Lawler, M.; Leiminger, M.; Mathot, S.; Mohler, O.; Nieminen, T.; Onnela, A.; Petaja, T.; Piel, F. M.; Miettinen, P.; Rissanen, M. P.; Rondo, L.; Sarnela, N.; Schobesberger, S.; Sengupta, K.; Sipila, M.; Smith, J. N.; Steiner, G.; Tome, A.; Virtanen, A.; Wagner, A. C.; Weingartner, E.; Wimmer, D.; Winkler, P. M.; Ye, P. L.; Carslaw, K. S.; Curtius, J.; Dommen, J.; Kirkby, J.; Kulmala, M.; Riipinen, I.; Worsnop, D. R.; Donahue, N. M.; Baltensperger, U. *Nature* **2016**, *533*, 527-+.

- (20) Ahlberg, E.; Falk, J.; Eriksson, A.; Holst, T.; Brune, W. H.; Kristensson, A.; Roldin, P.; Svenningsson, B. *Atmospheric Environment* **2017**, *161*, 210-220.

Chapter 5

CONCLUSIONS AND FUTURE DIRECTIONS

This dissertation is the first detailed study of aerosol chemical composition, formation mechanisms, and aerosol yield of aerosol generated from OH oxidation of the cyclic volatile methyl siloxane (cVMS), decamethylcyclopentasiloxane (D₅). The use of multiple methods of aerosol generation, reaction and molecular characterization has allowed the study of aerosol formation under a variety of reaction conditions that include atmospheric relevant conditions.

The first step of this research was to characterize the chemical composition of molecular products in secondary aerosol produced from the OH-initiated oxidation of decamethylcyclopentasiloxane (D₅, C₁₀H₃₀O₅Si₅) by high performance mass spectrometry. Both of monomer (300 < m/z < 470) and dimer (700 < m/z < 870) oxidation products were observed among the hundreds of molecular species assigned. With the aid of high resolution ESI-MS and MS/MS, it was shown that oxidation leads mainly to the substitution of a CH₃ group by OH or CH₂OH, and that a single D₅ molecule can undergo many CH₃ group substitutions. Dimers also exhibit OH and CH₂OH substitutions and can be linked by O, CH₂ and CH₂CH₂ groups. GC-MS confirmed major building blocks were D₅, one OH substituted D₅ and dimers linked by O and CH₂, which is consistent with the ESI-MS results. Oxidation of D₄ (C₈H₂₄O₄Si₄) exhibited similar substitutions and oligomerizations to D₅, though the degree of oxidation was greater under the same conditions and there was direct evidence for the formation of peroxy groups (CH₂OOH) in addition to OH and CH₂OH.

The next step was to study the aerosol formation mechanisms under varying experimental conditions. In Chapter 3, aerosol mass concentrations were controlled by adjusting the initial D₅ concentrations, both in the absence and

presence of ammonium sulfate seed. Aerosol yield was measured for 1 to 5 ppbv of reacted D₅. For unseeded experiments, the aerosol mass yield ranged from ~0.08 to 0.15 for aerosol mass concentrations between ~1 and 12 μg/m³. For the unseeded experiments, chemical characterization showed that the molecular composition is aerosol mass loading dependent in the 1-12 μg/m³ range. Monomers (5 Si atoms/molecule) and dimers (10 Si atoms/molecule) dominated the mass spectra of aerosols at higher mass loadings while ring opened species (neither 5 nor 10 Si atoms/molecule) dominated the mass spectra of aerosols at lower mass loadings.

Molecular signal intensity dependencies on the aerosol volume-to-surface area ratio suggested that nonvolatile ring opened species are formed in the gas phase and assist particle formation through condensation, favored in smaller particles, while dimers are formed by accretion reactions within the particle phase as the particles grow, favored in larger particles. These conclusions were supported by experiments in the presence of seed aerosol with similar siloxane aerosol mass loading but higher volume to surface area ratio, where ring-opened species are much less prevalent than monomers or dimers and the aerosol yield is higher.

Finally, Chapter 4 studied the aerosol generated from OH oxidation of D₅ mixed with β-pinene in the photo-oxidation chamber. Under the conditions studied, β-pinene oxidation was much faster than D₅ and its secondary aerosol dominated the overall chemical composition of mixed aerosol. Those produced β-pinene SOA with large volume would take up more monomers formed from D₅ oxidation to partition and also promote the particle phase reaction of dimers.

Future directions of this research should focus on a wider range of experimental conditions. Relative humidity should be changed to make the seed more liquid-like or to be solid to see the effect on the particle phase reaction. This overall graph of siloxane-derived aerosol could also be utilized into field measurement or modeling research.

Appendix A

MOLECULAR FORMULAS FOR IONS DETECTED IN D₅-DERIVED AEROSOL

Formula	M+H ⁺	M+Na ⁺	M-H
C ₆ H ₁₈ O ₂ Si ₂	√		
C ₃ H ₁₀ O ₃ Si ₂			√
C ₃ H ₁₂ O ₃ Si ₂			√
C ₄ H ₁₄ O ₃ Si ₂			√
C ₆ H ₁₈ O ₃ Si ₃	√		
C ₅ H ₁₆ O ₄ Si ₃			√
C ₆ H ₂₀ O ₄ Si ₃			√
C ₄ H ₁₄ O ₅ Si ₃			√
C ₅ H ₁₆ O ₅ Si ₃			√
C ₅ H ₁₈ O ₅ Si ₃			√
C ₈ H ₂₄ O ₄ Si ₄	√		
C ₇ H ₂₂ O ₅ Si ₄	√		√
C ₈ H ₂₄ O ₅ Si ₄			√
C ₈ H ₂₆ O ₅ Si ₄		√	√
C ₆ H ₂₀ O ₆ Si ₄			√
C ₆ H ₂₂ O ₆ Si ₄			√
C ₇ H ₂₂ O ₆ Si ₄			√
C ₇ H ₂₄ O ₆ Si ₄		√	√
C ₅ H ₁₈ O ₇ Si ₄			√
C ₄ H ₁₆ O ₈ Si ₄			√
C ₈ H ₂₆ O ₅ Si ₅			√
C ₉ H ₂₆ O ₅ Si ₅	√		
C ₁₀ H ₂₈ O ₅ Si ₅	√		
C ₇ H ₂₀ O ₆ Si ₅	√		
C ₈ H ₂₄ O ₆ Si ₅	√		√
C ₆ H ₂₀ O ₇ Si ₅			√
C ₇ H ₂₂ O ₇ Si ₅	√		√
C ₇ H ₂₄ O ₇ Si ₅			√
C ₅ H ₁₈ O ₈ Si ₅			√
C ₆ H ₂₀ O ₈ Si ₅			√
C ₆ H ₂₂ O ₈ Si ₅			√
C ₅ H ₁₈ O ₉ Si ₅			√
C ₄ H ₁₆ O ₁₀ Si ₅			√
C ₁₀ H ₃₂ O ₆ Si ₆			√
C ₈ H ₂₆ O ₇ Si ₆			√
C ₉ H ₂₈ O ₈ Si ₆			√

$C_{10}H_{32}O_8Si_6$			√
$C_7H_{22}O_9Si_6$			√
$C_8H_{26}O_9Si_6$			√
$C_9H_{28}O_9Si_6$			√
$C_9H_{30}O_9Si_6$			√
$C_8H_{28}O_{10}Si_6$			√
$C_7H_{26}O_{11}Si_6$			√
$C_9H_{30}O_{11}Si_6$			√
$C_6H_{24}O_{12}Si_6$			√
$C_{11}H_{34}O_9Si_7$			√
$C_9H_{28}O_{10}Si_7$			√
$C_{10}H_{32}O_{10}Si_7$			√
$C_{11}H_{36}O_{10}Si_7$			√
$C_8H_{26}O_{11}Si_7$			√
$C_9H_{30}O_{11}Si_7$			√
$C_{11}H_{34}O_{11}Si_8$			√
$C_{12}H_{38}O_{11}Si_8$			√
$C_9H_{28}O_{12}Si_8$			√
$C_{10}H_{32}O_{12}Si_8$			√
$C_{11}H_{36}O_{12}Si_8$			√
$C_{13}H_{40}O_{12}Si_9$			√
$C_{13}H_{40}O_{14}Si_{10}$			√

Table A- 1: Assigned ring-opened formulas for ions detected in D₅-derived aerosol.

Formula	M+H ⁺	M+Na ⁺	M-H ⁻
C ₁₀ H ₃₀ O ₅ Si ₅	√	√	
C ₉ H ₂₈ O ₆ Si ₅	√	√	√
C ₁₀ H ₃₀ O ₆ Si ₅	√	√	√
C ₈ H ₂₆ O ₇ Si ₅	√	√	√
C ₉ H ₂₈ O ₇ Si ₅	√	√	√
C ₁₀ H ₃₀ O ₇ Si ₅			√
C ₇ H ₂₄ O ₈ Si ₅		√	√
C ₈ H ₂₆ O ₈ Si ₅		√	√
C ₉ H ₂₈ O ₈ Si ₅		√	√
C ₁₀ H ₃₀ O ₈ Si ₅		√	√
C ₆ H ₂₂ O ₉ Si ₅			√
C ₇ H ₂₄ O ₉ Si ₅		√	√
C ₉ H ₂₈ O ₉ Si ₅		√	√
C ₁₀ H ₃₀ O ₉ Si ₅			√
C ₅ H ₂₀ O ₁₀ Si ₅			√
C ₈ H ₂₆ O ₁₀ Si ₅			√
C ₉ H ₂₈ O ₁₀ Si ₅		√	√
C ₁₀ H ₃₀ O ₁₀ Si ₅			√
C ₉ H ₂₈ O ₁₁ Si ₅			√
C ₁₀ H ₃₀ O ₁₁ Si ₅			√
C ₅ H ₂₀ O ₁₃ Si ₅			√
C ₁₉ H ₅₆ O ₁₀ Si ₁₀		√	
C ₂₀ H ₅₈ O ₁₀ Si ₁₀		√	
C ₁₈ H ₅₄ O ₁₁ Si ₁₀	√	√	
C ₁₉ H ₅₆ O ₁₁ Si ₁₀		√	
C ₂₀ H ₅₈ O ₁₁ Si ₁₀		√	
C ₁₇ H ₅₂ O ₁₂ Si ₁₀	√	√	
C ₁₈ H ₅₄ O ₁₂ Si ₁₀		√	
C ₁₉ H ₅₆ O ₁₂ Si ₁₀		√	
C ₂₀ H ₅₈ O ₁₂ Si ₁₀		√	
C ₁₆ H ₅₀ O ₁₃ Si ₁₀		√	√
C ₁₇ H ₅₂ O ₁₃ Si ₁₀		√	√
C ₁₈ H ₅₄ O ₁₃ Si ₁₀		√	√
C ₁₉ H ₅₆ O ₁₃ Si ₁₀		√	
C ₂₀ H ₅₈ O ₁₃ Si ₁₀		√	
C ₁₅ H ₄₈ O ₁₄ Si ₁₀		√	√
C ₁₆ H ₅₀ O ₁₄ Si ₁₀		√	√
C ₁₇ H ₅₂ O ₁₄ Si ₁₀		√	√
C ₁₈ H ₅₄ O ₁₄ Si ₁₀		√	
C ₁₉ H ₅₆ O ₁₄ Si ₁₀		√	√
C ₂₀ H ₅₈ O ₁₄ Si ₁₀		√	
C ₁₄ H ₄₆ O ₁₅ Si ₁₀		√	√
C ₁₅ H ₄₈ O ₁₅ Si ₁₀		√	
C ₁₆ H ₅₀ O ₁₅ Si ₁₀		√	

$C_{17}H_{52}O_{15}Si_{10}$		√	
$C_{18}H_{54}O_{15}Si_{10}$		√	
$C_{19}H_{56}O_{15}Si_{10}$		√	
$C_{13}H_{44}O_{16}Si_{10}$			√
$C_{16}H_{50}O_{16}Si_{10}$		√	
$C_{17}H_{52}O_{16}Si_{10}$		√	
$C_{18}H_{54}O_{16}Si_{10}$		√	
$C_{17}H_{52}O_{17}Si_{10}$		√	√

Table A- 2: Assigned saturated formulas for ions detected in D₅-derived aerosol.

Formula	M+H ⁺	M+Na ⁺	M-H ⁻
C ₉ H ₂₆ O ₆ Si ₅	√		
C ₉ H ₂₆ O ₇ Si ₅			√
C ₁₀ H ₂₈ O ₇ Si ₅	√	√	
C ₇ H ₂₂ O ₈ Si ₅			√
C ₈ H ₂₄ O ₈ Si ₅			√
C ₉ H ₂₆ O ₈ Si ₅		√	√
C ₁₀ H ₂₈ O ₈ Si ₅		√	√
C ₆ H ₂₀ O ₉ Si ₅			√
C ₈ H ₂₄ O ₉ Si ₅		√	√
C ₉ H ₂₆ O ₉ Si ₅			√
C ₁₀ H ₂₈ O ₉ Si ₅		√	√
C ₇ H ₂₂ O ₁₀ Si ₅			√
C ₉ H ₂₆ O ₁₀ Si ₅			√
C ₁₀ H ₂₈ O ₁₀ Si ₅			√
C ₈ H ₂₄ O ₁₁ Si ₅			√
C ₉ H ₂₆ O ₁₁ Si ₅			√
C ₁₀ H ₂₈ O ₁₁ Si ₅			√
C ₇ H ₂₂ O ₁₂ Si ₅			√
C ₁₀ H ₂₈ O ₁₄ Si ₅			√
C ₁₆ H ₄₈ O ₁₂ Si ₁₀	√		
C ₁₅ H ₄₆ O ₁₃ Si ₁₀	√	√	√
C ₁₆ H ₄₈ O ₁₃ Si ₁₀			√
C ₁₇ H ₅₀ O ₁₃ Si ₁₀		√	
C ₁₉ H ₅₄ O ₁₃ Si ₁₀		√	
C ₁₄ H ₄₄ O ₁₄ Si ₁₀		√	√
C ₁₅ H ₄₆ O ₁₄ Si ₁₀			√
C ₁₃ H ₄₂ O ₁₅ Si ₁₀			√

Table A- 3: Assigned unsaturated formulas for ions detected in D₅-derived aerosol.

Appendix B

MOLECULAR FORMULAS AND VOLATILITIES (LOG C*) OF THE CORRESPONDING CANDIDATE STRUCTURES AT 299.15K FOR PRODUCTS DETECTED IN D₅-DERIVED SECONDARY AEROSOL

Formula	logC*($\mu\text{g}/\text{m}^3$)	Formula	logC*($\mu\text{g}/\text{m}^3$)
C ₄ H ₁₂ O ₂ Si ₂	8.75	C ₁₄ H ₄₂ O ₁₁ Si ₈	-3.08
C ₆ H ₁₈ O ₃ Si ₃	7.75	C ₉ H ₂₈ O ₁₂ Si ₈	-5.27
C ₅ H ₁₆ O ₄ Si ₃	6.41	C ₁₀ H ₃₂ O ₁₂ Si ₈	-5.33
C ₄ H ₁₄ O ₅ Si ₃	4.56	C ₁₁ H ₃₄ O ₁₂ Si ₈	-5.51
C ₇ H ₂₀ O ₄ Si ₄	6.82	C ₁₁ H ₃₆ O ₁₂ Si ₈	-5.35
C ₈ H ₂₄ O ₄ Si ₄	6.82	C ₁₂ H ₃₆ O ₁₂ Si ₈	-5.76
C ₅ H ₁₄ O ₅ Si ₄	5.04	C ₁₂ H ₃₈ O ₁₂ Si ₈	-5.54
C ₆ H ₁₈ O ₅ Si ₄	5.04	C ₁₂ H ₄₀ O ₁₂ Si ₈	-5.33
C ₇ H ₂₀ O ₅ Si ₄	5.21	C ₁₃ H ₄₀ O ₁₂ Si ₈	-5.78
C ₇ H ₂₂ O ₅ Si ₄	5.40	C ₁₄ H ₄₂ O ₁₂ Si ₈	-6.08
C ₄ H ₁₂ O ₆ Si ₄	2.80	C ₈ H ₂₆ O ₁₃ Si ₈	-8.51
C ₅ H ₁₆ O ₆ Si ₄	3.17	C ₉ H ₃₀ O ₁₃ Si ₈	-8.53
C ₆ H ₁₈ O ₆ Si ₄	3.04	C ₁₀ H ₃₄ O ₁₃ Si ₈	-8.52
C ₆ H ₂₀ O ₆ Si ₄	3.55	C ₁₁ H ₃₈ O ₁₃ Si ₈	-8.47
C ₅ H ₁₈ O ₇ Si ₄	1.20	C ₁₂ H ₃₆ O ₁₃ Si ₈	-9.14
C ₇ H ₂₂ O ₆ Si ₄	-1.98	C ₁₂ H ₃₈ O ₁₃ Si ₈	-8.86
C ₄ H ₁₄ O ₇ Si ₄	0.80	C ₁₃ H ₄₀ O ₁₃ Si ₈	-9.13
C ₅ H ₁₈ O ₇ Si ₄	1.20	C ₁₄ H ₄₂ O ₁₃ Si ₈	-9.46
C ₆ H ₂₀ O ₇ Si ₄	1.14	C ₁₁ H ₃₄ O ₁₄ Si ₈	-12.62
C ₄ H ₁₆ O ₈ Si ₄	-1.75	C ₁₂ H ₃₈ O ₁₄ Si ₈	-12.58
C ₇ H ₂₂ O ₈ Si ₄	-1.98	C ₁₃ H ₄₀ O ₁₄ Si ₈	-12.87
C ₆ H ₂₀ O ₉ Si ₄	-5.21	C ₉ H ₂₈ O ₁₅ Si ₈	-16.61
C ₉ H ₂₆ O ₅ Si ₅	5.95	C ₁₀ H ₃₂ O ₁₅ Si ₈	-16.56
C ₇ H ₂₀ O ₆ Si ₅	4.20	C ₁₃ H ₄₀ O ₁₅ Si ₈	-17.03
C ₈ H ₂₄ O ₆ Si ₅	4.20	C ₁₄ H ₄₂ O ₁₁ Si ₉	-0.94
C ₉ H ₂₆ O ₆ Si ₅	4.22	C ₁₁ H ₃₂ O ₁₂ Si ₉	-3.25
C ₉ H ₂₈ O ₆ Si ₅	4.42	C ₁₂ H ₃₆ O ₁₂ Si ₉	-3.25
C ₅ H ₁₄ O ₇ Si ₅	2.06	C ₁₃ H ₃₈ O ₁₂ Si ₉	-3.68
C ₆ H ₁₈ O ₇ Si ₅	2.06	C ₁₃ H ₄₀ O ₁₂ Si ₉	-3.43
C ₇ H ₂₂ O ₇ Si ₅	2.29	C ₁₄ H ₄₄ O ₁₂ Si ₉	-3.57
C ₈ H ₂₄ O ₇ Si ₅	2.12	C ₁₁ H ₃₄ O ₁₃ Si ₉	-6.12
C ₈ H ₂₆ O ₇ Si ₅	2.54	C ₁₂ H ₃₈ O ₁₃ Si ₉	-6.26
C ₉ H ₂₈ O ₇ Si ₅	2.36	C ₁₃ H ₄₂ O ₁₃ Si ₉	-6.37
C ₅ H ₁₆ O ₈ Si ₅	-0.32	C ₉ H ₂₈ O ₁₄ Si ₉	-9.21
C ₆ H ₂₀ O ₈ Si ₅	-0.06	C ₁₀ H ₃₂ O ₁₄ Si ₉	-9.36
C ₇ H ₂₂ O ₈ Si ₅	-0.17	C ₁₁ H ₃₆ O ₁₄ Si ₉	-9.47

C ₇ H ₂₄ O ₈ Si ₅	0.22	C ₁₂ H ₄₀ O ₁₄ Si ₉	-9.54
C ₈ H ₂₆ O ₈ Si ₅	0.09	C ₁₁ H ₃₈ O ₁₅ Si ₉	-13.13
C ₅ H ₁₈ O ₉ Si ₅	-2.91	C ₁₃ H ₄₀ O ₁₅ Si ₉	-13.66
C ₆ H ₂₂ O ₉ Si ₅	-2.60	C ₁₁ H ₃₄ O ₁₆ Si ₉	-17.53
C ₉ H ₂₈ O ₉ Si ₅	-3.03	C ₁₂ H ₃₈ O ₁₆ Si ₉	-17.56
C ₆ H ₂₂ O ₉ Si ₅	-2.60	C ₁₆ H ₄₈ O ₁₂ Si ₁₀	-2.44
C ₅ H ₁₈ O ₉ Si ₅	-2.91	C ₁₃ H ₃₈ O ₁₃ Si ₁₀	-4.83
C ₇ H ₂₂ O ₁₀ Si ₅	-6.45	C ₁₄ H ₄₂ O ₁₃ Si ₁₀	-4.83
C ₈ H ₂₆ O ₁₀ Si ₅	-6.14	C ₁₅ H ₄₆ O ₁₃ Si ₁₀	-5.16
C ₉ H ₂₆ O ₇ Si ₆	3.58	C ₁₁ H ₃₂ O ₁₄ Si ₁₀	-7.56
C ₁₀ H ₃₀ O ₇ Si ₆	3.58	C ₁₂ H ₃₆ O ₁₄ Si ₁₀	-7.56
C ₇ H ₂₀ O ₈ Si ₆	1.54	C ₁₃ H ₄₀ O ₁₄ Si ₁₀	-7.91
C ₈ H ₂₄ O ₈ Si ₆	1.54	C ₁₄ H ₄₄ O ₁₄ Si ₁₀	-8.21
C ₉ H ₂₈ O ₈ Si ₆	1.65	C ₁₅ H ₄₈ O ₁₄ Si ₁₀	-8.47
C ₁₀ H ₃₂ O ₈ Si ₆	1.79	C ₁₁ H ₃₄ O ₁₅ Si ₁₀	-11.05
C ₆ H ₁₈ O ₉ Si ₆	-0.91	C ₁₂ H ₃₈ O ₁₅ Si ₁₀	-11.38
C ₇ H ₂₂ O ₉ Si ₆	-0.80	C ₁₃ H ₄₀ O ₁₅ Si ₁₀	-11.49
C ₈ H ₂₄ O ₉ Si ₆	-0.96	C ₁₃ H ₄₂ O ₁₅ Si ₁₀	-11.65
C ₈ H ₂₆ O ₉ Si ₆	-0.66	C ₁₄ H ₄₆ O ₁₅ Si ₁₀	-11.88
C ₉ H ₂₈ O ₉ Si ₆	-0.82	C ₁₀ H ₃₂ O ₁₆ Si ₁₀	-14.99
C ₉ H ₃₀ O ₉ Si ₆	-0.50	C ₁₁ H ₃₆ O ₁₆ Si ₁₀	-15.28
C ₇ H ₂₄ O ₁₀ Si ₆	-3.41	C ₁₂ H ₄₀ O ₁₆ Si ₁₀	-15.52
C ₈ H ₂₈ O ₁₀ Si ₆	-3.22	C ₁₁ H ₃₈ O ₁₇ Si ₁₀	-19.86
C ₅ H ₁₆ O ₁₀ Si ₆	-3.74	C ₁₅ H ₄₆ O ₁₅ Si ₁₁	-7.92
C ₆ H ₂₀ O ₁₀ Si ₆	-3.59	C ₁₃ H ₄₀ O ₁₆ Si ₁₁	-10.90
C ₇ H ₂₄ O ₁₀ Si ₆	-3.41	C ₁₄ H ₄₄ O ₁₆ Si ₁₁	-11.21
C ₈ H ₂₆ O ₁₀ Si ₆	-3.51	C ₁₅ H ₄₈ O ₁₆ Si ₁₁	-11.47
C ₈ H ₂₈ O ₁₀ Si ₆	-3.22	C ₁₁ H ₃₄ O ₁₇ Si ₁₁	-14.28
C ₆ H ₂₂ O ₁₁ Si ₆	-6.67	C ₁₂ H ₃₈ O ₁₇ Si ₁₁	-14.60
C ₉ H ₂₈ O ₁₁ Si ₆	-7.00	C ₁₃ H ₄₂ O ₁₇ Si ₁₁	-14.87
C ₁₀ H ₃₂ O ₁₁ Si ₆	-6.80	C ₁₄ H ₄₆ O ₁₇ Si ₁₁	-15.10
C ₈ H ₂₆ O ₁₂ Si ₆	-10.53	C ₁₅ H ₅₀ O ₁₇ Si ₁₁	-15.28
C ₁₁ H ₃₂ O ₈ Si ₇	2.74	C ₁₃ H ₄₄ O ₁₈ Si ₁₁	-19.13
C ₁₂ H ₃₆ O ₈ Si ₇	2.74	C ₁₄ H ₄₈ O ₁₈ Si ₁₁	-19.27
C ₉ H ₂₆ O ₉ Si ₇	0.73	C ₁₇ H ₅₂ O ₁₆ Si ₁₂	-8.86
C ₁₀ H ₃₀ O ₉ Si ₇	0.73	C ₁₅ H ₄₆ O ₁₇ Si ₁₂	-11.81
C ₁₁ H ₃₄ O ₉ Si ₇	0.73	C ₁₆ H ₅₀ O ₁₇ Si ₁₂	-12.19
C ₇ H ₂₀ O ₁₀ Si ₇	-1.65	C ₁₇ H ₅₄ O ₁₇ Si ₁₂	-12.52
C ₈ H ₂₄ O ₁₀ Si ₇	-1.65	C ₁₅ H ₄₈ O ₁₈ Si ₁₂	-15.87
C ₉ H ₂₈ O ₁₀ Si ₇	-1.65	C ₁₆ H ₅₂ O ₁₈ Si ₁₂	-16.17
C ₁₀ H ₃₂ O ₁₀ Si ₇	-1.62	C ₁₇ H ₅₂ O ₁₈ Si ₁₂	-16.41
C ₁₁ H ₃₆ O ₁₀ Si ₇	-1.54	C ₁₃ H ₄₀ O ₁₈ Si ₁₂	-15.13
C ₇ H ₂₂ O ₁₁ Si ₇	-4.47	C ₁₄ H ₄₄ O ₁₈ Si ₁₂	-15.53
C ₈ H ₂₆ O ₁₁ Si ₇	-4.43	C ₁₅ H ₄₈ O ₁₈ Si ₁₂	-15.87
C ₉ H ₂₈ O ₁₁ Si ₇	-4.36	C ₁₆ H ₅₂ O ₁₈ Si ₁₂	-16.17
C ₉ H ₃₀ O ₁₁ Si ₇	-4.36	C ₁₄ H ₄₆ O ₁₉ Si ₁₂	-19.94
C ₁₀ H ₃₄ O ₁₁ Si ₇	-4.26	C ₁₅ H ₅₀ O ₁₉ Si ₁₂	-20.19
C ₇ H ₂₄ O ₁₂ Si ₇	-7.66	C ₁₆ H ₅₀ O ₁₉ Si ₁₂	-20.39

$C_8H_{28}O_{12}Si_7$	-7.55	$C_{16}H_{54}O_{19}Si_{12}$	-20.41
$C_9H_{32}O_{12}Si_7$	-7.42	$C_{17}H_{50}O_{18}Si_{13}$	-13.06
$C_{11}H_{34}O_{12}Si_7$	-8.04	$C_{15}H_{46}O_{19}Si_{13}$	-16.04
$C_9H_{28}O_{13}Si_7$	-11.64	$C_{16}H_{48}O_{19}Si_{13}$	-16.32
$C_{10}H_{32}O_{13}Si_7$	-11.52	$C_{16}H_{50}O_{19}Si_{13}$	-16.50
$C_8H_{26}O_{14}Si_7$	-15.66	$C_{17}H_{54}O_{19}Si_{13}$	-16.91
$C_{12}H_{36}O_{10}Si_8$	-0.10	$C_{16}H_{52}O_{20}Si_{13}$	-20.99
$C_{13}H_{40}O_{10}Si_8$	-0.18	$C_{17}H_{56}O_{20}Si_{13}$	-21.31
$C_9H_{26}O_{11}Si_8$	-2.44	$C_{15}H_{50}O_{21}Si_{13}$	-25.46
$C_{10}H_{30}O_{11}Si_8$	-2.44	$C_{16}H_{54}O_{21}Si_{13}$	-25.74
$C_{11}H_{32}O_{11}Si_8$	-2.76	$C_{17}H_{58}O_{21}Si_{13}$	-25.98
$C_{11}H_{34}O_{11}Si_8$	-2.53	$C_{15}H_{46}O_{21}Si_{14}$	-20.62
$C_{12}H_{36}O_{11}Si_8$	-2.76	$C_{17}H_{52}O_{20}Si_{14}$	-16.98
$C_{12}H_{38}O_{11}Si_8$	-2.59	$C_{16}H_{50}O_{21}Si_{14}$	-21.17
$C_{13}H_{40}O_{11}Si_8$	-2.81	$C_{17}H_{54}O_{21}Si_{14}$	-21.65

Table B-1: Molecular formulas and volatilities ($\log C^*$) of the corresponding candidate structures at 299.15K for products detected in D₅-derived secondary aerosol. The products listed were positively detected in all four samples of at least one secondary aerosol studied.